CRISTHIANE ASSENHAIMER

Evaluation of Emulsion Destabilization by Light Scattering Applied to Metalworking Fluids

Tese apresentada à Escola Politécnica da Universidade de São Paulo para obtenção do título de Doutor em Engenharia

São Paulo
2015

CRISTHIANE ASSENHAIMER

Evaluation of Emulsion Destabilization by Light Scattering Applied to Metalworking Fluids

Tese apresentada à Escola Politécnica da Universidade de São Paulo para obtenção do título de Doutor em Engenharia

Área de concentração:
Engenharia Química

Orientador:
Prof. Dr. Roberto Guardani

São Paulo
2015

Este exemplar foi revisado e corrigido em relação à versão original, sob responsabilidade única do autor e com a anuência de seu orientador.

São Paulo, 07 de outubro de 2015

Assinatura do autor: Cristhiane Assenhaimer

Assinatura do orientador: Roberto Pecora

Catalogação-na-publicação

Assenhaimer, Cristhiane
Evaluation of Emulsion Destabilization by Light Scattering Applied to Metalworking Fluids / C. Assenhaimer -- versão corr. -- São Paulo, 2015.
130 p.

Tese (Doutorado) - Escola Politécnica da Universidade de São Paulo. Departamento de Engenharia Química.

1.Emulsões 2.Espectroscopia 3.Redes neurais 4.Distribuição de tamanho de gotas 5.Fluidos de corte I.Universidade de São Paulo. Escola Politécnica. Departamento de Engenharia Química II.t.

To my parents, my inspiration to pursue my goals,
and to my husband, who made this possible.

ACKNOWLEDGEMENTS

Primeiramente, agradeço a Deus, que me deu a vida e essa curiosidade que me leva à busca incessante pelo conhecimento.

Agradeço ao professor Dr. Roberto Guardani, pela orientação, pelo constante estímulo transmitido durante todo o trabalho e por estar sempre pronto a ajudar; ao professor Dr. Udo Fritsching, pela orientação durante meu período sanduíche na Universidade de Bremen; aos demais professores da Escola Politécnica da USP pelo conhecimento transmitido e críticas construtivas durante a elaboração da minha tese; aos colegas da Universidade de São Paulo e da Universidade de Bremen, por sua colaboração acadêmica e amizade; e a todos os meus alunos de Iniciação Científica que me ajudaram durante esse trabalho; a contribuição de cada um foi muito valiosa.

Agradeço à minha família; aos meus pais, por me incentivarem nos estudos e me ensinarem a sempre perseguir meus objetivos; ao meu marido, por me apoiar em todos os momentos e contribuir para que fosse possível esse tempo de dedicação exclusiva aos estudos; ao meu filho, pelo carinho nas horas de desânimo; à minha irmã, simplesmente por ser minha irmã e por sua amizade; à minha sogra, que esteve sempre presente para me ajudar toda vez que eu precisei.

Agradeço também aos amigos que me apoiaram e a todos aqueles que direta ou indiretamente colaboraram na execução desse trabalho. Não teria como citar o nome de todos aqui, mas agradeço em especial às gurias, aos amigos do GP, à família Takahashi e aos amigos da USP pela amizade e por muitas vezes ajudarem a tornar essa jornada mais leve.

Finalmente, agradeço à FAPESP pela concessão da bolsa de doutorado direto (processo n° 2010/20376-7). Agradeço também às agências financiadoras do programa Bragecrim, CNPq, CAPES e DFG, pelo suporte financeiro ao projeto de pesquisa, onde o esse estudo está inserido.

It seems I was like a little kid playing on the seashore,
and diverting myself now and then
finding a smoother pebble or a prettier shell than ordinary,
whilst the great ocean of truth lay all undiscovered before me.
(Isaac Newton)

CONTENTS

LIST OF FIGURES

LIST OF TABLES

ABREVIATIONS

ANN	Artificial neural network
DSD	Droplet size distribution
Discr. Lin	Linear discriminant
Discr. Q	Quadratic discriminant
ECM	Expected cost of failures
GC-MS	Gas chromatography–mass spectrometry
HIPR	Holdback input randomization
HLB	Hydrophilic-lipophilic balance
LDA	Linear discriminant Analysis
MSE	Mean squared error
MWF	Metalworking fluid
MWFs	Metalworking fluids
NMR	Nuclear magnetic resonance
O/W	Oil-in-water
PCA	Principal component analysis
PDW	Photon density wave
QDA	Quadratic discriminant analysis
W/O	Water-in-oil

SYMBOLS

A_{calc}	area under the calculated DSD curve
A_{exp}	area under the experimental DSD curve
C	cost
c_p	specific heat capacity
$D_{4.3}$	volumetric mean diameter
e_i	components
E	error
E_v	dissipated energy
f(x)	density function
L	optical path length
I	received light intensity
I_0	emitted light intensity
N_p	total particle number per unit volume of the system
P	probability
p_i	priori probability
Oj	response function of the ANN
O_k	calculated value of the output of the ANN
Q_{ext}	extinction efficiency

R^2	coefficient of determination
S_j	weighted sum of the inputs of the ANN
W_{ij}	weights
X_i	inputs of the ANN
x	particle size, diameter
x_i	observations
Y_i	experimental value of the output of the ANN
z	wavelength exponent
ΔT	variation of temperature
ε	quadrature and measurement error
λ	wavelength
μ	mean
ρ	density
Σ	covariance matrix
τ	turbidity
φ	volumetric fraction of the dispersed phase

ABSTRACT

Monitoring of emulsion properties is important in many applications, like in foods and pharmaceutical products, or in emulsion polymerization processes, since aged and 'broken' emulsions perform worse and may affect product quality. In machining processes, special types of emulsions called metalworking fluids (MWF) are widely used, because of its combined characteristics of cooling and lubrication, increasing the productivity, enabling the use of higher cutting speeds, decreasing the amount of power consumed and increasing tool life. Even though emulsion quality monitoring is a key issue in manufacturing processes, traditional methods are far from accurate and generally fail in providing the tools for determining the optimal useful life of these emulsions, with high impact in costs.

The present study is dedicated to the application of a spectroscopic sensor to monitor MWF emulsion destabilization, which is related to changes in its droplet size distribution. Rapeseed oil emulsions, artificially aged MWF and MWF in machining application were evaluated, using optical measurements and multivariate calibration by neural networks, for developing a new method for emulsion destabilization monitoring. The technique has shown good accuracy in rebuilding the droplet size distribution of emulsions for monomodal and bimodal distributions and different proportions of each droplet population, from the spectroscopic measurements, indicating the viability of this method for monitoring such emulsions.

This study is part of a joint project between the University of São Paulo and the University of Bremen, within the BRAGECRIM program (Brazilian German Cooperative Research Initiative in Manufacturing) and is financially supported by FAPESP, CAPES, FINEP and CNPq (Brazil), and DFG (Germany).

Keywords: Emulsion. Spectroscopic sensor. Droplet size distribution. Metalworking fluids. Neural Networks.

1. BACKGROUND AND MOTIVATION

Emulsions are utilized in industrial and medical applications for a variety of reasons, such as encapsulation and delivery of active components; modification of rheological properties; alteration of optical properties; lubrication; modification of organoleptic attributes. Traditionally, conventional emulsions consist of small spherical droplets of one liquid dispersed in another immiscible liquid, where the two immiscible liquids are typically an oil phase and an aqueous phase, although other immiscible liquids can sometimes be used.

In machining processes, special types of emulsions called metalworking fluids (MWFs) are widely used, because of their combined characteristics of cooling and lubrication. Although some fluids are composed of oil and additives, only, most of them are oil-in-water emulsions, with complex formulations that can change according to the application. Their use increases the productivity and reduces costs by enabling the use of higher cutting speeds, higher feed rates and deeper cuts. Effective application of cutting fluids can also increase tool life, decrease surface roughness and decrease the amount of power consumed (EL BARADIE, 1996).

The consumption of cutting fluids in a typical metal working facility is around 33 t/year (OLIVEIRA; ALVES, 2007). The worldwide annual usage is estimated to exceed $2x10^9$ L and the waste could be more than ten times the usage, as MWFs have to be diluted prior to use (CHENG; PHIPPS; ALKHADDAR, 2005). From 7 to 17% of the total costs of machining processes are due to the metalworking fluids, while only 2 to 4% are due to the costs of tools (KLOCKE; EISENBLÄTTER, 1997).

One of the main problems observed in these emulsions consists of degradation by contamination with substances from the manufacturing process and losses in its stability. This degradation promotes coalescence of the dispersed droplets, increasing the mean droplet size of the dispersed fluid. Although the complete separation of emulsion due to coalescence should not be a problem to be found in real metalworking processes, since the fluid is replaced before reaching such condition, the increase in droplet size affects the attributes of the MWFs and its performance in machining processes. At this point, the fluid is considered “old” or “aged”, and traditional practice has been to dispose the used MWF, as well as the

fluids with high contaminant levels. However, due to their nature as stable oil-in-water mixtures, MWFs create both monetary and environmental problems in their treatment and disposal. It is estimated that for each dollar of MWF concentrate purchased, eleven dollars are spent in mixing, managing, treating and disposing spent emulsions. This is an important aspect in a sector that has traditionally focused on tool costs. MWFs are also a major source of oily wastewater in the effluents of industries in the metal products and machinery sector. About 10 years ago, it was estimated that 3.8 to 7.6 millions m^3 of oily wastewater resulted annually from the use of MWFs (GREELEY; RAJAGOPALAN, 2004).

Due to that, new technologies are been developed to improve MWFs quality, maximize its useful life or minimize its environmental impact. Machado and Wallbank (1997), for example, studied the effect of the use of extremely low lubricant volumes in machining processes, reducing therefore the volume of old fluid to be disposed. Benito et al. (2010) carried out experiments to obtain optimal formulations for MWFs, and proposed the disposal of spent O/W emulsions using techniques such as coagulation, centrifugation, ultrafiltration, and vacuum evaporation. Zimmerman et al. (2003) designed a mixed anionic/nonionic emulsifier system for petroleum and bio-based MWFs that improve the useful life by providing emulsion stability under hard water conditions, a common cause of emulsion destabilization leading to MWF disposal. Vargas et al. (2014) studied the use of an ecofriendly emulsifier for the production of oil-in-water emulsions for industrial consumption. Doll and Sharma (2011) investigated the application of chemically modified vegetable oils to substitute conventional oils in lubricant use. Guimarães et al. (2010) focused his work on the destabilization and recoverability of oil used in the formulation of cutting fluids.

Greeley and Rajagopalan (2004) carried out an analysis on the impact of environmental contaminants on machining properties of metalworking fluids and the possibility of extended use of aged fluids. Several experiments were performed to evaluate the lubricating, cooling, corrosion inhibition, and surface finishing functionalities of MWFs in presence of natural contaminants. Their conclusion was that, as long as stability is maintained, natural contaminants have little or no impact in the performance of the MWF. However, when there is some level of destabilization of the fluid, there are also losses in lubrication and cooling. Hence, the monitoring of

emulsion destabilization could possibly be used as an indicator of potential loss of lubrication and cooling properties. In this way, it could be helpful in determining the optimal useful life of MWFs.

The monitoring of MWF consists conventionally of periodic measurements of oil concentration, pH, viscosity and contamination. In this way, changes in fluid characteristics are detected only when the destabilization of the emulsion is already significant, leading to problems in machining processes, decreasing tool life, among others. In other occasions, fluids with no loss of performance are discarded because one or more of the measured items has reached the stipulated limit. In both situations, it has a significant impact on costs for this industry sector. Therefore, there is a growing market estimated in 1.2 Million t/a emulsions for new stability or destabilization detection methods (GROSCHE, 2014 apud Kissler, 2012). One possible method is based on the droplet size distribution (DSD), which is directly linked to the quality and physical stability of an emulsion because of its influence on the free interactive surface (GROSCHE, 2014), i.e., changes in DSD are an indicator of destabilization of the emulsion.

In this context the objective of this study is to evaluate changes in the droplet size distribution of emulsions, with focus on MWFs, using optical measurements and multivariate calibration by neural networks, in order to developing a new method for emulsion destabilization monitoring.

The present document shows results of experiments carried out to measure absorbance spectra of rapeseed oil emulsions (taken as simple oil-in-water emulsions) and commercially available MWFs with a spectroscopic sensor. The data obtained from the spectroscopic measurements were used treated in different ways, in order to select an efficient criterion to identify the condition of a given MWF emulsion, based on estimates of the DSD.

Commercially available MWF emulsions were evaluated in terms of their artificial destabilization with addition of calcium salts, thus increasing the coalescence rate. The destabilization process was monitored by means of droplet size distribution measurements as well as by on-line measurement of the absorbance spectra. The

data were used to evaluate the destabilization of emulsions based on existing criteria like the wavelength exponent and to estimate the DSD using neural network models.

In addition, several commercially available MWFs were evaluated during use in a machining facility in order to obtain data as near as possible of a real case scenario. The destabilization process was monitored by means of droplet size distribution measurements as well as by on-line measurement of the absorbance spectra.

This study is part of the project entitled “Emulsion Process Monitor”, within the scope of the BRAGECRIM program – “Brazilian German Collaborative Research Initiative in Manufacturing”, a partnership of CAPES, FINEP and CNPq (Brazil), and DFG (Deutsche Forschungsgemeinschaft) (Germany), coordinated by Prof. Roberto Guardani (USP) and Prof. Udo Fritsching (University of Bremen). The main objective of the project is the development of an optical sensor for monitoring metalworking fluid characteristics, and to study emulsion stability and flow characteristics.

In this project, different aspects related to MWF monitoring, and the destabilization process have been investigated. Thus, experiments under different conditions and with different arrangements of the optical sensor have been carried out by the Brazilian and German teams, coupled with simulations of the interaction between the MWF and the sensor based on computational fluid dynamic techniques (GROSCHE, 2014). Coalescence models have also been compared in simulations aimed at studying the effect of the flow conditions on the coalescence rate and droplet size distribution (VARGAS, 2014). An intensive study has also been dedicated to the behavior of MWF emulsions with respect to optical properties and the treatment of spectroscopic data to evaluate the emulsion in different conditions, mainly based on inversion methods; the results evidenced the limitation of these methods in retrieving droplet size information of real MWF from spectroscopic data. The inversion methods produced satisfactory results only for a specific subset of simulated data and monodisperse polystyrene particle suspensions (GLASSE, 2015).

The present thesis is based on the results of the previous studies mentioned, and is dedicated to the application of the spectroscopic sensor to monitor MWF

emulsion destabilization. Based on the results of the application of different criteria to evaluate the MWF emulsions, a new method is proposed, based on the fitting of neural networks to estimate droplet size distribution from process operational data.

2. OBJECTIVE

The main objective of the present study is to evaluate the application of a spectroscopic sensor to monitor metalworking fluid emulsion destabilization during aging, thus proposing a new method for the monitoring of such emulsions and providing an innovative tool to optimize the useful life of metalworking fluids in industries. In order to achieve this overall objective, the following specific objectives are stated:

- To establish a methodology for estimating the droplet size distribution in emulsions based on spectroscopic data.
- To apply the methodology, i.e., the spectroscopic sensor and the data treatment procedure, to monitor emulsion destabilization based on changes in the droplet size distribution, with focus on metalworking fluids (MWF).

3. LITERATURE REVIEW

3.1. Emulsions

Emulsions are dispersions of at least two immiscible liquids and appear most commonly as two types: water droplets dispersed in an organic liquid (an “oil”), designated W/O, and organic droplets dispersed in water, designated O/W. In this study, only oil-in-water emulsions (O/W) are considered. Emulsions are generally stabilized by a third component, an emulsifier, which is often a surfactant. Other examples of emulsifiers include polymers, proteins, and finely divided solids, each one influencing the final physical-chemical properties of the emulsion. Emulsions do not form spontaneously but rather require an input of energy, contrary to the thermodynamically stable microemulsions. Therefore, the term “emulsion stability” refers to the ability of an emulsion to keep its characteristics unchanged over a certain period of time and, as a consequence, emulsions are only kinetically stabilized, with destabilization occurring over time with a time constant varying from seconds to years (EGGER; MCGRATH, 2006). The more slowly the characteristics change, the more stable the emulsion is.

Microbiological contamination and external influences such as UV light, changes in temperature or reactions between individual components can also result in losses in stability or even "breaking" of an emulsion, by increasing the droplet size due to the coalescence of drops of the dispersed phase. Coalescence is defined as a process where two or more droplets of the dispersed phase merge together forming a larger droplet. Its rate depends on the number of collisions, on the energy or efficiency of those collisions and on the properties of the adsorption layers The final stage of the coalescence consists of the complete separation of the phases. In addition to droplet coalescence, other processes, including aggregation or flocculation, Ostwald ripening, sedimentation and creaming can take place (MOLLET; GRUBENMANN, 2001), as illustrated in Figure 1. In the flocculation process, the dispersed droplets form aggregates in which the individual droplets can still be recognized, and such aggregation is often reversible by means of mechanical forces caused by stirring of shaking. Flocculation may occur under conditions when the van

der Waals attractive energy exceeds the repulsive energy and can be weak or strong, depending on the strength of inter-drop forces. It can cause local concentration differences within the emulsion due to the change of the droplet size distribution and often results in coalescence. While aggregation is a reversible process, coalescence is irreversible. Ostwald ripening refers to the mass diffusion of several small droplets that ceases to exist and their mass is added to a few larger drops. Creaming is an upward migration phenomenon due to the density difference between disperse and continuous phases (HARUSAWA; MITSUI, 1975). Different processes can occur simultaneously.

In this study, since the droplets of the evaluated emulsions are typically small and they can not be considered as highly concentrated systems, the ripening phenomenon is not significant (CHISTYAKOV, 2001; VARGAS, 2014). Besides, some exploratory evaluations of commercial MWFs artificially aged with $CaCl_2$, using an optical scanning turbidimeter, Turbiscan Lab Expert® (from Formulaction), have shown profiles typical of particle size variation, like coalescence process, as illustrated in Figure 2. Thus, in this study, only the coalescence is considered as a cause of emulsion destabilization.

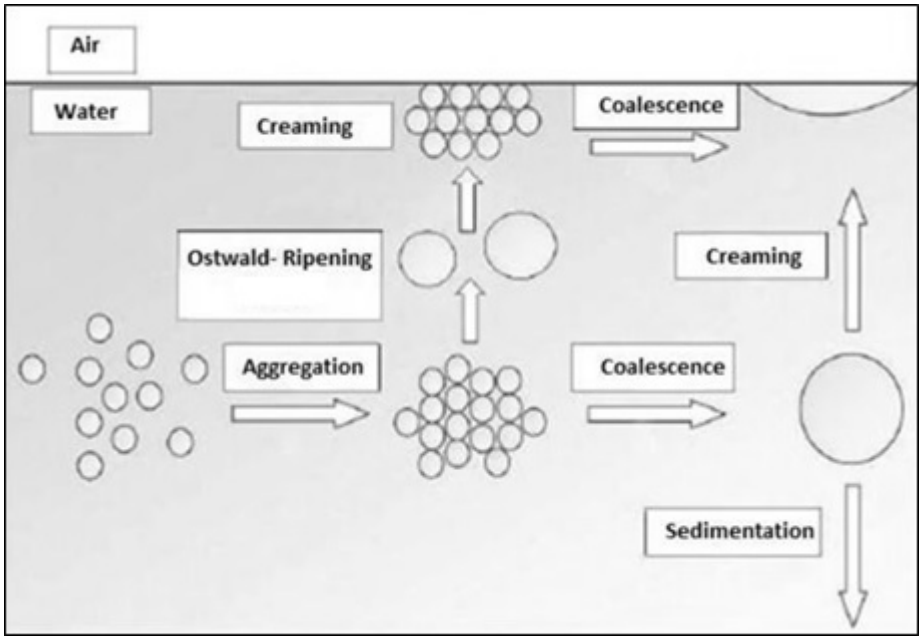

Figure 1: Illustration of the emulsion destabilization processes (MOLLET; GRUBENMANN, 2001).

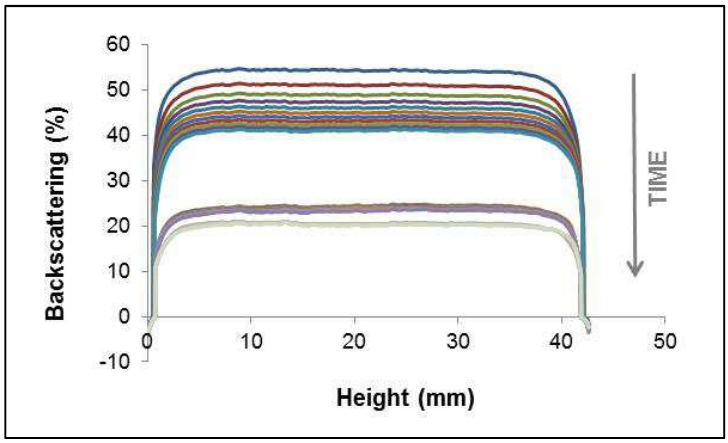

Figure 2: Illustration of the obtained profile of a commercial MWF during artificial aging with $CaCl_2$, using an optical scanning turbidimeter.

The stability of an emulsion depends on several factors, some of which are size distribution of the dispersed phase, the volume fraction of the dispersed phase and the type and quantity of the surfactant that, depending on the mechanism involved, promotes steric stabilization of the system or affect the repulsion forces between droplets of the dispersed phase. For this this factor, its dependency is explained by the DLVO Theory, proposed by Derjaguin and Landau and by Verwey and Overbeek (HIEMENZ; RAJAGOPALAN, 1997), by which it is possible to estimate the total interaction energy and the energy gap for coalescence or coagulation to occur. Otherwise, when the stabilization is steric, which is most likely the stabilization mechanism in the MWFs of this study, there are a formation of an adsorbed layer in the surface of the droplets, causing steric repulsion, which prevent the close approach of dispersed phase droplets (WILDE, 2000).

The size distribution of the dispersed phase affects the emulsion stability because it is related to the free-energy change in the coalescence of two droplets, which can be calculated by the product of the surface tension by the variation of the surface area, at constant volume, temperature, composition and surface tension. The area decreases as droplets coalesce, hence the change in the free-energy of the system is negative and the coalescence is therefore spontaneous. The larger the droplets, the larger is the surface area reduction, and more spontaneous is the coalescence process, and, therefore, less stable is the emulsion (MORRISON; ROSS, 2002). So, an increase in the droplet size of an emulsion is an indicator of its partial destabilization.

3.2. Metalworking Fluid Emulsions

Metalworking fluids are also known as “cutting and grinding fluids”, “metalforming fluids” or simply as “coolants”, but their function goes far beyond cooling: they transport the chips generated in the process away from the cutting zone, help to prevent rewelding and corrosion, reduce the power required to machine a given material, extend tool life, increase productivity, help to generate chips with specific properties, and are responsible for the cooling and lubrication (BYERS, 2006). They are not only used for machining metals, but can also be used for machining plastics, ceramics, glass and other materials.

These fluids can be classified as pure oils, soluble oils, semisynthetics and synthetics. Soluble oils are in fact O/W emulsions made from mineral or synthetic oils and constitute the largest amount of fluid used in metalworking – they are also the focus of this study. Usually they are sold as concentrated emulsions to be diluted in factory facilities, before filling up the machines. Typical dilution ratios for general machining and grinding are 1%-20% in water, with 5% being the most common dilution level (BYERS, 2006).

The major component of soluble oils is either a naphthenic or a paraffinic oil in usual concentrations of 40%-85%. Naphthenic oils have been predominantly used because of their historically lower cost and ease of emulsification. Vegetable based oils may also be used to prepare a water-dilutable emulsion for metalworking, but they have higher costs, larger tendency to undergo oxidation and hydrolysis reactions, and microbial growth issues. One favorable aspect related to the use of vegetable oils is that they are biodegradable, resulting in less environmental problems involved in waste destination.

Besides the oil and the water, there are several other components in MWF emulsions. The formulations are usually complex in order to ensure that the fluid has all the properties needed for machining, as well as chemical and microbiological stability. Several additives are added to fulfill the purpose of emulsification, corrosion inhibition, lubrication, microbial control, pH buffering, coupling, defoaming, dispersing

and wetting. While more than 300 different components can take part in the formulation of MWF emulsions, a single mixture may contain up to 60 different components (BRINKSMEIER et al., 2009; GLASSE et al., 2012). All additives are chosen according to the process and material type, so there is an infinite number of possible formulations.

In the so-called soluble oils, i.e., MWF emulsions, emulsion stability is the most critical attribute (BYERS, 2006), because losses in stability would affect all other fluid characteristics, like lubricating and cooling. Changes in droplet size, even in its first stages, can decrease the performance of the MWF and thereby cause several problems in machining processes, such as reduction of tool life, corrosion, foam formation and others (EL BARADIE, 1996). Consequently, emulsifiers and other additives are chosen carefully to guarantee the stability of the fluid for as long as possible. As previously mentioned, the droplet size is an important property, because it has large influence on stability (ABISMAÏL et al., 1999; CHANAMAI; MCCLEMENTS, 2000; DICKINSON, 1992). The size of the emulsion particles also determines its appearance: normal “milky” emulsions have particle sizes of approximately 2.0 to 50 μm in mean diameter and micro-like emulsions are translucent solutions and have particle sizes of 0.1 to 2.0 μm [1](BYERS, 2006). However, the droplet size range of an emulsion changes over time.

In machining processes there is a high rate of heat generation and it is estimated that about 10% of the heat produced is removed by the fluid, 80% by the chips, and 10% is dissipated over the tool. With time, this thermal stress can lead to partial degradation of emulsifiers and other additives, favoring microbiological contamination, which also contributes to degradation of emulsion components and its stability reduction, changing the droplet size profile over time (BRINKSMEIER et al., 2009; BYERS, 2006). The increase in droplet size over time is defined as the “aging” of an emulsion. At a certain stage of this destabilization process, the fluid is considered “old” or “aged” and is disposed.

Zimmerman et al. (2003) have found that a particle size shift from 20 to 2000 nm in a commercial MWF resulted in a 440% increase in microbial load during a 48-h

[1] The presented nomenclature for emulsion classification is typical of MWFs. Therefore, other types of emulsions may receive a different classification for different particle size range.

inoculation, leading to the release of acids, lowering pH, and further increasing particle size. As this process continues, it can ultimately lead to oil-water phase separation.

Even though emulsion stability is critical in manufacturing processes and, consequently, monitoring is a key issue, for MWF it is normally carried out only by what is required in local legislations, like periodic measurements of oil concentration (since fluid concentration changes over time due to water evaporation), pH, viscosity and contamination. In this way, changes in fluid characteristics usually are detected only when the destabilization of the emulsion is already significant, leading to problems in machining processes, decreasing tool life, among others. In other occasions, fluids with no loss of performance are disposed because some of these measurements have reached the stipulated limit. In both situations, it has a significant impact on costs for this industry sector. This is why Greeley and Rajagopalan (2004) suggest that the evaluation of emulsion destabilization could be possibly used as a better indicator for monitoring the quality of MWF.

Concerning the droplet size distribution (DSD), Figure 3 shows typical DSD curves of a fresh metalworking fluid, a metalworking fluid in use and an aged metalworking fluid. Due to this change in the distribution pattern, real-time monitoring of the DSD can be used as a more suitable and sensitive method than conventional techniques to detect changes in characteristics of these emulsions. This can be done, for example, by light scattering techniques, as discussed in later chapters.

In this study two types of oil-in-water emulsions were evaluated: rapeseed oil emulsions and commercial metalworking fluids. Rapeseed oil is one of the oils used in some MWF formulations. An emulsion prepared with this oil, emulsifier and water constitutes a relatively simple system to evaluate the proposed technique before applying it in more complex commercial fluids.

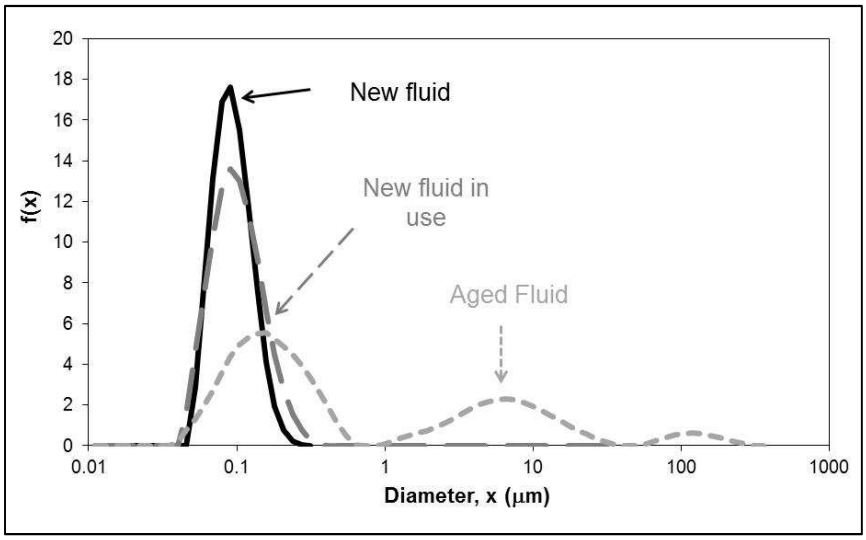

Figure 3: Illustration of changes in droplet size distribution of a typical MWF due to emulsion aging.

3.3. Methods for the Monitoring of Emulsion Destabilization Process

3.3.1. Conventional Methods

An indication of the thermodynamic work involved in creating an emulsion is provided by the area of interface produced. As the emulsion ages, the area of interface decreases (MORRISON; ROSS, 2002), and this decrease means that the size of droplets in the emulsion increase. Thus, emulsion stability (or emulsion destabilization) can be monitored by measuring the change in droplet size.

A direct way to estimate the average droplet size consists of examining the emulsion in a microscope. This involves placing a sample in the viewing area of a microscope, where an image can be captured and image analysis software can be used to extract a size-frequency distribution. The system studied needs to be transparent to light, which may require dilution of the emulsion. In addition, this technique produces a 2D image of the emulsion, which may affect the accuracy of the results. The number of droplets sampled is also small, unless a large number of repeated measurements are made. Confocal microscopy can be used to produce 3D images of emulsion droplets. However, in the absence of refractive index matching of

the continuous and discontinuous phases, this measurement is limited to the top layer of droplets (CHESTNUT, 1997).

Another method used for measuring droplet size is by means of ionic conductivity. The electrical conductivity of an emulsion depends on the concentration of the dispersed oil phase. An unstable emulsion can have a variation in the concentration of the dispersed oil droplets from bottom to top. Therefore, the stability of an emulsion can be checked by comparing the electrical conductivity at the top and the bottom of the container. In a different method, the conductivity measurements can be based on the effect of caused by a droplet passing through a small orifice, on either side of which is an electrical contact. For the case of an O/W emulsion, when the oil droplet passes through the orifice, there is a dip in the conductivity of the material that can be related to the droplet size. These methods can not always be applied to concentrated emulsions and often require an electrolyte to be added to the aqueous phase in order to enhance conductivity contrast, which may affect emulsion stability. In addition, the high shear in the orifice can cause further emulsion droplet break-up (JOHNS; HOLLINGSWORTH, 2007).

Acoustic methods are based on the fact that the speed of sound in an emulsion depends on the concentration of the dispersed oil phase. This speed is measured by transmitting a short pulse of sound and measuring the time required for the pulse to reach a detector opposite to the source. The advantage of determining emulsion stability by this method is that the sample can be measured without dilution, even for relatively concentrated emulsions, typically up to 30% (volume basis), and the container and the sample can be optically opaque. However, large errors can be caused by the presence of tiny gas bubbles. A large number of thermo-physical properties of both the continuous and discontinuous phases are required for the experimental data inversion procedure (COUPLAND; JULIAN MCCLEMENTS, 2001; MCCLEMENTS; COUPLAND, 1996).

Nuclear Magnetic Resonance (NMR) techniques can be used to measure droplet sizes in the range between 50 nm and 20 mm in concentrated emulsions which are opaque and contaminated with other materials (e.g. gas bubbles and suspended solids). NMR is generally able to measure an emulsion DSD via the application of magnetic field gradients; such gradients are also able to image

emulsion macroscopic structure as well as the velocity field of flowing emulsions. They are non-invasive techniques that have the advantage of requiring little sample preparation, but that are not yet established as a standard technique for o/w emulsions despite the fact that the principle of the measurement is not new. This is caused by technical limitations, mainly with respect to the size range of droplets that can be accurately sized, and by the fact that it often requires expensive equipments, making the technique unavailable for routine measurements in a practical sense (HOLLINGSWORTH et al., 2004; JOHNS; HOLLINGSWORTH, 2007; KIOKIAS; RESZKA; BOT, 2004).

Fiber-based Photon Density Wave (PDW) spectroscopy is a new method for the precise measurement of the optical properties of systems where conventional optical analysis is strongly hindered by multiple light scattering resulting from cells, particles or droplets. These properties are usually obtained without any dilution or calibration and are expressed as absorption and reduced scattering coefficients, which are linked to the chemical composition and physical properties of the sample. PDW spectroscopy is based on transport theory for photon propagation in multiple light scattering materials. A PDW is generated if intensity-modulated light is inserted in a strongly light scattering and weakly absorbing material. The amplitude and phase of the wave are characteristically influenced by the absorption and scattering properties of the investigated material. Thus, by quantifying shifts in the properties of the waves as a function of emitter/detector distance and modulation frequency enable the independent determination of absorption and reduced scattering coefficients. The scattering coefficients can be linked to the size of spherical particles by Mie theory and theories for dependent light scattering, with good results obtained in the equivalent diameter range of approximately 50 nm to 500 μm (HASS et al., 2015).

Light scattering is currently the most widely used method to size emulsion droplets and rely on the scattering of light by the droplets, which have a different refractive index from that of the continuous phase. The scattering patterns produced are related to the droplet size. The disadvantage of this technique is that relatively dilute systems are required, typically significantly less than 1% (volume basis) of the dispersed phase, as multiple scattering events may result in inaccurate estimations

of droplet size. The method also requires that the sample be reasonably transparent. The technique is flexible in that it can measure a wide range of droplet sizes, typically between 20nm and 2000 μm (COUPLAND; JULIAN MCCLEMENTS, 2001; JOHNS; HOLLINGSWORTH, 2007; NOVALES et al., 2003).

Although there are many available methods for emulsion stability evaluation, hardly any one of them is used for evaluation of MWF in machining processes. Some of them require expensive equipment; while others are difficult to be implemented under machining process conditions. New fluids have their stability evaluated only by standard methods (ASTM D3707 and ASTM D3709), which involve storage under special conditions for a certain period of time and, after that, phase separation is visually evaluated. In some cases, droplet size is also measured by light scattering methods, but only for new fluids. When in use, the controls are much simpler: only what is required in local legislation and visual changes, including visual phase separation.

3.3.2. Application of UV/VIS Spectroscopy and Optical Models

When a beam of light incides on a particle, the electrons of the particle are excited into oscillatory motion. The excited electric charges re-emit energy in all directions (scattering) and may convert a part of the incident radiation into thermal energy (absorption). The sum of both, scattering and absorption is called extinction. Depending on the chemical species, and on the energy of the incident light, scattering can be elastic or inelastic (like Raman scattering).

Extinction by an individual particle depends on its size, refractive index and shape, and the wavelength of the incident light. For a typical DSD in emulsions, the most suitable optical models for treatment of spectroscopic data are based on the Mie theory (MIE, 1908). This model enables to estimate the light scattering patterns for light sources with given properties interacting with spherical particles of known size and optical properties dispersed in a medium with known optical properties.

Detailed descriptions of the Mie model can be found, for example, in Bohren and Huffman (1983).

Thus, when a suspension of spherical particles of known refractive index is illuminated with light of different wavelengths, the resulting optical spectral extinction contains information that, in principle, can be used to estimate the particle size distribution of the suspended particles.

A number of papers have been published in recent years, showing the application of UV/Vis spectroscopy to obtain information on the DSD and stability of emulsions (e.g. ASSENHAIMER et al., 2014; CELIS; GARCIA-RUBIO, 2002, 2008; DELUHERY; RAJAGOPALAN, 2005; ELICABE; GARCIA-RUBIO, 1990; GLASSE et al., 2013, 2014).

Song et al. (2000) used spectroscopic measurements in a method called *Turbidity Ratio* for comparing stabilities of different emulsions. Deluhery and Rajagopalan (2005) proposed a method for rapid evaluation of MWF stability, by modifying the *Turbidity Ratio* method and establishing a stability coefficient called *Wavelength Exponent* (*z*). This coefficient was also based on the work of Reddy and Fogler (1981) and on the Mie Theory (MIE, 1908), and can be used to estimate stability of emulsions with nearly mono-disperse population of non-absorbing spheres by evaluating time-changes in the measured spectra.

Equation 1 relates the measured turbidity $\tau(\lambda)$ via spectrometry with the optical path length L, the emitted light intensity, I_0, and the received light intensity I, for light with wavelength λ. The term $ln(I_0/I)$ is referred to the absorbance or extinction.

$$\tau(\lambda) = \frac{1}{L} ln\left(\frac{I_0}{I}\right) \quad (1)$$

From the Mie Theory, the turbidity, $\tau(\lambda)$, can be related to the particle size[2] (x) by means of Equation 2, where $f(x)$ is the DSD density function, N_p is the total particle number per unit volume of the system, and Q_{ext} is the extinction efficiency, obtained from the Mie model.

$$\tau(\lambda) = N_p \frac{\pi}{4} \int_0^\infty Q_{ext}(\lambda, x) x^2 f(x) dx \quad (2)$$

The extinction of light by emulsions is the result of light absorption by the continuous and dispersed phases plus scattering. For a nonabsorbing system, the turbidity can be directly related to scattering by the suspended droplets. The extinction efficiency Q_{ext} depends on the particle size parameter and the refractive index of both phases, evaluated at λ. For dilute dispersions consisting of monodisperse spherical nonabsorbing particles significantly smaller than the wavelength of the incident light, scattering is described by the Rayleigh scattering regime (BOHREN, C.F., HUFFMAN, 1983). Under this regime, and if it is assumed that the refractive index ratio does not depend significantly on the wavelength, which usually is a good approximation for such systems, Q_{ext} can be expressed in a simplified form (REDDY; FOGLER, 1981), as shown in Equation 3, where the parameter k'' is the size-independent component that incorporates the properties contained in the expression for the scattering coefficient under the Rayleigh scattering regime, λ is the wavelength and z is the exponent of the wavelength, λ, dependent on particle size and refractive index.

$$Q_{ext} = k'' . \left(\frac{x}{\lambda}\right)^z \quad (3)$$

[2] The size parameter x can be defined as the particle diameter, but some authors prefer to define it as the particle radius, making the proper adjustments in the corresponding equations.

For this same dispersion of monodisperse spherical nonabsorbing particles, Equation 2 can be simplified and rewritten as Equation 4.

$$\tau(\lambda) = N_p \frac{\pi}{4} x^2 k'' \left(\frac{x}{\lambda}\right)^z \quad (4)$$

Under Rayleigh regime, the exponent *z* is equal to 4 (BOHREN, C.F., HUFFMAN, 1983) and decreases as the particle size increases. Note that the only variables in this equation are the size parameter *x*, the exponent *z*, the turbidity *τ(λ)* and the wavelength *λ*. Thus, for a given particle diameter, i.e., if *x* is constant, the wavelength exponent *z* can be expressed as the slope of ln(τ) versus ln(1/λ), as indicated in Equation 5.

$$z = \frac{d\left(ln(\tau)\right)}{d\left(ln\left(\frac{1}{\lambda}\right)\right)} \quad (5)$$

Therefore, under the mentioned assumptions, the wavelength exponent for a given emulsion can be determined from turbidity measurements at different values of λ by fitting Equation 5 to the data.

The same concept can also be applied to other particle systems, e.g. aerosols. However, in the study of the particle size of aerosols, the exponent of the wavelength is called Angstrom Exponent (å) and some additional restrictions are imposed in its definition, like the assumption of a homogeneous atmospheric layer, where the aerosol is distributed uniformly over the ranges of altitudes (ANGSTRÖM, 1930; JUNG; KIM, 2010; SEINFELD; PANDIS, 2006).

Because of its dependency on particle size, Deluhery and Rajagopalan (2005) used the wavelength exponent *z* as an indicator of emulsion stability. In their paper,

the decrease in the exponent over time is related to the destabilization of emulsions by associating this process with the increase in droplet size by coalescence.

This author and the team of researchers in the BRAGECRIM project generalized the application of this method, showing that, although the wavelength exponent is in its definition valid for monodisperse systems only, it can also be used for evaluation of stability of polydisperse systems, with monomodal and even bimodal distributions (GLASSE et al., 2013). In addition to that, we have also shown that there is no need to exclusively evaluate time-changes in the spectra, as proposed by Deluhery and Rajagopalan (2005), since the emulsion stability can also be evaluated by performing instantaneous measurement of turbidity and evaluating the quality of the fitting of the corresponding correlations. Although the use of the wavelength exponent for emulsion stability (or destabilization) evaluation is easy to be implemented, it performs not so well when applied to droplet populations with high polydispersity or above a certain range of droplet diameter. Figure 4 exemplifies the simulated behavior of the wavelength exponent with the increase of droplet diameter for a monodisperse distribution; there is a decrease in *z* values with the increase of the diameter. However, between 1 μm and 10 μm it increases again, with oscillatory behavior. Therefore, it was not chosen in this study as the method of MWF quality evaluation, but it was used as an auxiliary method, with other techniques, for comparison.

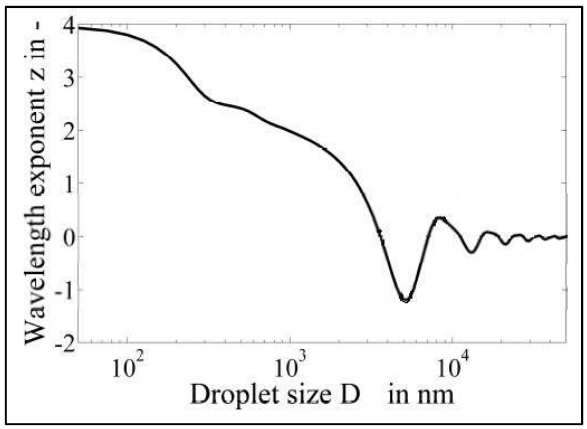

Figure 4: Illustration of the simulated behavior of the wavelength exponent *z* versus the droplet size of a monodispersed distribution (GLASSE, 2015).

In a different approach Celis and Garcia-Rubio (2002, 2008, 2004) and Celis et al. (2008) used spectroscopic data treated by optical models and inversion methods using regularization to obtain information on the DSD of a dispersed system in which the time variation of the extinction pattern can be correlated with properties of the emulsion. Most of these models were also based on the Mie Theory.

Eliçabe and Garcia-Rubio (1990) used an algorithm based on optical models to estimate the DSD in emulsions and dispersions based on the optical properties of its components and on spectroscopic measurements and inversion methods. The method enables the acquisition of real-time data, enabling *in-line* monitoring of DSD in emulsions. In the model proposed by the authors, by defining the function *K* as

$$K(\lambda, x) \equiv \frac{\pi}{4} Q_{ext}(\lambda, x) x^2, \tag{6}$$

then Equation 2 can be identified as a Fredholm integral equation of the first kind, in which *K(λ,x)* is the corresponding Kernel and the numerical solution can be found by using an appropriate discrete model. If the integrand in this equation is discretized into *(n-1)* intervals, the integral can be approximated at a given wavelength λ_i with a sum,

$$\tau_i = \sum_{j=1}^{n} a_{ij} f_j \tag{7}$$

where:

$$\tau_i \equiv \tau(\lambda_i) \ , i = 1, 2, \ldots m \tag{8}$$

$$f_j \equiv f(x_j) \ , j = 1, 2, \ldots n \tag{9}$$

$$a_{ij} = \frac{1}{\Delta x}\sum_{x_{j-1}}^{x_j} K_i(x)x\Delta x - \frac{x_{j-1}}{\Delta x}\sum_{x_{j-1}}^{x_j} K_i(x)\Delta x + \frac{x_{j+1}}{\Delta x}\sum_{x_j}^{x_{j+1}} K_i(x)\Delta x - \frac{1}{\Delta x}\sum_{x_j}^{x_{j+1}} K_i(x)x\Delta x \ ,$$

j = 2, 3, ...n-1 (10)

$$a_{i1} = \frac{x_2}{\Delta x}\sum_{x_1}^{x_2} K_i(x)\Delta x - \frac{1}{\Delta x}\sum_{x_1}^{x_2} K_i(x)x\Delta x \quad (11)$$

$$a_{in} = \frac{1}{\Delta x}\sum_{x_{n-1}}^{x_n} K_i(x)x\Delta x - \frac{x_{n-1}}{\Delta x}\sum_{x_{n-1}}^{x_n} K_i(x)\Delta x \quad (12)$$

The details of the discretization procedure are given in the referenced paper. The Kernels can be calculated by the Mie theory with the corresponding equations presented, for instance, in Bohren and Huffman (1983).

If the extinction is evaluated at m wavelengths, λ_i, *i=1, 2, …m*, then Equation 7 can be written in matrix form as

$$\bar{\tau} = \bar{\bar{A}}\bar{f} \quad (13)$$

where

$$\bar{\tau} = \begin{bmatrix} \tau_1 \\ \dots \\ \tau_m \end{bmatrix}, \ \bar{\bar{A}} = \{a_{ij}\}, \ \bar{f} = \begin{bmatrix} f_1 \\ \dots \\ f_n \end{bmatrix}$$

If quadrature and measurement errors are considered, Equation 13 can be rewritten as the following equation.

$$\bar{\tau} = \bar{\bar{A}}\bar{f} + \varepsilon \quad (14)$$

Direct inversion of Equation 14 to obtain the DSD density function *f* is not possible due to the highly correlated elements, making this matrix singular and, consequently, not invertible. So, for solving this problem, it is necessary to apply some adequate inversion technique.

Eliçabe and Garcia-Rubio (1990) used an inversion algorithm combining regularization techniques and generalized cross-validation for obtaining the DSD from the spectroscopic measurements – further details can be found in the referenced paper. Exploratory studies were carried out using the model proposed by the mentioned authors, but with poor results. These results are presented in the Appendix. Since the implementation of inversion algorithms usually does not provide accurate results for multimodal droplet populations, as the ones that can be found in aged emulsions (Figure 3), and generally the established optical models are not suitable for emulsions with high droplet concentration due to multiple scattering effects, no further investigations were carried out in this topic. Furthermore, Glasse (2015) has intensively studied the application of several inversion methods for retrieving DSD from the spectroscopic measurements and poor results were obtained for real emulsions like rapeseed oil emulsion and MWF; only a specific subset of simulated data produced acceptable results.

In view of the difficulties associated with the application of inversion methods, an alternative approach was adopted in this thesis, applied to emulsions under high droplet concentration, based on pattern recognition techniques. In this case, the data measured by a spectroscopic sensor was associated with the corresponding DSD by means of a previously calibrated multivariate model. More specifically, light extinction spectra as the one illustrated in Figure 5 obtained for oil-in-water emulsions by spectroscopic measurements can be associated with the DSD density function by means of multivariate empirical models.

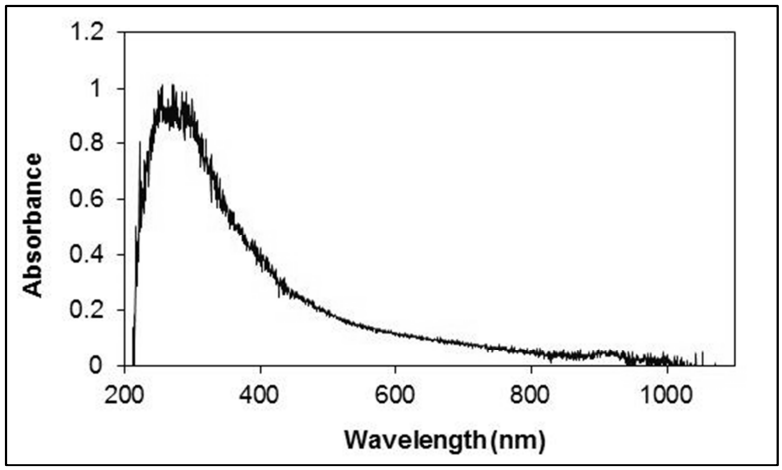

Figure 5: Example of a light extinction spectrum.

Among different techniques that can be applied, non-linear models such as neural networks have been successfully applied in place of light scattering models to estimate particle size distributions in concentrated solid-liquid suspensions (GUARDANI; NASCIMENTO; ONIMARU, 2002; NASCIMENTO; GUARDANI; GIULETTI, 1997) and to predict the stability of suspensions (VIÉ; JOHANNET; AZÉMA, 2014). Thus, neural networks model were adopted in this thesis to associate light extinction spectra with the DSD.

4. MATERIALS AND METHODS

4.1. Materials

The experiments reported in this text were carried out at the University of Bremen by this author with the support of the German team of the BRAGECRIM joint project. In this study rapeseed oil emulsions as well as commercial metalworking fluids were evaluated. Rapeseed oil is one of the possible oils used in metalworking fluids. An emulsion prepared with this oil, emulsifier and water constitutes a simple system to evaluate the technique before applying it to more complex commercial fluids. Rapeseed oil emulsions were prepared in laboratory, with different droplet sizes, thus simulating both new and aged emulsions. For the MWF, aging was simulated in the laboratory by adding $CaCl_2$ to the system in order to disturb the interface layer and thus enable droplet coalescence. For evaluation of MWF aging in machining application, thus simulating a real-case scenario, no further treatment was carried out besides dilution for achieving the recommended concentration.

4.1.1. Rapeseed Oil Emulsions

For the preparation of oil-in-water emulsions a commercial rapeseed oil was used (from the German company Edeka, density 0,92 g/mL, refraction index 1.47). The volume of the samples was 30 mL and the mass fraction of oil in the emulsions ranged from 0.06% to 1.59%. Other substances used in the experiments were an emulsifier, Polysorbate 80 (Tween 80, HLB 15, from Alfa Aesar, 0.07% to 0.42%), and deionized water.

In the emulsification, an ultrasound equipment by Bandelin (Sonopuls HD 200, with deep probe Sonopuls Kegelspitze KE76) was used. The intensity was set at 50% of the maximum for 1 to 5 minutes. The temperature variation was monitored

and used to estimate the dissipated energy in ultrasound emulsification by means of Equation 15, where ρ is the density of the dispersed or continuous phases, φ is the volumetric fraction of the dispersed phase, c_p is the specific heat capacity and ΔT is the measured temperature difference of the fluid before and after the sonication. The initial temperatures of the samples was 20±1°C and typical ΔT of the emulsions were in the range of 10°C to 50ºC, varying according to the sonication time. A total of 105 formulations were prepared by this method.

$$E_v = \frac{P_{diss}}{V_E} = \left(\varphi . \rho_d . c_{p,d} + (1 - \varphi) . \rho_c . c_{p,c}\right) . \Delta T . \quad (15)$$

4.1.2. Metalworking Fluids

4.1.2.1. Artificial Aging

Commercial metalworking fluid, Kompakt YV Neu (oil concentration of approximately 40 wt.%, density 0,96 g/mL, refraction index 1.25), was obtained from Jokisch GmbH and prepared by dilution with deionized water to reach the MWF desired concentrations (3.5 - 5.2 wt.%). Artificial aging, i.e., partial chemical destabilization, was promoted by adding to the emulsions 0 - 0.3 wt.% of $CaCl_2$ ($CaCl_2$.$2H_2O$, purity of 99.5%), from Grüssing GmbH. This salt was chosen because its presence is common in hard water used in machining facilities in Germany, where the tests were conducted, and poses as a problem precisely for accelerating the aging of the MWF diluted with this water. A total of 104 formulations were prepared by this method.

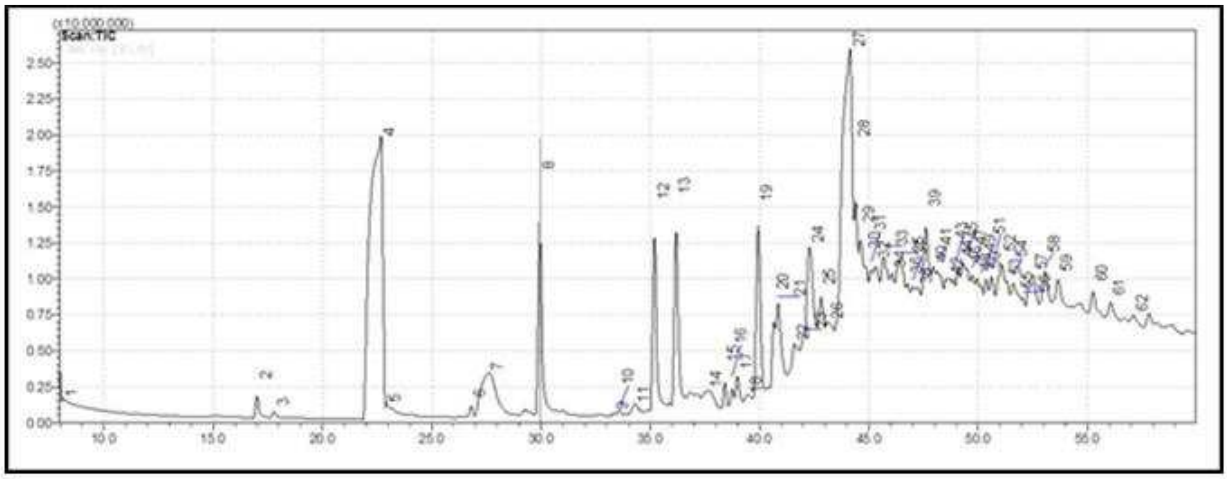

Peak	Retention Time	Identification	Peak	Retention Time	Identification
1	8.1	3-Hexanol	32	45.7	Tetracosane
2	17.0	Acetophenone	33	46.0	Tetratetracontane
3	17.8	Benzenemethanol, .alpha.,.alpha.-dimethyl-	34	46.4	Ethanol, 2-(octadecyloxy)-
			35	46.8	Benzene, (2,3-dimethyldecyl)-
4	22.7	Ethanol, 2-phenoxy-	36	47.0	Triacontane
5	26.8	Silane, trimethyl(2-phenoxyethoxy)-	37	47.2	Undecane, 2-cyclohexyl-
6	27.6	Triethanolamine	38	47.6	Octacosane
7	29.9	1-Dodecanol	39	47.9	Cyclooctacosane
8	33.3	9-Eicosene, (E)-	40	48.1	Hexadecane, 2,6,10,14-tetramethyl-
9	33.6	Pentadecane	41	48.6	Octanamide, N-(2-hydroxyethyl)-
10	34.3	2,8,9-Trioxa-5-aza-1-borabicyclo[3.3.3]undecane	42	48.9	Heneicosane
			43	49.1	Pentatriacontane
11	35.2	1-Tridecanol	44	49.3	Eicosane
12	36.2	Ethanol, 2-(dodecyloxy)-	45	49.5	Heptadecane, 3-methyl-
13	37.6	3.alpha.-(Trimethylsiloxy)cholest-5-ene	46	49.7	1-Eicosanol
14	38.4	Nonadecane	47	49.9	Tetratetracontane
15	38.7	Hexadecane, 2,6,10,14-tetramethyl-	48	50.1	1-Eicosanol
16	39.0	2H-1,4-Benzothiazine, 3,4-dihydro-	49	50.4	Cyclohexane, eicosyl-
17	39.4	Hexadecane, 7-methyl-	50	50.6	Heneicosane
18	39.9	1-Heptadecene	51	51.1	Tetracosane
19	40.7	Heneicosane	52	51.3	Tetratriacontane
20	40.8	Ethanol, 2-(hexadecyloxy)-	53	51.6	Tetrapentacontane, 1,54-dibromo-
21	41.6	Hentriacontane	54	51.8	1-Tricosene
22	42.0	Silane, (hexadecyloxy)trimethyl-	55	52.0	1-Eicosanol
23	42.3	1-Propanol, 3-(octadecyloxy)-	56	52.5	Tetracosane
24	42.8	Heneicosane	57	53.1	Tetracontane
25	43.1	13-Tertadecen-1-ol acetate	58	53.7	Pentatriacontane
26	44.1	cis-9-Tetradecen-1-ol	59	55.3	Hexatriacontane
27	44.4	1-Octadecene	60	56.1	Squalane
28	44.6	1,E-11,Z-13-Hexadecatriene	61	57.1	2,6-Nonadienoic acid, 7-ethyl-9-(3-ethyl-3-methyloxiranyl)-3-methyl-, methyl ester, [2R-
29	44.9	Eicosane			
30	45.1	trans-2-Undecen-1-ol			
31	45.3	1,E-11,Z-13-Heptadecatriene	62	57.8	Heneicosane

Figure 6: Chromatogram of MWF Kompakt YV Neu obtained by Gas Chromatography–Mass Spectrometry analysis in a GCMS-QP2010 chromatograph.

Although it was not possible to have access to fluid formulation, GC-MS (Gas Chromatography–Mass Spectrometry) analysis was performed in a GCMS-QP2010 chromatograph, from Shimadzu, for characterization purposes only. The resulting chromatogram is presented in Figure 6, where is shown over 60 substances used in the formulation of this fluid. The chemistry of metalworking fluids is as diverse as its

applications. Each formulating chemist develops his own fluid formula to meet the performance criteria of the metalworking operation; however additives with function of surfactants, biocides, emulsifiers and waxes are always present in the formulation. Analyzing the main peaks of the chromatogram, it is possible to identify some of these substances and its function in the MWF formulation: 2-phenoxiethanol (biocidal); 3-octadecyloxy-1-propanol, 3-octadecyloxy-1-propanol and cis-9-tetradecen-1-ol (emulsifiers); 1-dodecanol and 2-dodecyloxy-ethanol (surfactants); E-9-eicosene (lubricant); 1-octadecene (dispersant); heneicosane (paraffin wax).

For the experiments aimed at applying the spectroscopic sensor and the neural network model to the monitoring of MWF aging, 0.3 wt.% of $CaCl_2$ was added to metalworking fluid emulsions with concentration of 4 wt.% and the aging was monitored over time.

4.1.2.2. Machining Application

In the last stage of the experiments, a campaign was carried out aimed at obtaining data as near as possible of a real case scenario. In this campaign, a total of 7 different commercial metalworking fluids (Acmosit 65-66, from Acmos Chemie KG; Grindex 10, from Blaser Swisslube; Unimet 230 BF, from Oemeta; Rhenus r.meta TS 42, Rhenus XY 121 HM and Rhenus R-Flex, from Rhenus Lub; Zubora 10 M Extra, from Zeller-Gmelin) were monitored for a period of 13 months while they were used in 3 different machines in a machining facility at the University of Bremen (a vertical turning machine, Index C200-4D, a precision milling machine, Sauer 20 Linear, and a cylindrical grinding machine, Overbeck 600 R-CNC). All these MWF samples are oil-in-water emulsions, made from synthetic oils and several additives to fulfill the purpose of emulsification, corrosion inhibition, microbial control, among others. Each emulsion was previously diluted to the recommended concentration for each corresponding application. Once the fluid loses water due to evaporation during the process, some adjustments in concentration where carried out over time.

4.2. Measurements

4.2.1. Spectroscopic Measurements

Light extinction spectra measurements were performed in all samples with a UV-Vis-NIR spectrometer, model HR2000+ES, from OceanOptics, with light source DH 2000-BAL, spectral resolution of 0.5 nm, and a dip probe with 6.35 mm diameter, 127 mm of length and optical length of 2 mm, which enables *in-line* and real-time monitoring (Figure 7). The dark noise and the reference signal were recorded prior to measurement and subtracted from the measurement signal. Prior to the measurements, the light source was warmed up for 30 min to reach full intensity. Absorbance was measured for light wavelength in the range 200–1000 nm by probe immersion in the samples.

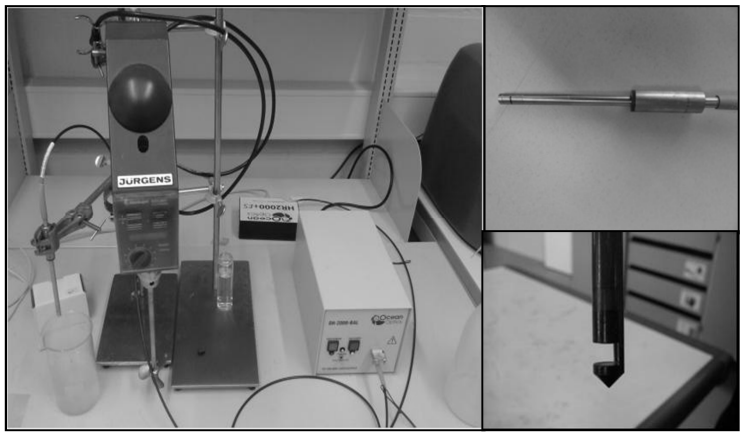

Figure 7: Spectrometer with deep probe for *in-line* monitoring. Images at the right: detail of deep probe.

4.2.2. Reference Measurements: Droplet Size Distribution

The evaluation of the droplet size distribution for neural network calibration was based on measurements with a Malvern Mastersizer 2000 laser diffractometer, with particle size detection range from 0.02 to 2000 µm. The measurements of the emulsion samples were performed using the universal model for spherical particles in the measurement suite and the corresponding refractive index of each phase of the

emulsion. For each sample the mean values of the DSD from three consecutive runs carried out over 35s were recorded.

Particle size analysis with Malvern Mastersizer is a well-established technique, but the samples need to be diluted prior to the analysis in order to prevent multiple scattering. Emulsion stability can be affected by dilution, although MWF formulations should not be affected by that, especially considering that the manufacture recommendation is for diluting it, within a certain range of concentration, before use. However, in order to confirm that the dilution of the samples for analyzing the DSD does not affect the result and can be trusted, a sample of the MWF Kompakt YV Neu was left in the Malvern Mastersizer for 1h and the DSD was recorded in 1 min intervals. Since no change in droplet size was observed during 1h (Figure 8), it is safe to say that the dilution in the Malvern Mastersizer does not affect the stability of the sample and this technique can be used for analyzing the DSD of MWF.

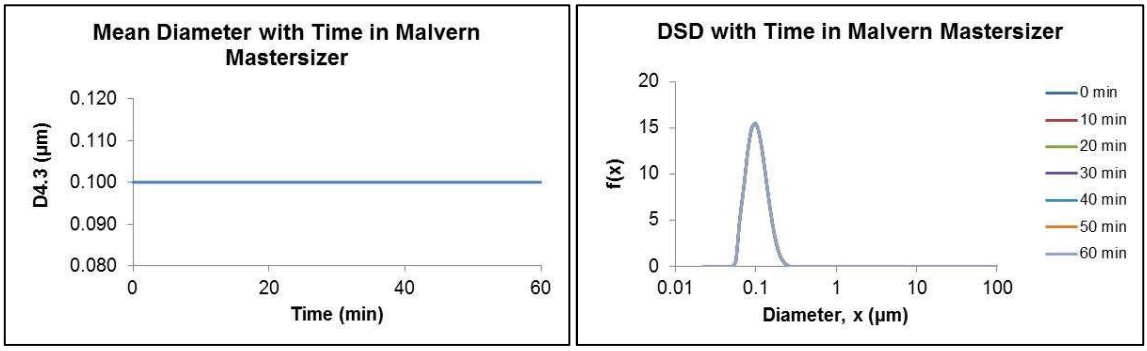

Figure 8: Evolution of particle size with time for MWF Kompakt YV Neu.

4.2.3. Wavelength Exponent

As previously mentioned, the extinction of light by emulsions is the result of light absorption by the continuous and dispersed phases plus scattering. For a nonabsorbing system, the turbidity can be directly related to scattering by the suspended droplets and, therefore, can be directly related to the measured absorbance of the emulsion. So, the exponent *z* can be found by measuring the

absorbance (*Abs*) of the emulsion at different wavelengths and determining the slope of the *ln(Abs)* versus *ln(1/λ)* curves in a selected wavelength range (Figure 9).

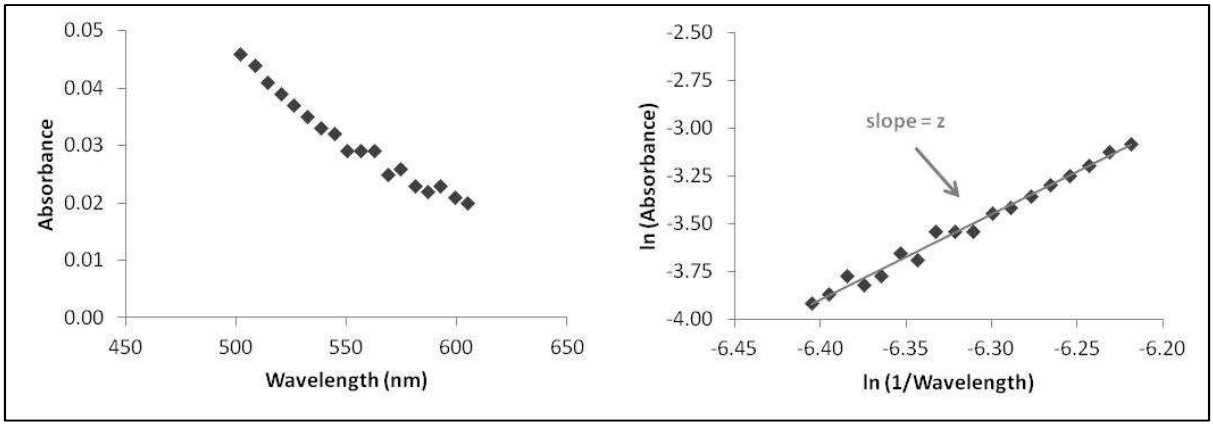

Figure 9: Illustration of wavelength exponent calculation.

However, in order to use the wavelength exponent, it is necessary to assume that there is no absorption in the selected wavelength range and that all the measured absorbance is due to scattering. So, in order to choose the best range for these evaluations, it was obtained from the supplier of this MWF the absorbance spectrum of its main components, in different concentrations (Figure 10 and Figure 11). Not much information was provided about these measurements, but it was possible to see the range of absorption of the main chemical species of the fluid prior to emulsification, i.e., without interference of droplets scattering in absorbance measurements. Based on this information, it is a good approximation to defined that the best range to assume absence of absorption by the emulsion is from 400-700 nm. Thus, for the calculation of exponent *z*, it was chosen a 100nm interval in this range, from 500 to 600nm, and all the fittings were carried out for this wavelength range.

In the evaluation of MWF in machining application, the linear coefficient of the fittings was also included in the collected data set. Although this coefficient itself does not have a physical meaning, it is related to the concentration and optical properties of the analyzed samples. Since it was not possible to have access to the optical properties of the MWF in this part of the study, the linear coefficient of the fittings was

used in this evaluation to compensate this lack of information and to help differentiate the data for different fluids.

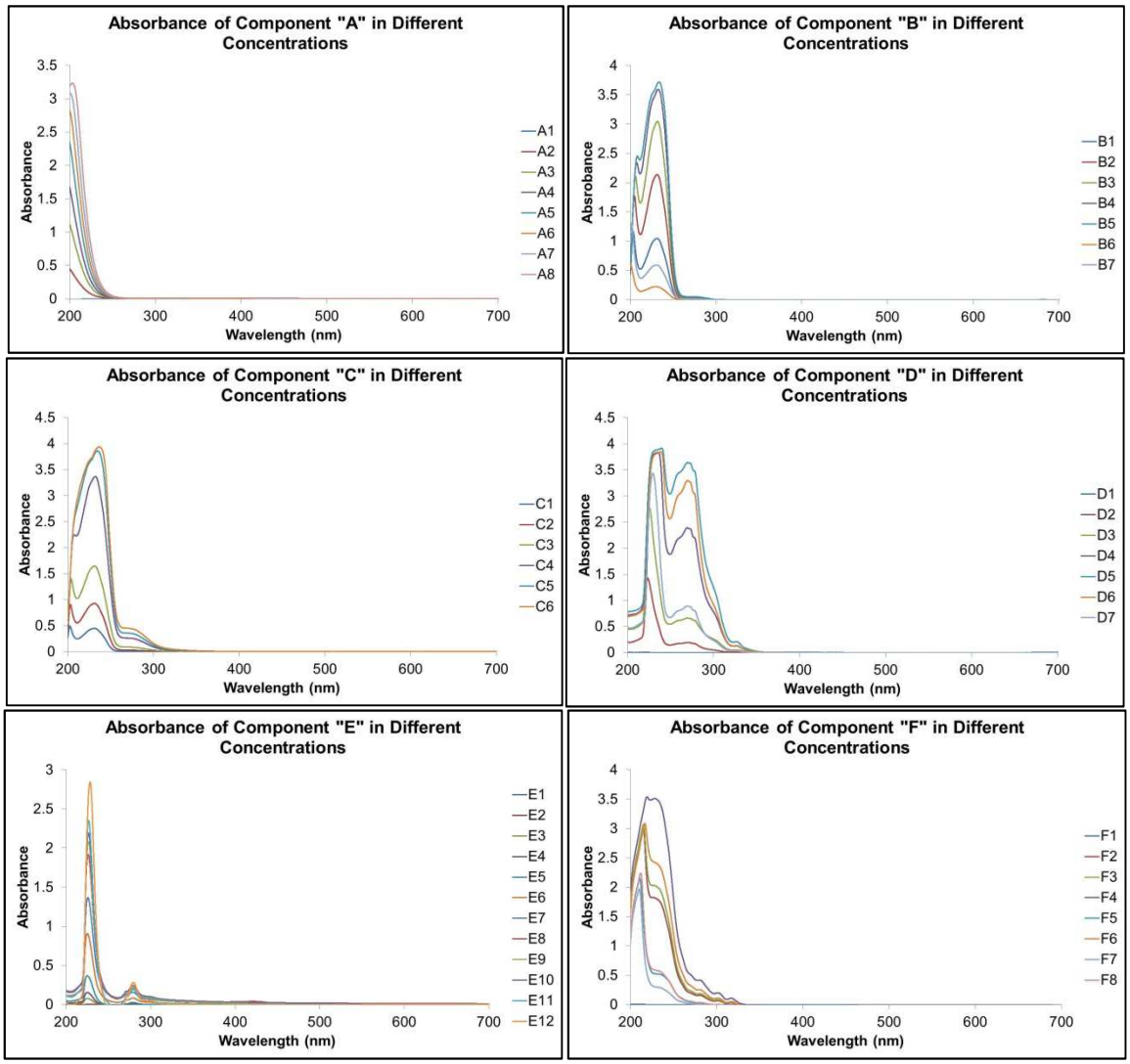

Figure 10: Absorbance spectrum of main components of MWF Kompakt YV Neu, in different concentrations (for components “A” to “F”).

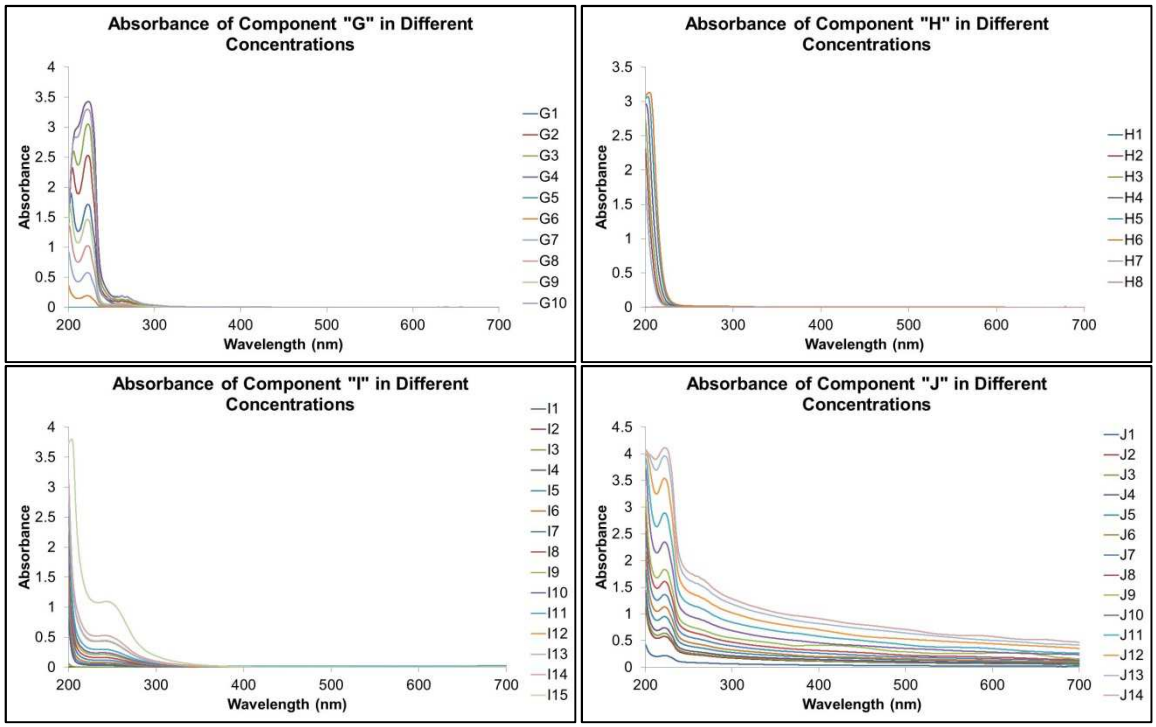

Figure 11: Absorbance spectrum of main components of MWF Kompakt YV Neu, in different concentrations (for components “G” to “J”).

4.2.4. Application to Long Term Monitoring of MWF Destabilization

For the evaluation of MWF in machining applications, periodic physical-chemistry and microbiological analysis of the fluid (pH, oil concentration, nitrite content and microbiological contamination by ATP method, according to German regulation requirements in norm VDI 3397) were performed over time as a routine of the facility’s employers, with supervision of the project team. Samples were collected weekly during 13 months and the measurements were performed by the machining operators in the laboratory facility. MWF also receive a classification in each analysis according to the machine operator perception concerning the performance of the MWF at the time when the samples were collected for analysis. The MWF samples were thus classified according to their “status” in three classes: 1, or green (no signs of deterioration), 2, or yellow (initial signs of deterioration), and 3, or red (high degree of deterioration). Although the machine operator perception of quality not always receives this qualitative classification in the facilities, generally it is one of the determinant factors for deciding when a MWF can be considered aged and has to be

disposed and replaced. Spectroscopic measurements and analysis of DSD of all collected samples were performed by the German team of the project, as previously described.

4.3. Characterization Methods

4.3.1. Pattern Recognition Techniques: Artificial Neural Networks

An Artificial Neural Network (ANN) is a non-linear computational model based on the structure and function of biological Neural Networks. Like human brain but in a simpler level, ANN has the ability to recognize patterns and behaviors hidden in a data set organized as inputs and outputs and to generalize it for similar observations. Because of that it is said that these networks have the ability to “learn” about the behavior of a given system and then simulate it.

The basic unit of an ANN is the neuron, an information-processing unit that is fundamental to its operation. The manner in which these neurons are structured is intimately linked with the learning algorithm used to train the network. In general there are three different classes of network architecture: Single Layer Feedforward Networks, Multilayer Feedforward Networks and Recurrent Networks (HAYKIN, 1999). In the first class, all the neurons are organized in the form of a layer and there is an input layer of source nodes that projects onto an output layer of neurons, but not vice-versa. The second type distinguishes itself from the first by the presence of one or more hidden layers, whose computation nodes are correspondingly called hidden neurons. By adding one or more hidden layers, the network is able to extract higher order statistics. The last class of networks architecture distinguishes itself from Feedforward Neural Networks in that it has at least one feedback loop. In this study, only Multilayer Feedforward Networks were used. More specifically, a three layer feedforward network was fit to the experimental data.

Neural networks have been applied to several systems of high complexity in different fields where phenomenological modeling is not suitable or is difficult to be implemented. In the field of this study, some examples of previous applications of the method to retrieve particle size distribution from optical measurement methods include the study by Guardani et al. (2002), who used ANN models to replace the optical model and to obtain particle size distribution of three different suspensions from forward light scattering measurements. The advantage is the possibility of analysis of suspensions with higher concentrations, which cannot be accurately measured by optical models due to multiple scattering phenomena.

Berdnik and Loiko (2006) and Berdnik et al. (2006) used ANN for retrieving size and refractive index of spherical particles by angular dependence of scattered light in scanning flow cytometry as an easier way for obtaining this information than with the application of other methods involving the calculation of complex integrals or trial-and-error methods.

In this thesis, multivariate models based on neural networks are used as an alternative to optical models to associate spectroscopic measurements with DSD. Thus, with the calibration of multivariate models, an association is established between the extinction pattern and the DSD of a given emulsion system. This approach provides a way to estimate the DSD in systems with high droplet concentration, in which multiple scattering does not enable the application of optical light scattering models.

Figure 12 shows an illustration of a three-layer feedforward neural network, like the ones used in this study. To neuron i (i=1,2,...,q), located in layer j (j=1,2,3) of a network, the received information S_j is a weighted sum of the inputs X_i by the weights $W_{i,j}$ (Equation 16). The last input, with value equal to 1, is a bias, which has the effect of increasing or lowering the net input of the activation function, depending on whether it is positive or negative, respectively. In this way, bias neurons may help the neural network to learn patterns, by allowing it to output a value of zero even when the input is near one.

$$S_j = \sum_{i=1}^{q} W_{i,j} X_i + W_{q+1,j} \quad (16)$$

The output from neuron *j* is a response function $O_j = f(S_j)$, in which $f(S_j)$ can consist of different mathematical forms. In most cases a sigmoidal function is used (Equation 17).

$$f(S_j) = \frac{1}{1-e^{-S_j}} \quad (17)$$

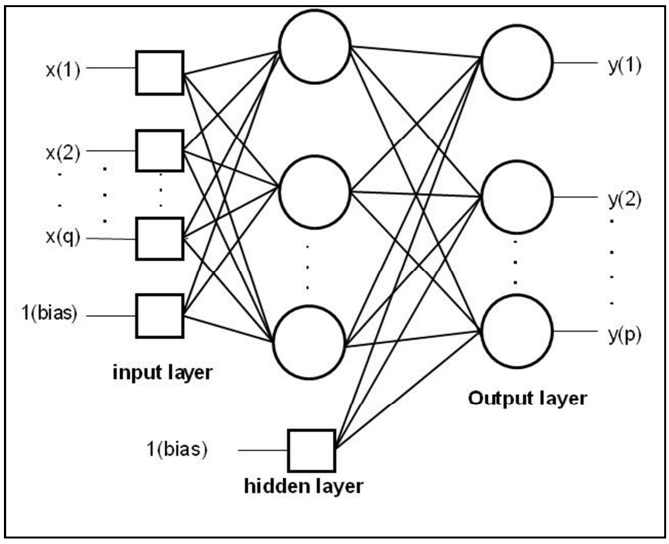

Figure 12: Illustration of a feed-forward neural network (ASSENHAIMER et al., 2014).

The fitting of a neural network consists of two steps: training, consisting of the adjustment of the parameters, or weights, for a given neural network structure, and validation. In the first part, known values of inputs and outputs are presented to the network and the set of weights is selected so that a minimum squared error *E* between calculated and observed values of the outputs is achieved. The squared error *E* is defined in Equation 18, where y_k is the experimental (observed) value and O_k is the calculated value of output *k*. In this thesis the fitting was based on the backpropagation algorithm (RUMMELHART, D., MCCLELLAND, 1986).

$$E = \sum_{m=1}^{r} \sum_{k=1}^{p} \left(y_k^{(m)} - O_k^{(m)} \right)^2 \quad (18)$$

The second part of the fitting consists of the validation of the model. The calculated outputs are compared with experimental values of another set of observations, which have not been used in the training step, in order to check if the model is able to predict the desired results adequately.

The computational programs used in this work for neural network model fitting, validation and simulations were developed in the Chemical Engineering Department, Escola Politécnica, Universidade de São Paulo (USP).

4.3.1.1. Architecture of the ANN

The architecture of the network is very important to define its capacity of convergence and generalization. The choice of a suitable architecture, with an adequate number of parameters, is the main factor for the success of the data training.

The number of neurons in the input and output layers is determined by the problem structure. The difficulty is to find the ideal number of neurons in the hidden layer. This number, sometimes, may be determined by rules as in Loesch and Sari (TÁPIA, 2000, apud LOESCH and SARI, 1996), where "*the number of neurons in the hidden layer should be equal to the geometric mean of the number of inputs and outputs*", or by the rule in Eberhart (TÁPIA, 2000, apud EBERHART, 1999), where "*the number of neurons in the hidden layer should be equal to the square root of the sum of inputs and outputs*". Although these and other rules are sometimes suitable for solving specific problems, they have not been proven to be reliable in all applications. Thus, in most cases these rules can be adopted as a first estimation of the number of neurons in the intermediary layer of a feed-forward neural network, but

the most adequate number must be based on fittings carried out for different values of this parameter.

The higher is the number of neurons in the hidden layers, more complex will be the network and large networks normally require large amounts of training data, which may not be available. An analysis of the degree of freedom of an ANN suggests that the number of observations available for training the network should be higher than the number of parameters in the network, otherwise, significant overfitting and poor generalization will be evident, which means that the error on the training set is driven to a very small value, but when new data are presented to the network the error is large; the network was successfully fitted to the data set, but it is unable to generalize the fitted model for new data.

However, this is not necessarily true. Larger networks often result in lower generalization error, even with a training set smaller that may be expected (LAWRENCE; GILES; TSOI, 1997). The rule that states that "*the number of parameters in the network should be (significantly) less than the number of examples*" aim to prevent overfitting, but is unreliable as the optimal number of parameters is likely to depend on other factors, e.g. the quality of the solution found, the distribution of the data points, the amount of noise, and the nature of the function being approximated. Specific rules, such as the above, are not commonly accurate. In fact, larger networks may generalize well and better generalization is often possible because they have less difficulty to find with local minima (LAWRENCE; GILES; TSOI, 1997). This is also supported by the work of Bartlett (LAWRENCE; GILES; TSOI, 1997, apud BARTLETT, 1996), who also found that neural networks often perform successfully with training sets that are considerably smaller than the number of network parameters, because it may be difficult to approximate the training data with smaller networks. Nevertheless, some precautions may be taken to confirm the absence of overfitting, like the removal of 20% to 30% of the data, which is not used in the training step of the network, to validate the fitting of the model. This step may be incorporated in the algorithm used for the fitting of the ANN in order to minimize simultaneously the error of the testing set and the validation set. If good results are found in the validation set, the hypothesis of overfitting can be discarded.

In this study, the most adequate number of neurons in the hidden layer was determined based on fittings carried out for different values of this parameter and 30% of all data were used exclusively for the validation of the model, as explained in Chapter 4.3.1.

4.3.1.2. Holdback Input Randomization Method (HIPR method)

As shown in Figure 12, the structure of ANN models is characterized by the fact that the information provided by each input is distributed in a weighed among all neurons of successive layers. Thus, no model parameter is individually connected to a specific input variable, which hinders the evaluation of the relative importance of the ANN input variables. In view of this characteristic of ANN models, Kemp, Zaradic and Hansen (2007) proposed a method based on a sequential randomized perturbances in the input variables to determine the relative proportion to which each input variable contributes to the predictive ability of the ANN model in the evaluated range. This method was named by the authors Holdback Input Randomization Method, or HIPR method.

In the HIPR method, the data are divided into a learning set, a validation set and a test set following the ratio 3:1:1. The ANN is adjusted with data from the learning set in the conventional way, and afterwards the error in relation to the validation set is computed. The test set is used to calculate the error of the model and thus to estimate the overall training success of the net. After the model is adjusted and the error of the model is evaluated, then, according to the HIPR method, each individual input variable is randomly varied within its range of validity and sequentially, and the mean squared error (MSE) is computed for all random values of each individual input variable. The contribution of each input variable to the predictive ability of the ANN model can be estimated based on how much it affects the MSE, compared to the minimum MSE value obtained in the model fitting step. The procedure can be repeated a number of times in order to increase the representativity of the test. The evaluation of the relative importance of each input

variable is thus based on the effect of the random perturbations on the MSE. If a given input variable does not significantly contribute to the fitted model of the ANN, then the MSE of the randomized data set will be close to the MSE relative to the original data set. If a parameter contributes strongly to the fitted model of the ANN, then the MSE of the data set in which this parameter is randomized will be larger than the MSE relative to the original data set. This is a robust, simple, general procedure for interpreting complex systems based on model performance, and the results can be obtained without making any assumptions regarding the architecture of the ANN model used.

An executable version of the algorithm developed by the author of this method, using the C++ programming language, is available at http://www.bio.upenn.edu/faculty/dunham/hipr/PennNN.zip. The evaluation of the ANN models fitted in this study by the HIPR method was based on a computer program in FORTRAN developed at the Department of Chemical Engineering, Escola Politécnica, USP. More details about this method can be found in Kemp, Zaradic and Hansen (2007).

4.3.2. Classification Techniques: Discriminant Analysis

Discrimination is a multivariate technique where distinct sets of observations are separated and allocated in previously defined groups. As a separative procedure, it is often employed in order to investigate observed differences when correlations between observations from the data set are not well understood (JOHNSON; WICHERN, 2007). The goal of this technique is to find “discriminants”, which consist of quantitative criteria whose numerical values are used to separate variables or observations as much as possible and, sometimes, to establish a rule that can be used to optimally assign new observations to the labeled classes or groups. This “discrimination” can be carried out by several different techniques, like the Test of Hypothesis, the Linear Discriminant, the Quadratic Discriminant, the Fisher

Discriminant, among others. In this study, only linear and quadratic discriminant were evaluated.

Considering two populations of observations x_i, i =1,...n, with *a priori* probabilities of occurrence p_1 and p_2, where $p_1 + p_2 = 1$, and considering that the probability density functions *f1(x)* e *f2(x)* are as illustrated in Figure 13, then the probability of a given observation x_0, belonging to a group m, be designated to a given group g, $P(g|m)$, is expressed as Equation 19.

$$P(g|m) = P(x_0 \in R_g|G_m) = \int_{R_g} f_m(x)dx \quad (19)$$

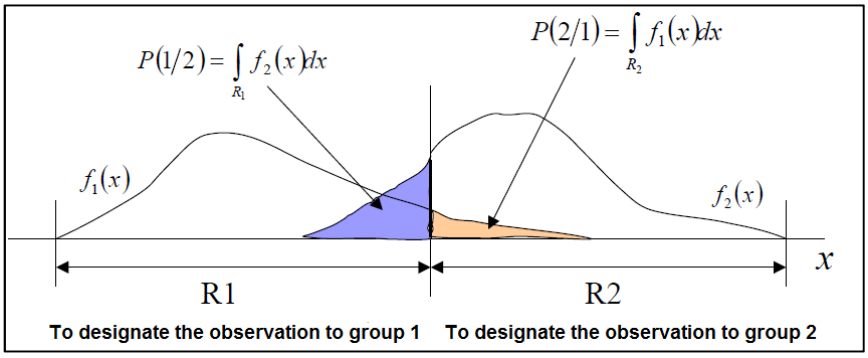

Figure 13: Illustration of the distribution of observations between the groups (GUARDANI; NASCIMENTO, 2007).

Thus, the probability of designating x_0 to the wrong group is given by

$$P(2|1) = P(x_0 \in R_2|G_1) = \int_{R_2} f_1(x)dx \quad (20)$$

$$P(1|2) = P(x_0 \in R_1|G_2) = \int_{R_1} f_2(x)dx \quad (21)$$

and the probability of designating x_0 to the correct group is

$$P(1|1) = P(x_0 \in R_1|G_1) = \int_{R_1} f_1(x)dx \quad (22)$$

$$P(2|2) = P(x_0 \in R_2|G_2) = \int_{R_2} f_2(x)dx \quad (23)$$

Therefore, these probabilities can be expressed as

$$P(x_0 \in R_1|G_1) = P(1|1).p(1) \quad (24)$$

$$P(x_0 \in R_2|G_2) = P(2|2).p(2) \quad (25)$$

when the observations are allocated in the correct group, and

$$P(x_0 \in R_2|G_1) = P(2|1).p(1) \quad (26)$$

$$P(x_0 \in R_1|G_2) = P(1|2).p(2) \quad (27)$$

when the observations are allocated in the wrong group.

"Costs" or "weights" may be assigned for misclassification, as shown in Table 1, and the Expected Cost of Misclassification, ECM, is defined as shown in Equation 28.

Table 1: Cost table for misclassification of the observations (GUARDANI; NASCIMENTO, 2007).

	Classification	
Group	G1	G2
G1	0	C(2|1)
G2	C(1|2)	0

$$ECM = C(2|1).P(2|1).p1 + C(1|2).P(1|2).p2 \quad (28)$$

The algorithms for classification are based on the minimization of this function, which may be rewritten as Equation 29,

$$ECM = C(2|1).p1 \int_{R_2} f_1(x)dx + C(1|2).p2 \int_{R_1} f_2(x)dx \quad (29)$$

where

$$\int_{R_1} f_1(x)dx + \int_{R_2} f_1(x)dx = \int_{R_1+R_2} f_1(x)dx = 1 \quad (30)$$

Thus,

$$ECM = C(2|1).p_1 \left[1 - \int_{R_1} f_1(x)dx\right] + C(1|2).p_2 \int_{R_1} f_2(x)dx \quad (31)$$

or

$$ECM = \int_{R_1} [C(1|2).p_2.f_2(x) - C(2|1).p_1.f_1(x)]dx + C(2|1).p_1 \quad (32)$$

The last term of the previous equation is constant and positive, so the function ECM only decreases in the region R_1 if the integrand is negative. Therefore, it is possible to establish the following criterion of classification: to designate x_0 to R_1 if Equation 33 is true.

$$\frac{f_1(x_0)}{f_2(x_0)} \geq \frac{C(1|2)}{C(2|1)} \cdot \frac{p_2}{p_1} \tag{33}$$

For R_2 it is possible to make the same assumptions and to obtain the following criterion of classification: to designate x_0 to R_2 if Equation 34 is true.

$$\frac{f_1(x_0)}{f_2(x_0)} < \frac{C(1|2)}{C(2|1)} \cdot \frac{p_2}{p_1} \tag{34}$$

Now considering *G* groups of multivariate observations (with dimension *p*), the probability density function corresponding to a normal distribution of observations in a given group *g* is expressed by Equation 35, where *g=1, 2, …G*.

$$f_g(x) = \frac{1}{(2\pi)^{p/2} |\sum|_g^{1/2}} exp\left[-\frac{1}{2}\left(\mathrm{x} - \mu_g\right)^T \sum_g{}^{-1} \left(\mathrm{x} - \mu_g\right)\right] \tag{35}$$

Considering that the covariance matrices of the groups are not the same, i.e., each group has its own covariance matrix, and that the cost of designating an observation to the correct group, *C(g|g)*, is equal to zero; and the cost of misclassification, *C(g|m)*, is equal to 1, then it is possible to define a criterion for allocation of observations similar to the previous criterion, based on the product $p_g.f_g(x)$ for each group. For this purpose, the linearized form of the normal probability

density function is more conveniently used, so that Equation 35 can be rewritten as Equation 36, where *g=1, 2, …G*.

$$ln[p_g f_g(x)] = ln(p_g) - \left(\frac{p}{2}\right) ln(2\pi) - \frac{1}{2} ln|\sum_g| - \frac{1}{2}(\mathrm{x} - \mu_g)^T \sum_g{}^{-1} (\mathrm{x} - \mu_g) \quad (36)$$

Therefore, a given observation, x_0, is allocated in a group that maximizes the value of this expression. Since the second term of the right side of the equation is the same for all groups, the comparison between groups is based on the remaining terms, and the so-called *Quadratic Discriminant* is thereby defined and expressed as Equation 37.

$$discr.Q_g = ln(p_g) - \frac{1}{2} ln|\sum_g| - \frac{1}{2}(\mathrm{x} - \mu_g)^T \sum_g{}^{-1} (\mathrm{x} - \mu_g) \quad (37)$$

According to this criterion, an observation x_0 is allocated to the group *g* if *discr.*Q_g is maximum for this group. The discriminant is denominated quadratic due to the quadratic statistical distance, present in the equation. A variation of the Quadratic Discriminant Analysis (QDA) is the Linear Discriminant Analysis (LDA). In LDA, the covariance matrices are assumed to be equal for all groups. Thereby, Equation 37 can be rewritten for expressing the linear discriminant as shown in Equation 38, which includes only the terms that depend on each group.

$$discr.Lin_g = ln(p_g) + \mu_g{}^T \Sigma^{-1} \mathrm{x} - \frac{1}{2} \mu_g{}^T \Sigma^{-1} \mu_g \quad (38)$$

More detailed information about discriminant analysis can be found in Johnson and Wichern (2007).

In this study, LDA and QDA were applied to the data using the statistical software Minitab, for convenience. All evaluations were based on cross-validation, which is a technique based on the exclusion of one or more observations from the data set used to estimate the discriminant and then test the criterion with these excluded observations. In the present thesis the cross-validation routine consisted of omitting one observation at a time, recalculating the classification function using the remaining data, and then classifying the omitted observation.

5. RESULTS

5.1. Treatment of the Spectral Results

Spectroscopic measurements of the samples resulted in spectra like the one illustrated in Figure 5, showing absorbance as a function of the wavelength. Due to the large resolution of the spectrometer, a large number of wavelengths is present in the data base. Since the absorbance values for close wavelength values are highly correlated, a preliminary treatment was necessary in order to reduce the number of input variables in the model. This consisted of applying a principal component analysis (PCA) to the data.

This analysis is able to identify implicit correlations among groups of variables, and enables to detect the most important variables that affect the variance of the experimental data. PCA consists of transforming the original variables of a multivariate system into non-correlated or independent new variables (components) that are linear combinations of the original variables. Thus, from a number of n original variables x_j (j = 1,…,n) a smaller number of p non-correlated components e_i (i = 1,…,p) can be obtained, which are linear combinations of the original variables with the general form: $e_i = w_{i1}x_1 + ...w_{ij}x_j + ...w_{in}x_n$, in which w_{ij} are the weights or loadings of variable x_j on the component e_i and are computed so that each component represents the maximum of the system variability in decreasing order. The technique is used to reduce the number of variables involved in an analysis, and to detect underlying relationships among groups of variables. Detailed descriptions of the method are presented in books on multivariate statistical analysis (e. g., JOHNSON; WICHERN, 2002). The weights correspond to the eigenvectors of the covariance matrix of the original variables. Components are ordered according to the decreasing value of variances, which correspond to the eigenvalues of the covariance matrix. In this thesis numerical differences among variables were eliminated by adopting standardized variables (zero mean, and scaled by the standard deviation). The interpretation of the results was based on the absolute value of the weights w_{ij},

(JOLLIFFE, 1986) for each component, in decreasing order of contribution to the variance.

Figures 14 and 15 show the result of the principal component analysis applied to rapeseed oil emulsions and artificially aged metalworking fluids, respectively. In both analyses, only three components represent 99% of the total variance of the system. Therefore, it was possible to reduce the set of input variables from the spectra to the corresponded measured absorbance to only three most important wavelengths, presented in Table 2. As expected the wavelengths selected for rapeseed oil emulsions are near the ones selected for the artificially aged MWF. The small differences between them are probably due to differences in the optical properties, since there is no significant light absorption in the selected wavelength range, as previously showed in chapter 4.2.

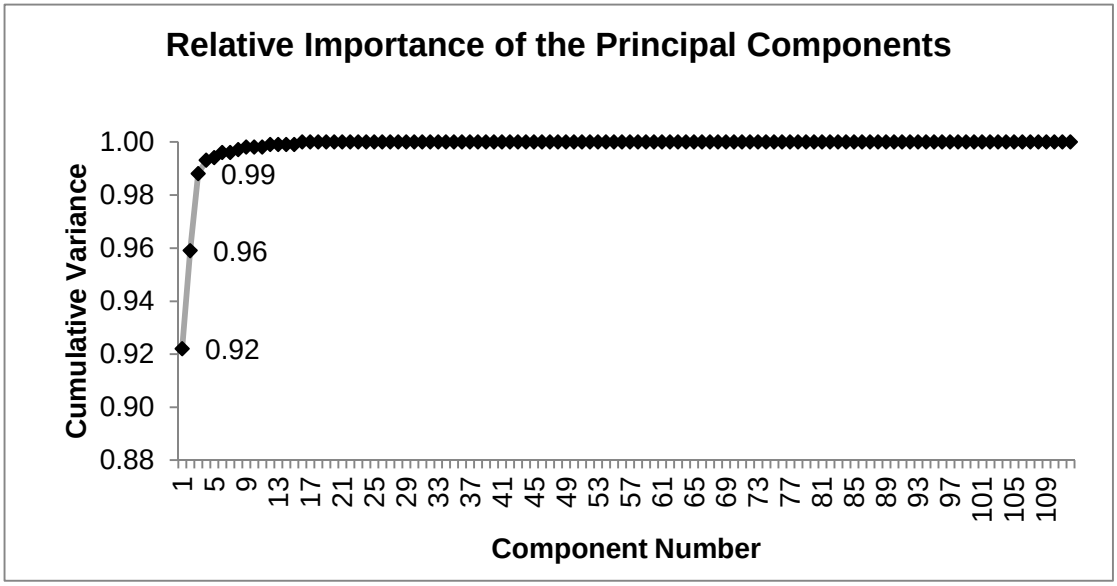

Figure 14: Relative importance of the principal components in the PCA of the rapeseed oil.

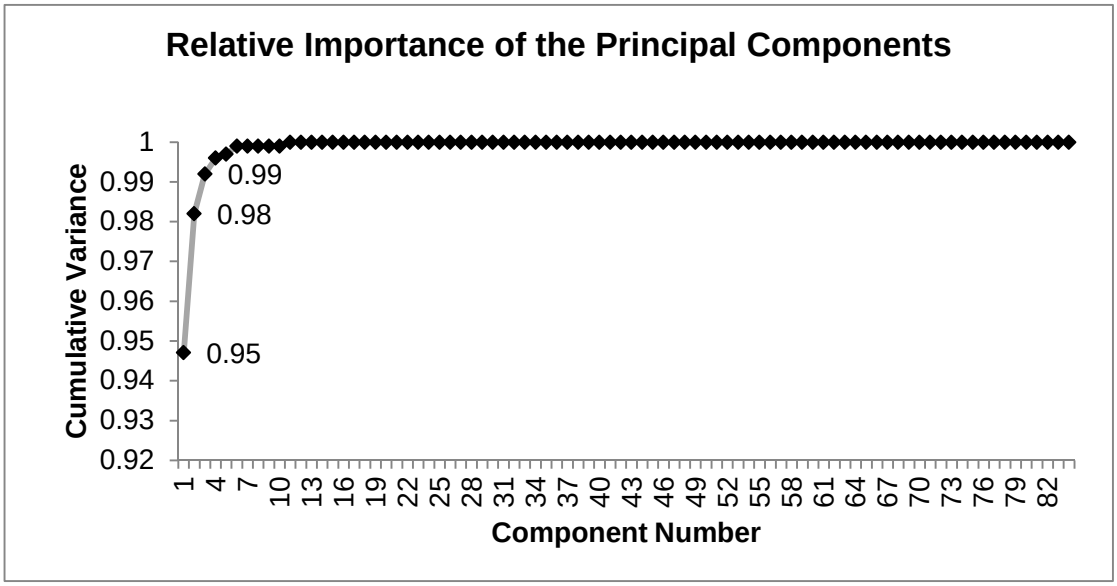

Figure 15: Relative importance of the principal components in the PCA of the metalworking fluid.

Table 2: Wavelengths selected by PCA for each type of emulsion.

Emulsion	Selected Wavelengths		
Rapeseed Oil	452 nm	662 nm	943 nm
Artificially Aged Metalworking Fluid	460 nm	695 nm	943 nm

Although there are other variables that can be used to characterize the MWF emulsions, like variables related to the composition of the emulsions, they were not included in the PCA analysis, because this preliminary treatment was aimed specifically at reducing the dimension of the spectroscopic data. The importance of non-spectroscopic variables for the fitting of the models was determined through manual experimentation.

5.2. Descriptive Statistic of the Collected Data Sets

As described in Chapter 4, two types of emulsions were evaluated, generating two data sets: one for rapeseed oil emulsions, which constitutes a simple system to evaluate the technique before applying it to more complex commercial fluids, and one for artificially aged MWF. All the samples were prepared according to the

procedure described in the previous chapter. Figure 16 shows the distribution of the measured volumetric mean diameter of all the samples of both data sets.

The rapeseed oil emulsions, which were prepared in laboratory, have significantly higher droplet size than commercial MWF, even after artificial aging. MWF formulations contain a combination of emulsifiers and other ingredients to achieve the desired droplet size and stability. Since rapeseed oil emulsions were prepared with much simpler formulations, it was not possible to achieve the same range of mean diameters. Although the higher frequency is in the range of smaller mean diameters, as desired, the presence of rapeseed oil samples with larger mean diameters represents a limitation for the application of the method of the wavelength exponent in the evaluation of the emulsions. Thus, this method was applied only in the evaluation of artificially aged MWFs.

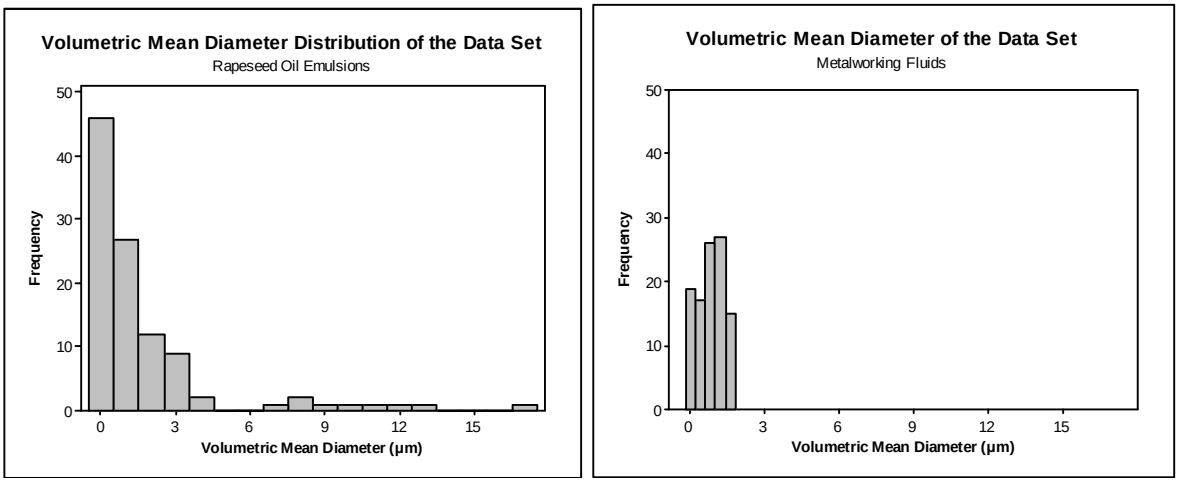

Figure 16: Volumetric mean diameter distribution of rapeseed oil emulsions and artificially aged MWFs data sets.

5.3. Study on the use of the Wavelength Exponent as a Measure of Emulsion Stability

The applicability of the wavelength exponent measurement was investigated by this author and the team of researchers in the BRAGECRIM project as an indication of the emulsion stability by monitoring both the turbidity spectra and the

DSD of emulsions over time, for MWF samples destabilized by adding calcium chloride, as well as by evaluating the time evolution of the wavelength exponent and the fitting quality of Equation 5 to the experimental data, presented before and repeated here.

$$z = \frac{d\left(ln(\tau)\right)}{d\left(ln\left(\frac{1}{\lambda}\right)\right)} \tag{5}$$

After the addition of $CaCl_2$ to the MWF, which has the purpose of promote the artificial aging of the emulsions, the samples, which were translucent solutions, became immediately cloudy. As illustrated in Figure 17, the absorbance measured by the spectrometer increased over the whole spectra. Changes in shape and an increase in the oscillations of the turbidity curves are also demonstrated in Figure 17, indicating that the turbidity spectra are very sensitive to the destabilization caused by adding the $CaCl_2$ to the MWF. As shown in Chapter 4.2, it was observed that no constituent of the studied MWF has significant absorption of the light in the range from 400 to 700 nm. Thus, the observed changes in the spectra in this range over time are mainly due to changes in the droplet population, although some interference of the $CaCl_2$ in the spectra is also possible. In this study, the results are based on the absorbance measured in the range from 500 to 600 nm, in order to avoid any oscillation in the spectra that could be related to light absorption effects.

Figure 18 presents results obtained with an MWF sample at two different times after addition of $CaCl_2$. The observed changes in the absorbance spectra (Figure 18a) correspond to a significant decrease in the slope of the straight lines (Figure 18b), i.e., the wavelength exponent *z* obtained by linear regression of the data based on Equation 5. Figure 18c indicates that this destabilized MWF contains two droplet populations.

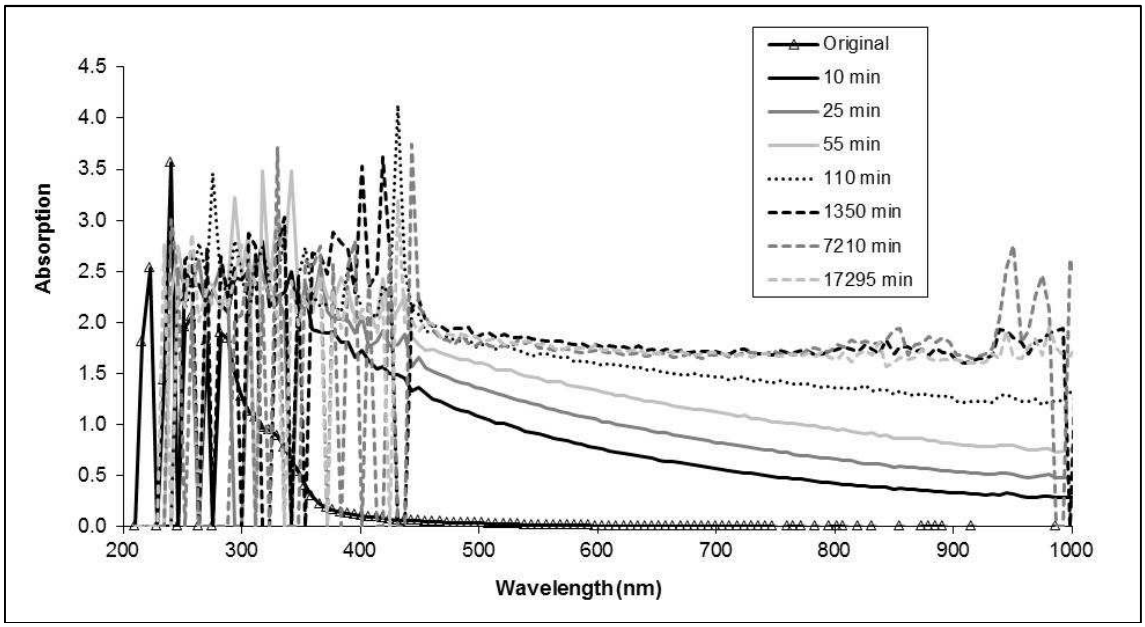

Figure 17: Absorption spectra the MWF at different times after addition of $CaCl_2$.

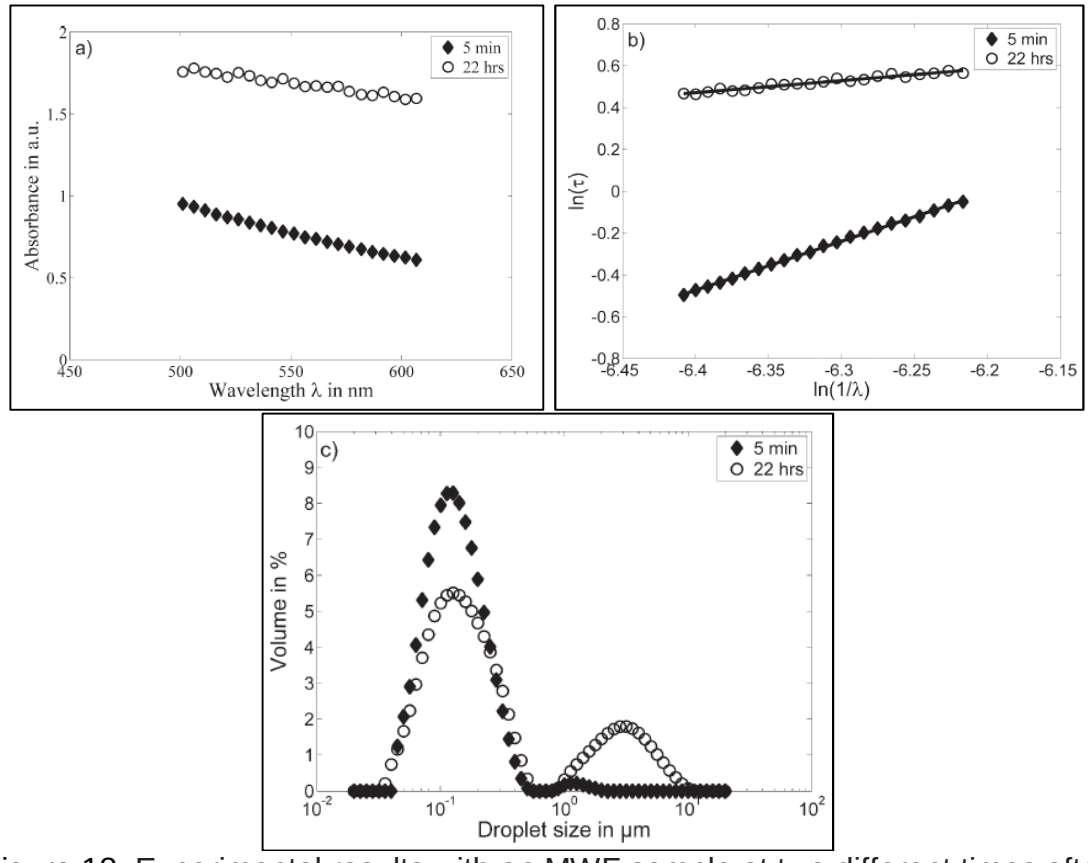

Figure 18: Experimental results with an MWF sample at two different times after addition of 0.3% $CaCl_2$. (a) Absorbance spectra; (b) ln(τ) versus ln(1/λ) (Equation 5); (c) DSD (GLASSE et al., 2013).

As illustrated in Figure 18, the addition of $CaCl_2$ resulted in substantial changes in the DSD of the MWF, with the formation of a second droplet population with larger diameters. The droplet size distribution was monitored over time for the artificially destabilized MWF samples and the results are displayed in Figure 19a. The DSD changes gradually from monomodal to bimodal. The larger mode corresponds to the new population formed. This larger mode gradually shifts towards larger droplet sizes and the DSD curve becomes progressively broader. Figure 19b illustrates for comparison the change of the DSD for a real MWF during machine operation within a time of 25 weeks of operation in a vertical turning machine, showing a similar behavior of the DSD of the MWF over time. The concentration of the samples from the turning machine was approximately 5-7% (volumetric basis).

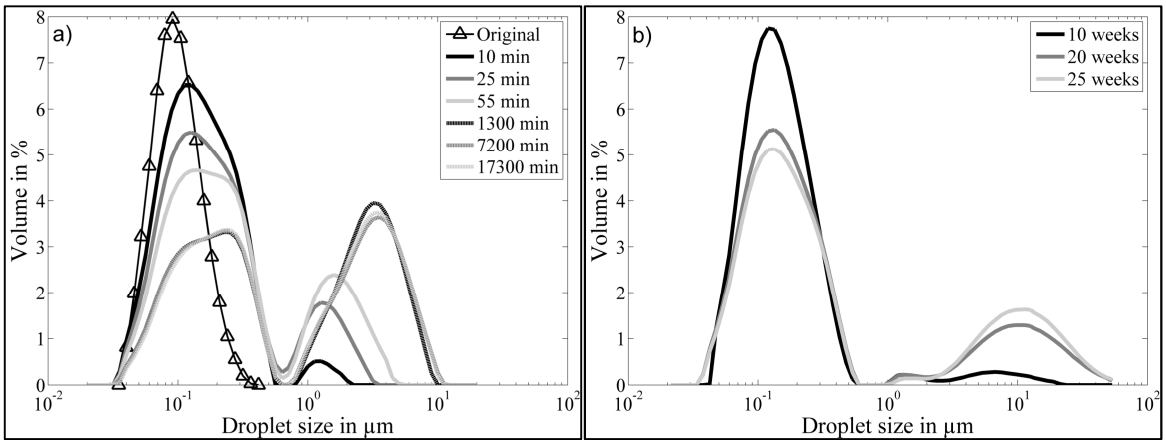

Figure 19: DSD of the MWF samples at different times after addition of $CaCl_2$ (a) and the weekly change of the DSD of a real MWF during machine operation in a vertical turning machine (b) (GLASSE et al., 2013).

Figures 20 to 22 present results for the artificially destabilized MWF samples after $CaCl_2$ addition. The volumetric mean droplet diameter, $D_{4.3}$, increased over time from approximately 150 nm to 700-1700 nm. This behavior was expected, since the addition of calcium may cause complexation between Ca^{2+} and the layer of additives adsorbed in the surface of the droplets, bridging between droplets and therefore reducing the electrostatic repulsion between them due to ion binding, thus facilitating the coalescence process. However, the DSD apparently tends to stabilize after 1000 min. The dispersion of the DSD curves also increases with time as a consequence of the formation of the bimodal distribution and tends to stabilize for longer times. The

corresponding values of the wavelength exponent, *z*, are indicated in Figure 22. These values were estimated by linear regression from turbidity wavelength data based on Equation 5, where *z* is obtained from the angular coefficient of the regression. The linear coefficient of the regression is related to the optical properties of the fluid and emulsion concentration, but it was not evaluated since it has no relevance for the purpose of this study.

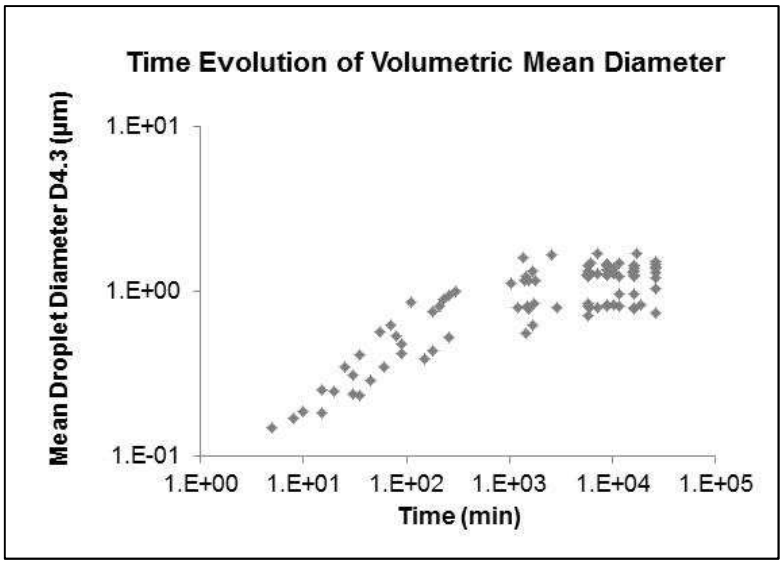

Figure 20: Time evolution of the volumetric mean droplet diameter $D_{4,3}$ for MWF samples after addition of $CaCl_2$.

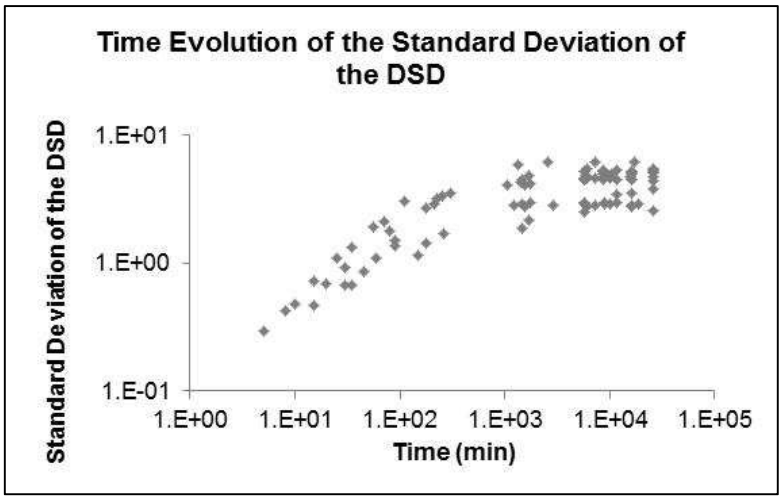

Figure 21: Time evolution of the standard deviation of the DSD for MWF samples after addition of $CaCl_2$.

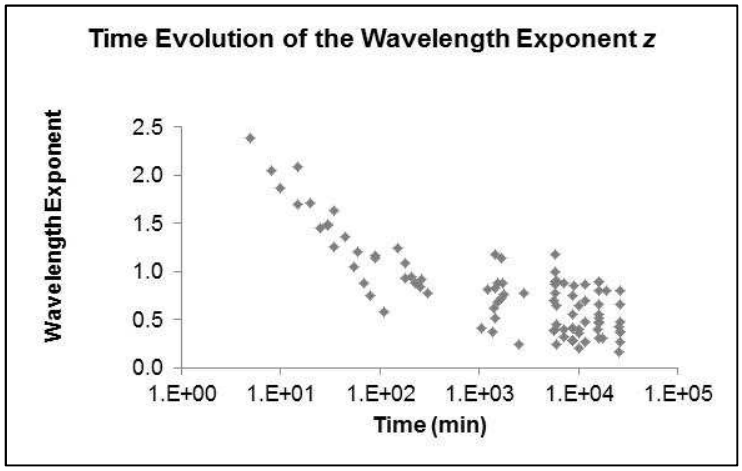

Figure 22: Time evolution of the wavelength exponent *z* for MWF samples after addition of $CaCl_2$.

The decrease of the *z*-values is in accordance with the predicted tendency from scattering equations (BOHREN, C.F., HUFFMAN, 1983) and also with the results reported by Deluhery and Rajagopalan (2005), who found that a rapidly decreasing wavelength exponent indicates a fast growth in droplet size while an unchanging or relatively constant wavelength exponent indicates a stable emulsion. However, the destabilization of the fluids leads to the formation of a bimodal DSD, resulting in a significant decrease in the quality of the fitting of Equation 5 to the data. This is illustrated in Figures 23 and 24 for the artificially destabilized samples. As expected, the wavelength exponent decreases gradually with the increase in $D_{4.3}$, but there is a significant reduction in the quality of the fitting as expressed by the coefficient of determination, R^2, when the volumetric mean diameter, $D_{4.3}$, reaches approximately 1μm.

The use of the wavelength exponent has been proposed under the assumption of a monomodal and monodisperse distribution (DELUHERY; RAJAGOPALAN, 2005), and the decrease in its value with time has been associated to the growth in droplet size by coalescence. Thus, according to Deluhery and Rajagopalan (2005), the stability of an emulsion can be evaluated by measuring the turbidity at different wavelengths over a certain time period and monitoring the time evolution of the wavelength exponent obtained by fitting Equation 5 to the data. However, based on the results in Figures 23 and 24, the fitting quality of Equation 5,

e.g., the coefficient of determination, and the resulting wavelength exponent are measured at specific instants of time, and then the condition of the MWF emulsion can be evaluated in real time. Nonetheless, the droplet size of the emulsion may be a limitation for the use of this method. In this evaluation, the quality of the fitting is reduced around 1 μm of the $D_{4.3}$, reducing therefore the reliability in the value obtained for z and consequently, the reliability of this method for being applied in the evaluation of emulsion destabilization, which is the purpose of this study, where is common the presence of bigger droplets.

Therefore, it is necessary to find another technique for the monitoring of MWF destabilization and it was decided to carry on the study with a multivariate calibration method using ANN. Nevertheless, since the wavelength exponent is an indicative of emulsion stability, it was used as one of the neural network inputs in the evaluations of MWFs.

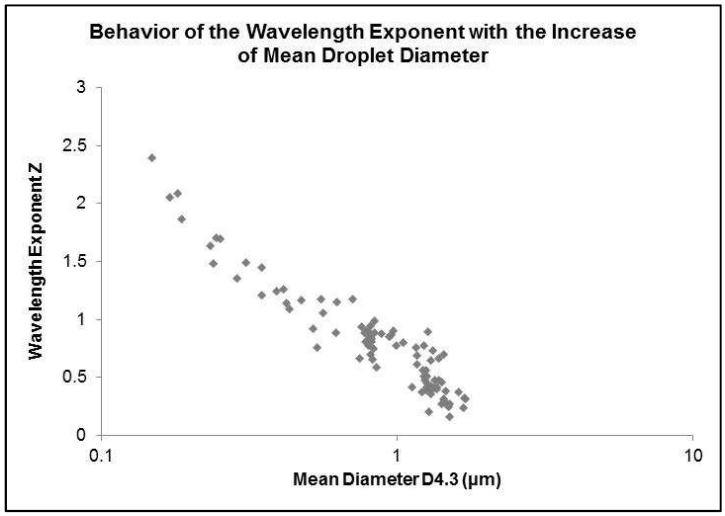

Figure 23: Wavelength exponent *z* of the artificially destabilized MWF samples as a function of $D_{4.3}$.

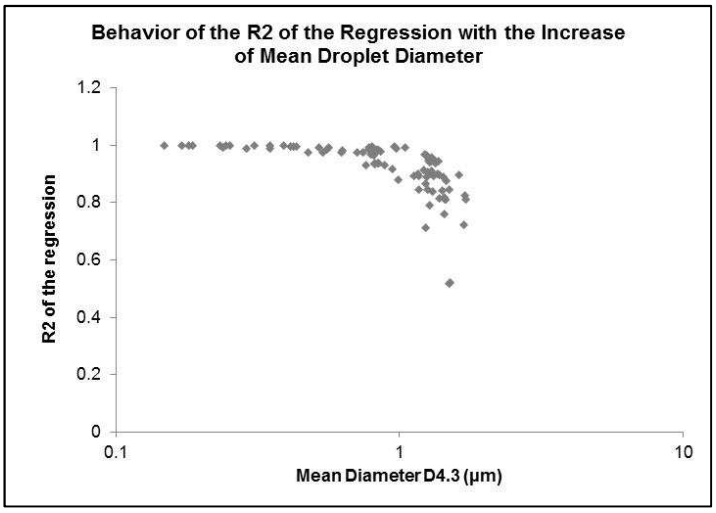

Figure 24: Coefficient of determination *R*2 for the fitting of Equation 5 to data of the artificially destabilized MWF samples as a function of $D_{4.3}$.

5.4. Studies to Estimate the Droplet Size Distribution of Rapeseed Oil Emulsions Based on Neural Network Fitting

As previously shown, the droplet size distribution of an emulsion changes with the destabilization. Therefore, the aging of an emulsion can be monitored by monitoring its DSD. For this purpose, it was evaluated the applicability of neural network models for obtaining DSD of emulsions using the data from the spectroscopic sensor described in Chapter 4.

The experimental data of rapeseed oil emulsion described in the previous items were used in the fitting of models to estimate the DSD of these emulsions based on spectroscopic measurements and fitting of the data by neural networks. As previously described and illustrated in Figure 12, the experimental data were fitted by a three-layer feed-forward neural network. Based on preliminary fittings trials, the following 7 variables were selected as inputs to the model: the measured values of extinction at the PCA-selected wavelengths (values at 452nm, 662nm e 943nm), the ultrasound energy transferred to the emulsion during the emulsification process and the mass fraction of water, oil and emulsifier (i.e., emulsion formulation, previously described in Chapter 4.1). It was not possible to use only data from spectra to fit an accurate model for obtaining the DSD of rapeseed oil emulsions due to the high

variability of the data, so variables related to emulsion formulation were included as inputs of the network. All the prepared samples were analyzed after the same time of preparation (after 5 minutes for absorbance spectrum and after 10 minutes for DSD analysis); however, most of the samples had presented low emulsion stability, especially the ones formulated to simulate old emulsions, which caused the high variability of the measured data. For this reason, it was necessary to add more information to the network to help in the learning process of the model and the best result were found using the 7 inputs previously cited. Since in a real application some of these inputs may not be available, like the inputs related to emulsion formulation, it is expected that this additional information will not be necessary in the studies of more stable emulsions and real-case scenario applications. As previously mentioned, the wavelength exponent *z* was not included as an input of the ANN due to the volumetric mean droplet diameter of the samples, with are outside the range of applicability of this method.

As outputs 20 size classes in the range of 0.03 μm to 20.3 μm were arbitrarily selected, as multiples of $\sqrt{2}$, aiming at reconstructing the DSD profile with an acceptable resolution. This number of size classes as well as its range can be changed according to the desired applications. In the present study 20 classes in the mentioned range were considered adequate, in order to compare the results and to evaluate the technique.

Thus, since the number of inputs and outputs is defined by the specific characteristics of the system, then the only degree of freedom was the number of neurons in the hidden layer. In the fitting step, for each value of this number, the minimum value of the error (Equation 18) was recorded and the best fitting was obtained with 6 neurons in the hidden layer and 500000 presentations of the data set.

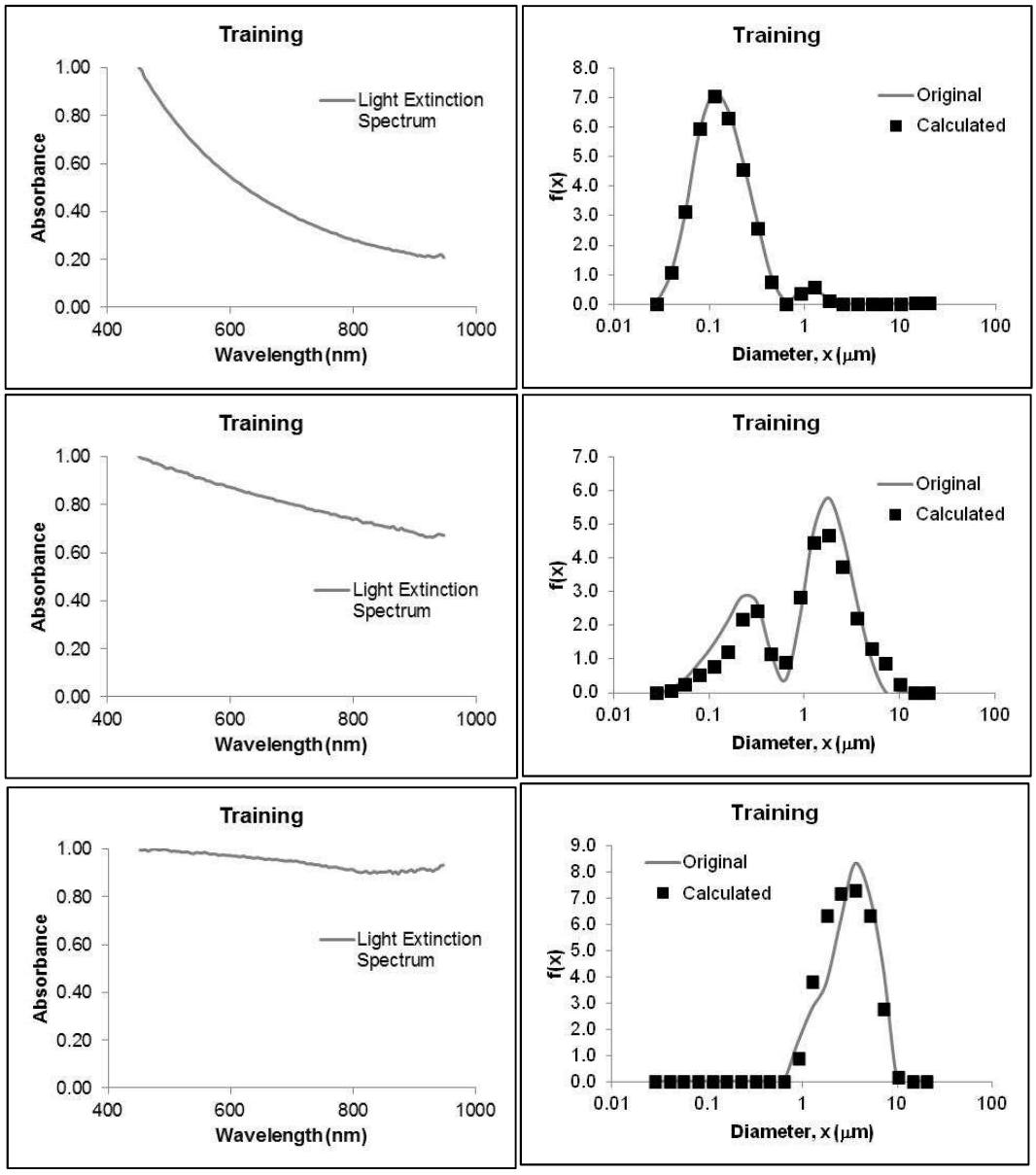

Figure 25: Neural network fitting results for corresponded spectra of rapeseed oil emulsions, with 7 inputs and 20 outputs (training set).

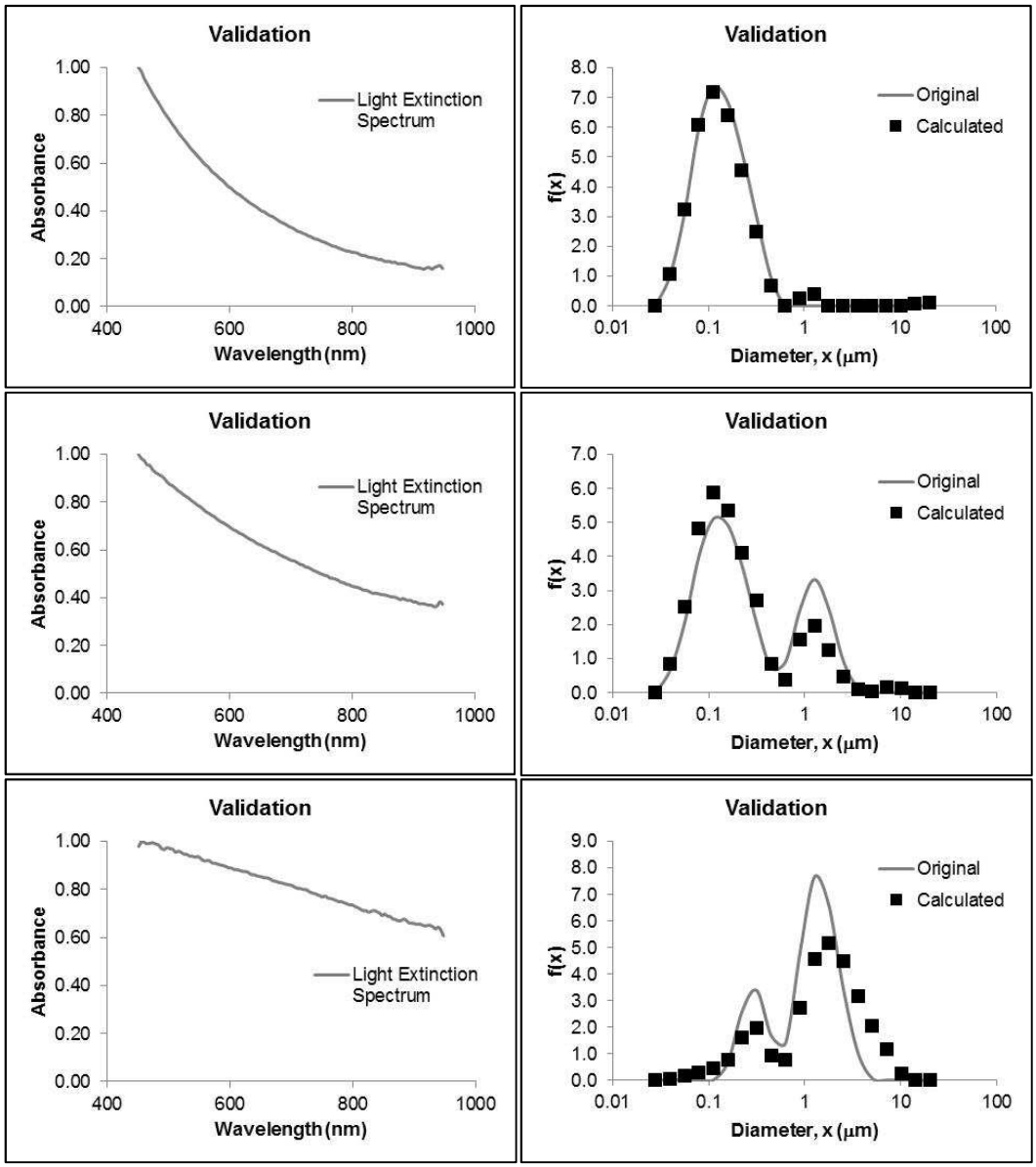

Figure 26: Neural network fitting results for corresponded spectra of rapeseed oil emulsions, with 7 inputs and 20 outputs (validation set).

Figures 25 and 26 show some results obtained in the best fitting, which are representative of the whole set. The plots in the left represent the normalized light extinction spectrum of the emulsion, measured with the spectroscopic sensor. The graphs in the right represent the corresponding DSD (measured distribution and distribution calculated by the network), where smaller droplet sizes are representative of newer emulsions and larger droplet sizes are representative of older emulsions. Good agreement between calculated and experimental values was obtained for monomodal as well as for bimodal distributions, indicating the potential of these models for monitoring oil-in-water emulsions in similar conditions. It is also possible

to observe how the measured spectra change with the destabilization of the emulsion and the growth of the droplet size, proving that they are indeed correlated to each other. The results of the fitting were presented as DSD curves instead of the more common “experimental *versus* calculated” curves because visualization of the results is better in DSD curves, due to the high number of outputs.

5.5. Studies to Estimate the Droplet Size Parameters Mean Diameter and Distribution Variance of Artificially Aged MWF Based on Neural Network Fitting

After the evaluation of rapeseed oil emulsions have indicated that the chosen technique has potential for the monitoring of emulsions, the same method was applied to artificially aged MWF.

A three-layer feed-forward neural network as illustrated in Figure 12 was fitted to the experimental data. In total, the following 8 variables were used as inputs: light extinction values selected by PCA (values at 460nm, 695nm and 943nm), wavelength exponent, concentration of oil, water and $CaCl_2$, and the time interval between addition of salt to the emulsion and each measurement (aging time). Once again, it was not possible to use only data from spectra to fit an accurate model. The presence of $CaCl_2$ in different concentrations in the emulsions affects the light absorbance in the measurements. For this reason, it was necessary to compensate this interference and to add more information to the network to help in the learning process of the model, being the best result found using the 8 inputs previously cited. In a real application some of these inputs will not exist (no chemicals are added to accelerate the emulsion destabilization in real application), so it is expected that this additional information will not be necessary in the studies of real-case scenario application.

As outputs of the neural network were selected the volumetric mean diameter ($D_{4,3}$) of the droplets (in μm) and variance of the droplet size distribution (in μm^2). The choice of $D_{4.3}$ as mean diameter was due to its higher sensitivity to the presence of

larger particles, which is related to the partial destabilization of the emulsion. However, it is possible that two populations with different distributions have the same mean diameter, so the variance of the droplet size distribution was also chosen as an input to provide information about the dispersivity of the distribution. The best fitting was obtained with 6 neurons in the hidden layer and 1 million presentations of the data set to the NN.

Figure 27 shows the results obtained in the fitting for emulsions with different aging times and consequently different mean diameters and variances. As shown in the plots, a good agreement between calculated and experimental values was obtained.

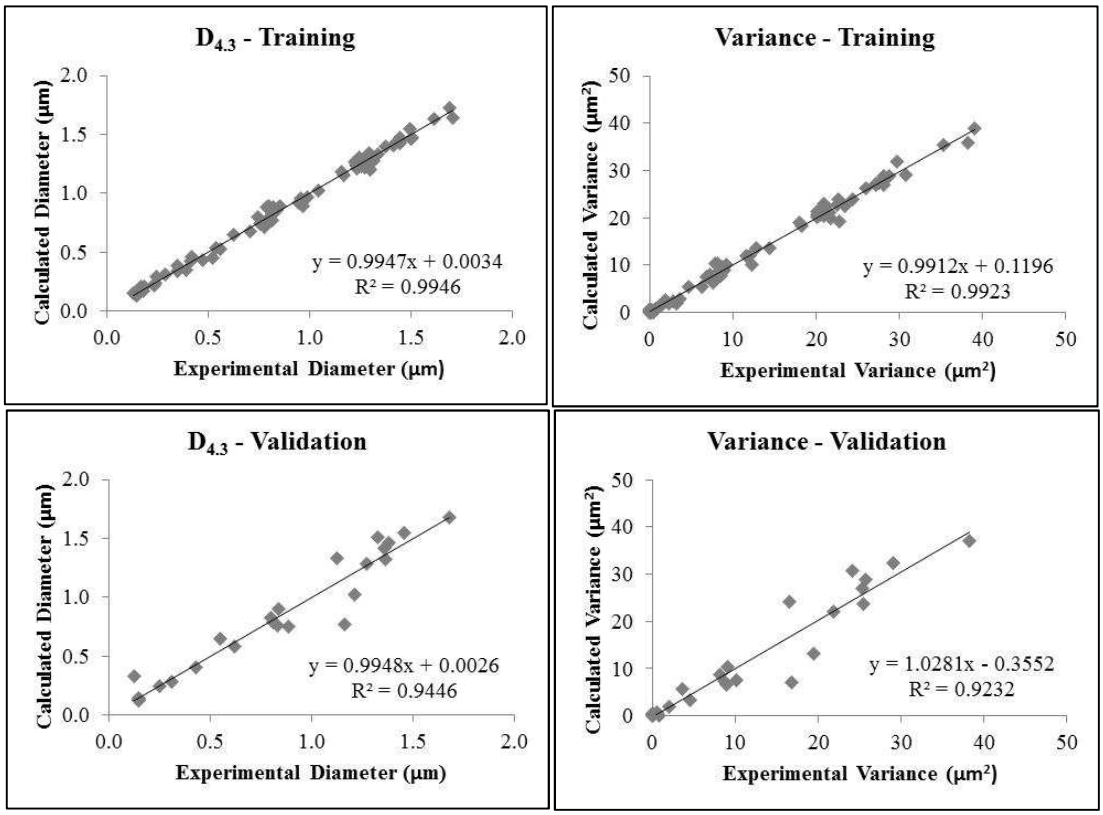

Figure 27: Neural network fitting results for a network with 6 neurons in the hidden (intermediary) layer.

The evaluation of the relative importance of each input variable of the model was carried out based on the HIPR method (“Holdback Input Randomization Method”), proposed by KEMP; ZARADIC and HANSEN (2007). The results are

shown in Figure 28. According to this analysis, the least important variable is the wavelength exponent. Thus, this variable was excluded from the inputs and a new neural network fitting was carried out based on the seven remaining model inputs. As shown in Figure 29, again there is a good correlation between calculated and experimental values. Removal of this input has in fact slightly improved the validation results. No improvement was obtained by removing the other least important inputs, indicating that this is the best fitted model for this system.

It is surprising that the evaluation of the relative importance of the neural network inputs has identified the wavelength exponent as the least important variable in the data set, since this has been a frequently adopted criterion in the literature associated with emulsion stability. However, since its value is estimated from the differentiation of spectral data in relation to the wavelength in log-log correlations, it is possible that, for this data set, the rather low accuracy of such estimation method, especially for the samples with longer aging times and, consequently, larger particles, causes too much noise in the data, and that the other variables from the spectral data (light extinction at 3 different wavelengths) provide similar information with less noise. This confirms previous findings that the particle size can indeed be a limitation for the application of the wavelength exponent method, since there are a significant number of samples in the data set with volumetric mean diameter larger than 1 μm, i.e., in the size range where it was previously shown to result in a poor fitting in the calculation of *z*. In Figure 28 it is also possible to see that the two main inputs of the model are the concentration of water and oil (MWF), justified by the fact that they have a direct impact on the droplet population and, consequently, on the spectroscopic measurements.

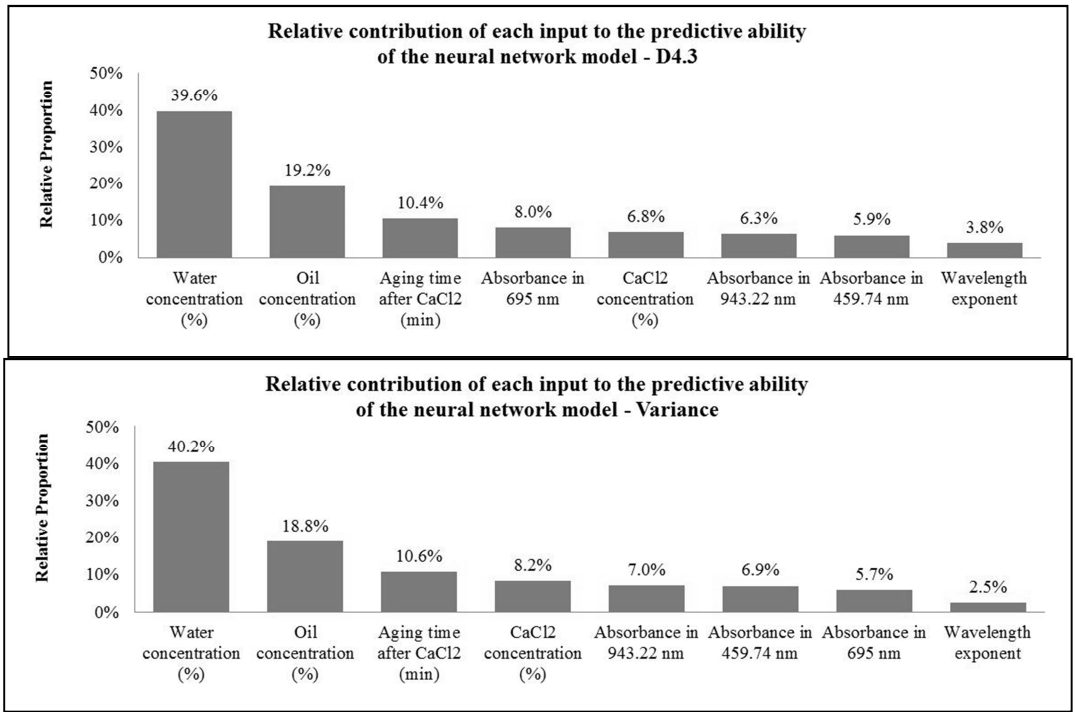

Figure 28: Relative contribution of each input to the predictive ability of the neural network model.

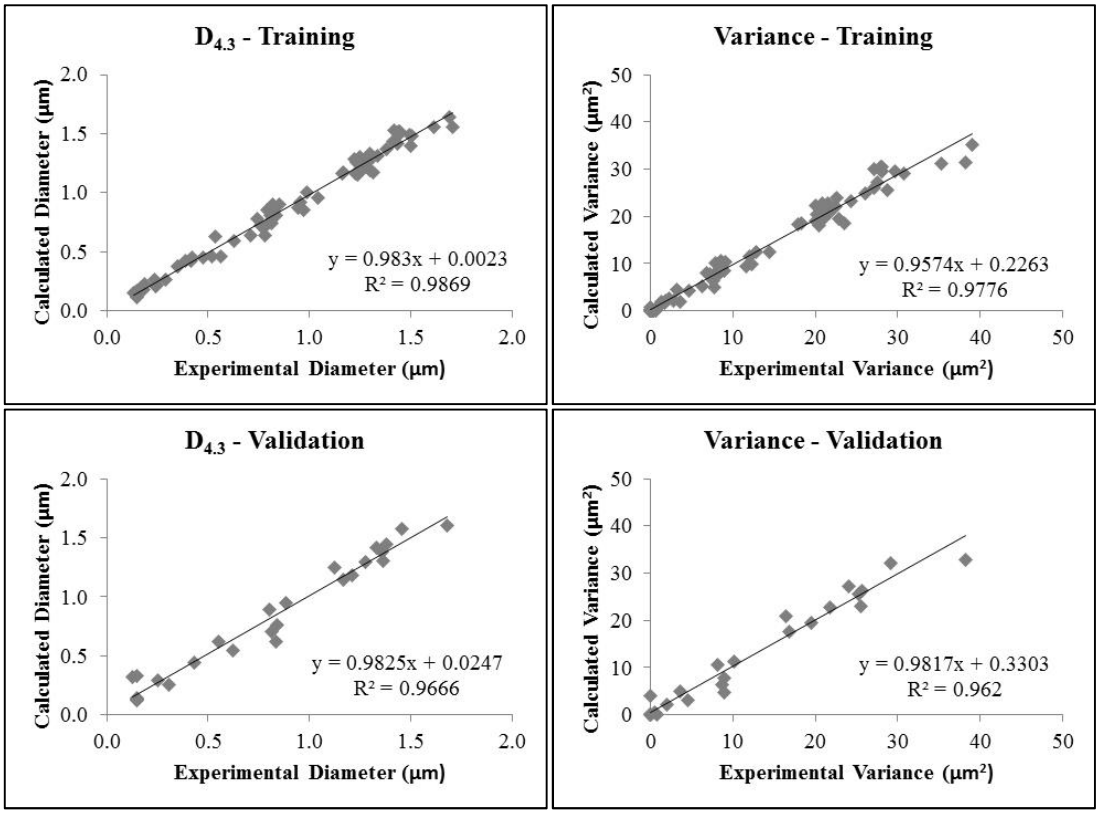

Figure 29: Neural network fitting results for a network with 6 neurons in the hidden (intermediary) layer reducing the number of inputs.

5.6. Studies to Rebuild the Droplet Size Distribution of Artificially Aged MWF Emulsions Based on Neural Network

Although parameters such as mean diameter and distribution variance can be used to monitor the aging and stability of emulsions, the droplet size distribution can provide more complete information about the emulsion structure. Due to that, another neural network fitting was performed. In this case, 7 variables were used as inputs: light extinction values selected by PCA at 460nm, 695nm and 943nm, concentration of oil, water and $CaCl_2$, and the time interval between addition of salt to the emulsion and each measurement (aging time). In this study the wavelength exponent was not used because the previous evaluation has shown that it is not so important to the model.

As outputs of the neural network 17 sizes classes were selected, from 0.04 μm to 10 μm, as multiples of $\sqrt{2}$, aiming at reconstructing the DSD profile with appropriate resolution. The best fitting was obtained with 6 neurons in the hidden layer and 500000 presentations of the data set.

Figures 30 and 31 show some of the results obtained in the best fitting, which are representative of the whole set, for emulsions with different aging times and consequently different DSD. The plots on the left represent the normalized light extinction spectrum of the emulsion, measured with the spectroscopic sensor. Those on the right represent the corresponding DSD (measured distribution and distribution calculated by the network), where smaller droplet sizes are representative of newer emulsions and larger droplet sizes are representative of emulsions with higher aging times. Again the results of the fitting were presented as DSD curves instead of the more common “experimental *versus* calculated” curves because visualization of the results is better in DSD curves, due to the high number of outputs.

A good agreement was obtained between calculated and experimental values, not only for monomodal but also for bimodal distributions, with different proportions between each droplet population. It is also possible to observe how the measured spectra change with the destabilization of the emulsion and the growth of the droplet

size, as expected. These results indicate the potential of these models for monitoring oil-in-water emulsions, although this fitted model is limited to evaluations with similar conditions and the same set of inputs. It would be interesting to find a model suitable for a more generic application, even if it is valid in the studied range only. This is discussed in other parts of this text, in the study of a real-case scenario.

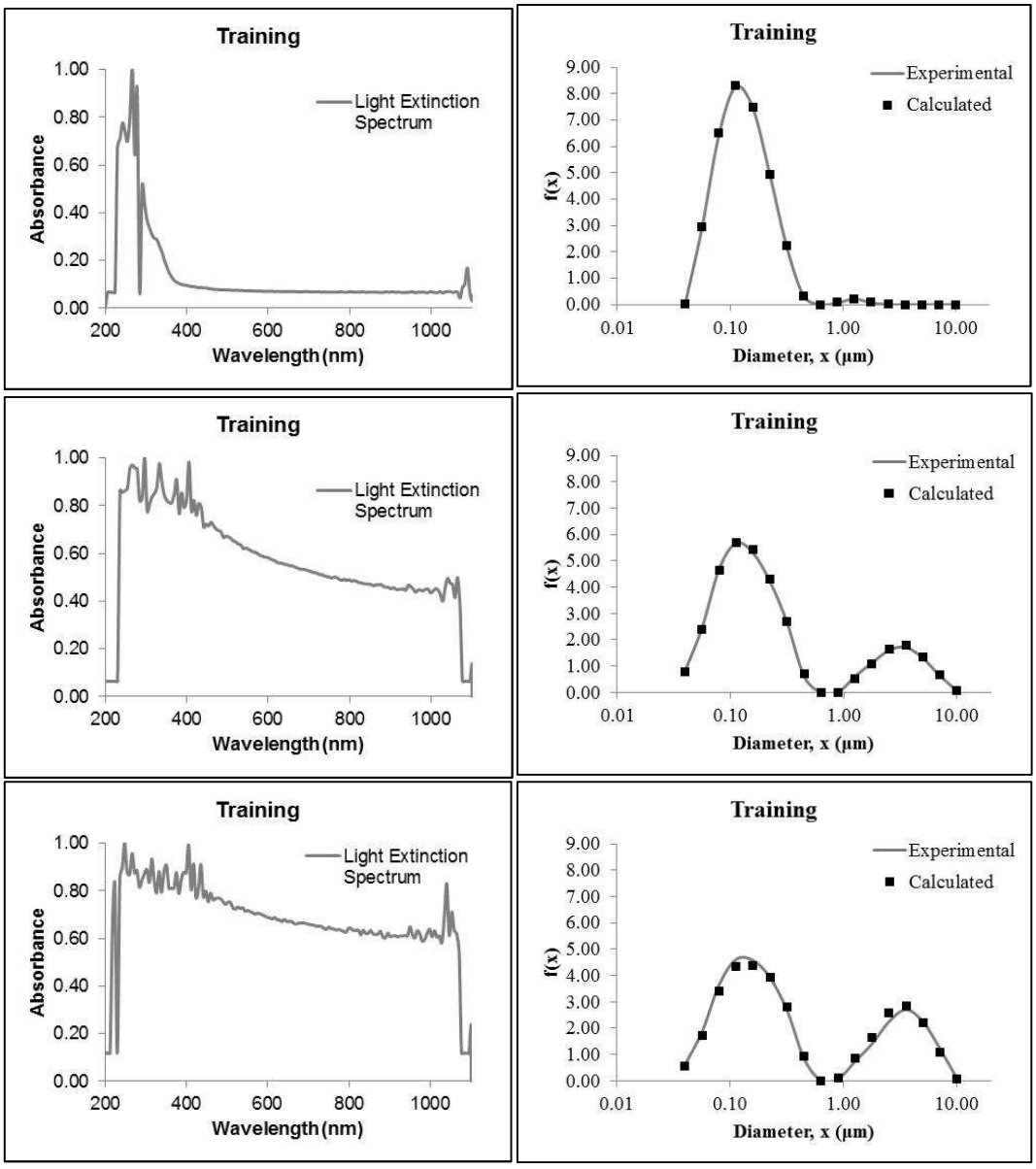

Figure 30: Neural network fitting results for artificially aged MWF, with 7 inputs and 17 outputs (training set).

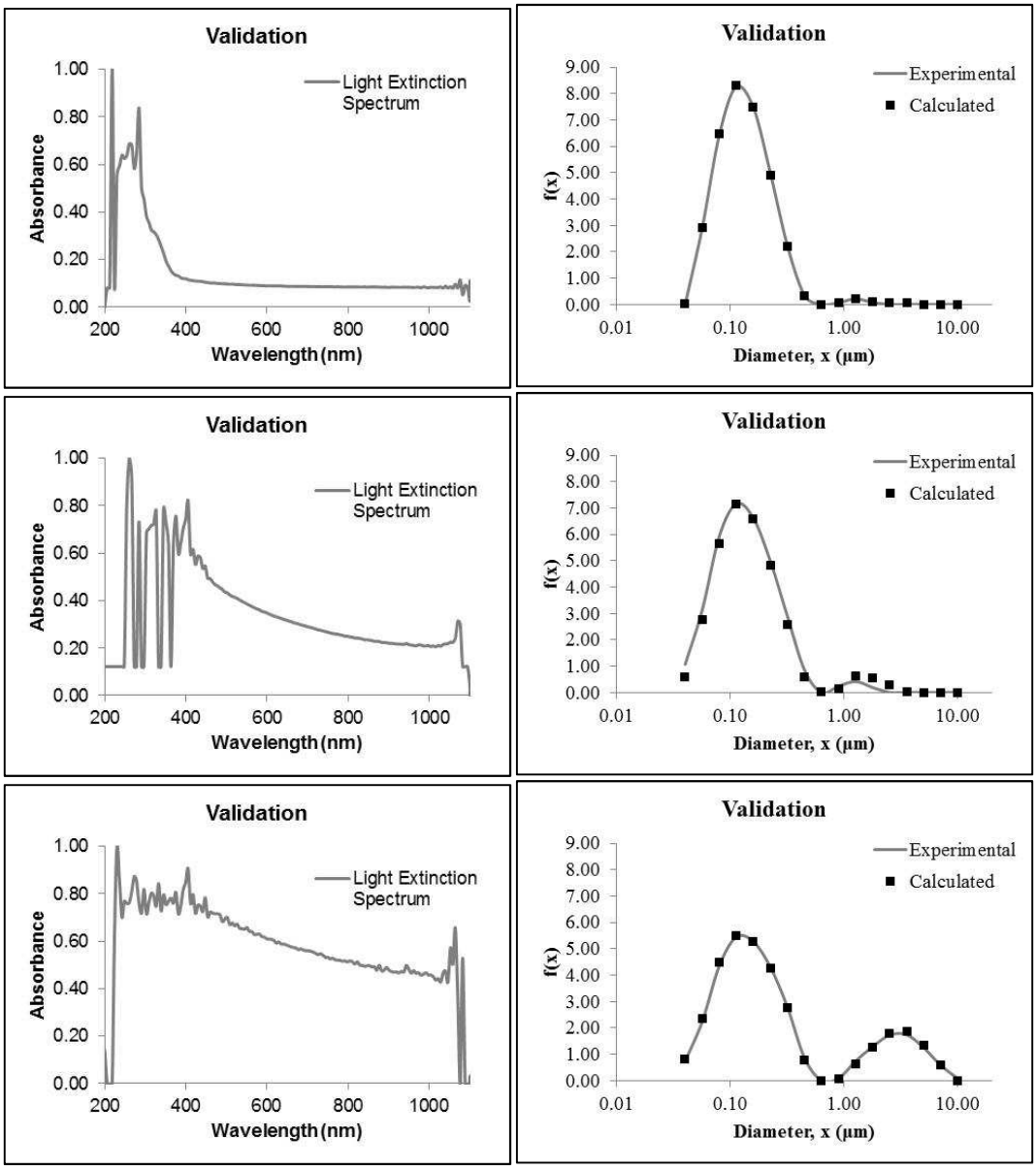

Figure 31: Neural network fitting results for artificially aged MWF, with 7 inputs and 17 outputs (validation set).

5.7. Application of the Neural Network Model to Monitor MWF Emulsion Destabilization

The previous model indicates that the combination of a UV/Vis spectrophotometric system with neural network models results in an optical sensor, which is capable of detecting changes in DSD during aging of MWF. In order to evaluate the potential use of this application, a monitoring experiment was carried out as follows. A commercial metalworking fluid emulsion with concentration of 4 wt.%

was artificially destabilized by adding 0.3 wt.% of calcium chloride and the aging was monitored over time with the optical sensor. These concentrations are within the range of fitting of the model, thus, of its validity. The spectroscopic data were fed to the adjusted model in order to estimate the droplet size distribution of the emulsion and evaluate its change over time.

In Figure 32, the plots on the left represent the normalized light extinction spectrum of the emulsion, as measured with the spectroscopic sensor, and the plots on the right represent the corresponding DSD (measured distribution and distribution calculated by the model). As shown in the plots, the DSD calculated by the model is similar to the DSD obtained by measuring the samples with the laser diffractometer. The model was able to calculate the distribution with good accuracy as well as to detect the evolution of the destabilization of the emulsion, which is associated with the change in the DSD from monomodal to bimodal. It is also possible to observe the evolution of the measured spectra with the destabilization of the emulsion and the growth of the droplet size, so it is clear that both phenomena are correlated.

Although the fitted model is suitable only for applications in similar systems, the results point out the potential of this technique for monitoring such emulsions, with the advantage that apparently the results are not affected by multiple scattering, suggesting that this approach may even be applied to more concentrated emulsions.

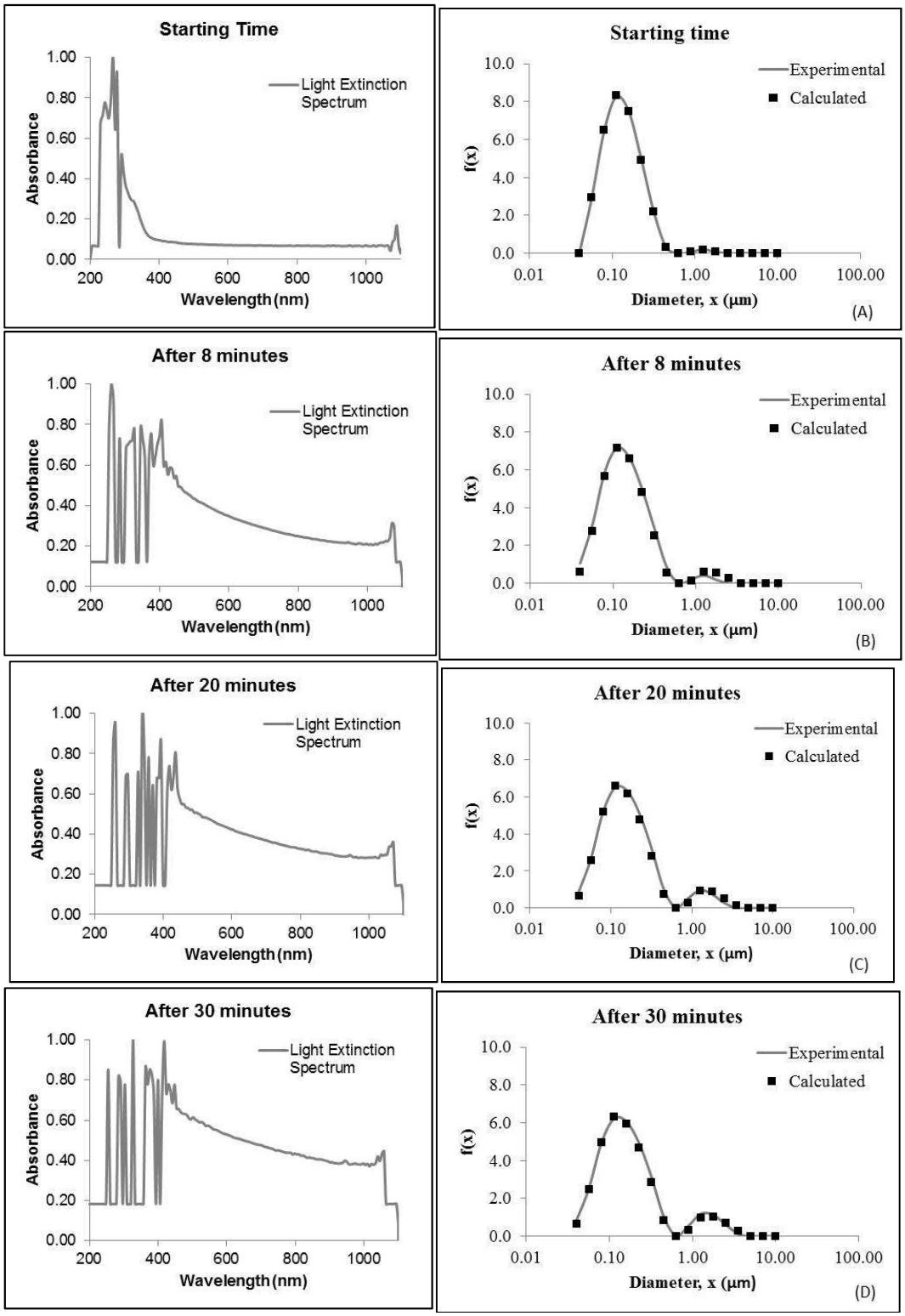

Figure 32a: Droplet size distribution calculated by the adjusted neural network model and measured by the laser diffractometer (Malvern Mastersizer) before $CaCl_2$ addition (A), and after 8 min (B), 20 min (C) and 30 min (D) after $CaCl_2$ addition.

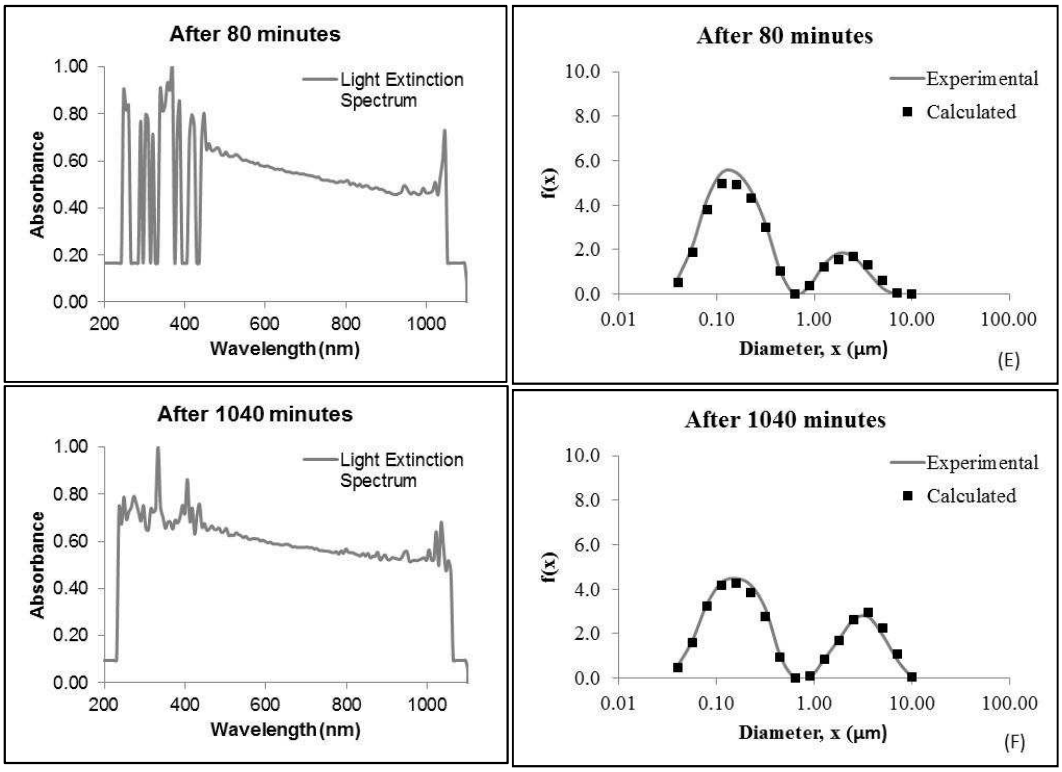

Figure 32b: Droplet size distribution calculated by the adjusted neural network model and measured by the laser diffractometer (Malvern Mastersizer) 80 min (E) and 1040 min (F) after $CaCl_2$ addition.

5.8. Application of the Spectroscopic Sensor to the Long-Term Monitoring of Metalworking Fluids Aging in a Machining Facility

The previous results indicate the potential of this technique for monitoring emulsion destabilization. However the obtained models are limited to a set of inputs that may not be available in common applications, like information about emulsion formulation or addition of chemicals to accelerate the destabilization process. In order to check the applicability of the method, a long-term monitoring study of commercial MWFs in a machining facility was carried out. The objective of this campaign was to obtain information as near as possible of a real-case scenario on the performance of the spectroscopic probe plus neural network as a sensor for monitoring MWF destabilization. Data were collected from 7 different commercial metalworking fluids, during a period of 13 months, from 3 different machines, as described in Chapter 4.1.2. After cleaning of the raw data set, to eliminate wrong or

missing recordings, as well as outliers, the resulting data set contained a total of 88 observations.

The usual control of quality of MWFs consists of periodic analyses of some properties of the fluid only, and the judgment by the machine operation personnel. These periodic analyses are the basis for the judgment of the fluid quality by the machine operation personnel. In this thesis, these results are expressed in the form of a status classification of the fluid. Thus, in the specific machining facility used in this study, MWFs are classified as: status 1/green (no signs of deterioration), status 2/yellow (initial signs of deterioration), and status 3/red (high degree of deterioration).

Figure 33 shows the distribution of the collected data of the long-term monitoring study, grouped by the status in which each sample was classified by the machine operation personnel. The measured variables in this study, as described in Chapter 4, are listed below.

- Variables commonly used in the monitoring of MWF quality in the studied machining facility, whose control is required by specific legislation applied to machining industry:
    - pH;
    - Concentration of the fluid, measured in wt.%;
    - Nitrite content in the MWF, measured in mg/L;
    - Microbiological contamination by ATP method, expressed as log(ATP) and measured in CFU/mL (colony forming unit per mL).
- Variables from the spectroscopic sensor:
    - Wavelength exponent of the samples, *z*, calculated by the fitting of Equation 5, where *z* is the slope of the curve, calculated between 500-600 nm;
    - Linear coefficient of the wavelength exponent fitting, i.e., of the fitting of Equation 5, which is related to optical properties of the fluid and emulsion concentration.
- Reference measurements:
    - Volumetric mean diameter $D_{4.3}$, calculated from the obtained DSD, measured in a Malvern Mastersizer diffractometer.

Although the previous studies showed the limitation of the application of the wavelength exponent method, this limitation is related to the reliability in the value obtained in the fitting, i.e., its accuracy. However, higher values of *z* for younger emulsions and lower values of *z* for older emulsions are obtained, so the trend is maintained. The mentioned inaccuracy may have high impact in simpler systems, like the one previously studied, where other variables were probably providing equivalent information, but these measurements may contribute to the evaluation of more complex systems, like in this long-term monitoring experiment, where the spectra are very noisy, as illustrated in Figure 34. As previously mentioned, the linear coefficient of the fittings was also used in this evaluation to compensate for the lack of information on the optical properties of the MWFs and to help differentiate the data for different fluids.

By analyzing Figure 33, it was expected that some correlation between the measured variables and the status of the fluid would be apparent. However, this correlation is not clear. Samples classified as Status 1/green should belong to new fluids, i.e., fluids without signs of deterioration. As expected, these samples show higher values of pH. The pH of MWFs tends to decrease during its use, due to chemical degradation, caused by thermal stress. However, the broadness of the distribution of this variable for Status 1 is higher than for Status 2/yellow. Once lowering the pH favors microbiological contamination, usually chemicals are added to the MWF during operation when the pH shows a significant decrease, in order to increase it again to its original value, but the control is not much accurate, so a higher standard deviation in pH values was expected for samples of older fluids, i.e., for Status 2 and Status 3. In addition, the distribution of the concentration values of the MWF samples should be similar for all cases, since the value is periodically corrected by the addition of water, otherwise an increase in the concentration from Status 1 to Status 3 would be observed. However, these expected tendencies are not observed in Figure 33.

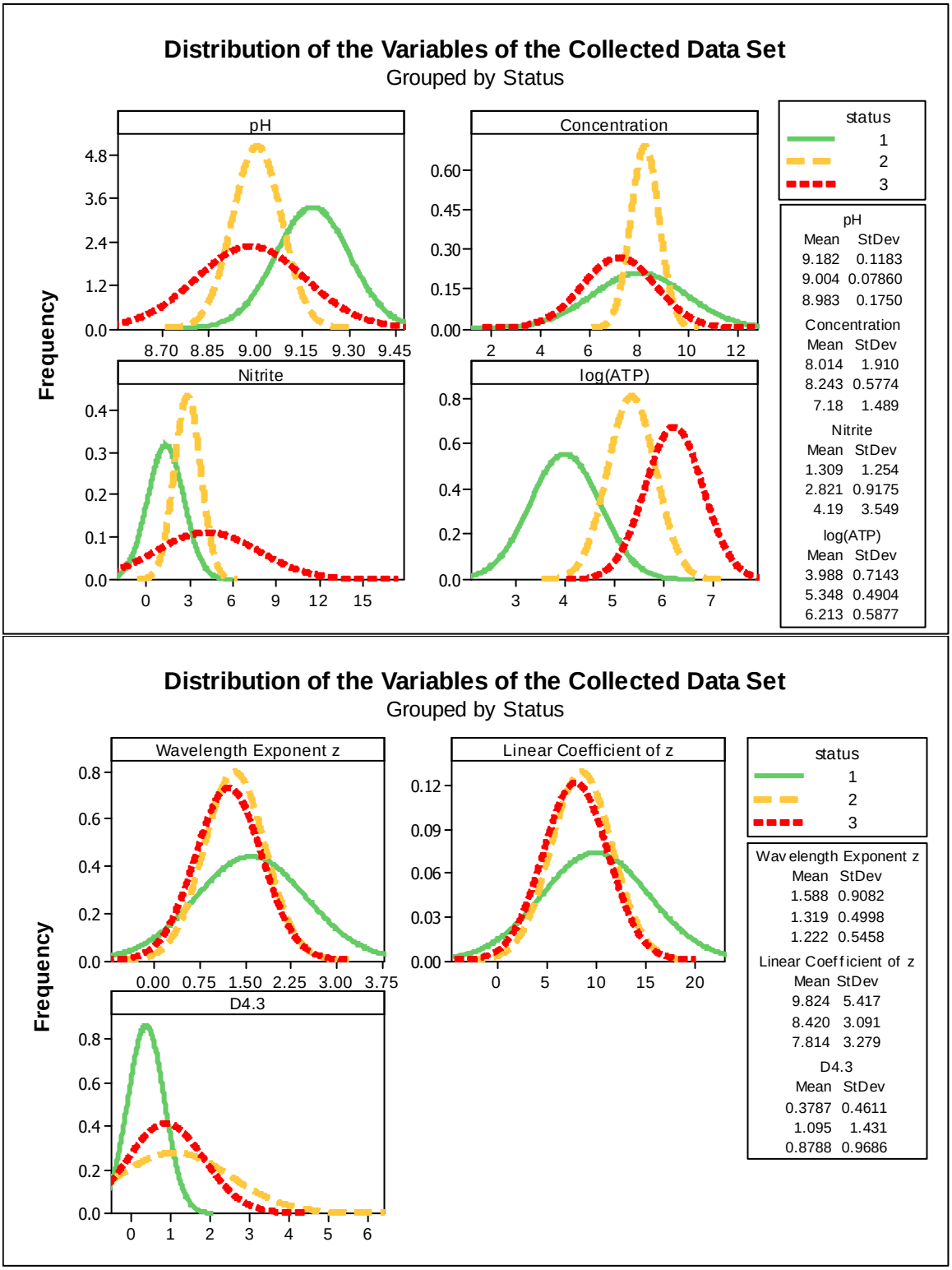

Figure 33: Distribution of the variables of the collected data set, grouped by status. (Concentration was measured in %, nitrite in mg/L, microbiological contamination in CFU/mL and volumetric mean diameter in μm)

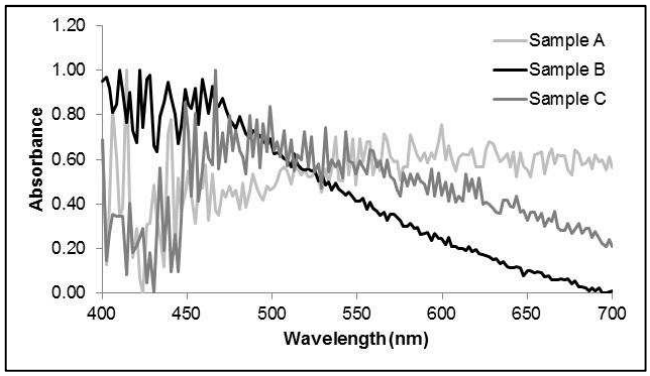

Figure 34: Illustration of the obtained spectra of three randomly chosen samples in the long-term monitoring experiment.

Water-mixed MWFs contain various nutrients for bacteria so that they are always contaminated with microorganisms. The microbiological contamination is measured by ATP method, expressed in Figure 33 as log(ATP), and for this variable some correlation with status is observed. As expected, the log(ATP) increases from Status 1 to Status 3, since the increase in microbiological contamination favors the degradation of the fluid. Anaerobic bacteria degrade nitrate or nitrite to ammonia and sulphate or sulphonate to hydrogen sulphide, causing unpleasant odors, so the monitoring of nitrite content in the MWFs is also required by specific legislation applied to machining industry. Fluids with higher nitrite content will present altered levels of odor, so it was indeed expected to find higher values for this variable in samples classified as Status 3/red, i.e. with higher signs of deterioration. However, the corresponding plot in Figure 33 shows no clear tendency regarding this variable. Although different distribution curves are observed, no clear tendency exists based on the value of this variable. The analysis of the distribution of the volumetric mean diameter in Figure 33, used as the reference measurement, does not show any visual correspondence between the $D_{4.3}$ and the status, although it is known that the mean diameter should increase with the aging of the fluid and, consequently, from Status 1 to Status 3. These results indicate that the MWF monitoring evaluation adopted by the machine operation personnel is mostly determined by factors related to microbiological contamination of the fluid, while factors that may affect the performance of the MWF appear to have less importance. Nevertheless, it was decided to use of a statistical method to find out if there is a correlation between all the measured variables and the status classification given by machine operators, which supposedly should exist.

5.8.1. Discriminant Analysis for Evaluating the Status Classification

Assuming that the variables used in monitoring the quality of the MWF (pH, concentration, nitrite content and microbiological contamination by ATP method) are adequate for the characterization of the MWF status, these variables were included in a classification procedure based on the discriminant analysis technique. The objective in this part of the study is to compare the results obtained with this statistical technique and the judgment criteria used by the operation personnel in the machining facility in terms of the three groups: 1/green, 2/yellow and 3/red. The efficiency of the classification method was based on the fraction of correctly classified observations in the original groups. Here, the denomination “original group” or “original status” refers to each of the three groups resulting from the classification made by the machine operating personnel. Two types of discriminants were tested: linear and quadratic. Besides the mentioned variables, the wavelength exponent and the linear coefficient of the linearly adjusted spectra were also included as predictors in the discriminant analysis. The effect of using only the variables measured by the spectroscope plus concentration and pH as predictors was also evaluated in these tests.

Table 3 presents the results obtained with different groups of predictors tested and the efficiency of each discriminant, indicated as “quality of the fitting”. The maximum rate of success was 81% and the addition of the wavelength exponent and the linear coefficient to the group of predictors did not bring any significant improvement in the quality of the fitting. However, the exclusion of the nitrite content and microbiological contamination as predictors for the status decreased the quality of the classification significantly. Since the previous analysis suggests that status classification done by machine operation personnel may be mostly determined by factors related to microbiological contamination of the fluid, the effect of using the two variables related to microbiological contamination as predictors, i.e., nitrite content and microbiological contamination by ATP method, was evaluated. The maximum rate of success was 81% in this case, too. Thus, no improvement in the quality of the fitting was obtained. These results confirm the hypothesis that the variables pH and concentration do not have much influence on the status classification of the MWF,

and also suggest that the factors related to microbiological contamination of the fluid are not sufficient for determining its quality classification, here represented by the status.

Table 3: Predictors used for status discrimination and quality of resulting fitting.

	Fitting 1	Fitting 2	Fitting 3	Fitting 4	Fitting 5	Fitting 6
Predictors	pH Concentration Nitrite Log(ATP) -	pH Concentration Nitrite Log(ATP) Wavelength Exponent	pH Concentration Nitrite Log(ATP) Wavelength Exponent Liner Coefficient of Wavelength Exponent Fitting	pH Concentration - - Wavelength Exponent	pH Concentration - - Wavelength Exponent Liner Coefficient of Wavelength Exponent Fitting	- - Nitrite Log(ATP) -
Quality of Linear Fitting	80%	80%	81%	55%	53%	80%
Quality of Quadratic Fitting	80%	78%	81%	58%	62%	81%

Figures 35 to 40 show the distribution of the data in all fittings. Discriminant analysis was based on the selected predictors for classifying each observation of the data set in one of the three groups of status, 1/green, 2/yellow or 3/red, and each group of this classification is presented in a separated panel of those figures. For each panel, i.e., each group of classification of the data, the distribution of the original status of the corresponding set of observations is presented, with the purpose of analyzing the accuracy of the fitting in each group.

For fittings 1 to 3 (Figures 35 to 37), most of the observations classified as status 1 or 3, really belong to that group. However, the discriminant analysis was not able to correctly discriminate the observations that should originally belong to group 2, and observations from all groups were classified in this group. Thus, the boundaries between these groups of data classification used in the current method of MWF monitoring are apparently diffuse. For fittings 4 and 5 (Figures 38 and 39) the results are even worse, with poor quality of fitting observed in all groups. In fitting 6 (Figure 40) most of the observations classified as status 1 or 2, really belong to that group, so it was the only fitting to improve the results obtained for Status 2. However, a significant number of observations were misclassified as Status 3.

In conclusion, the results of the discriminant analysis show that there is much overposition of the three groups, which are hardly discriminated by statistical criteria. This confusion among resulting groups can be caused by one of the following hypotheses:

- *The data were not correctly classified by machine operators and actually should receive a different status classification*. If this hypothesis is true, then a new method is needed for quality monitoring of MWF.
- *The data were correctly classified by machine operators*. If this is true, then there may exist subjective or unmeasured variables besides the currently measured ones that may have affected the status classification.

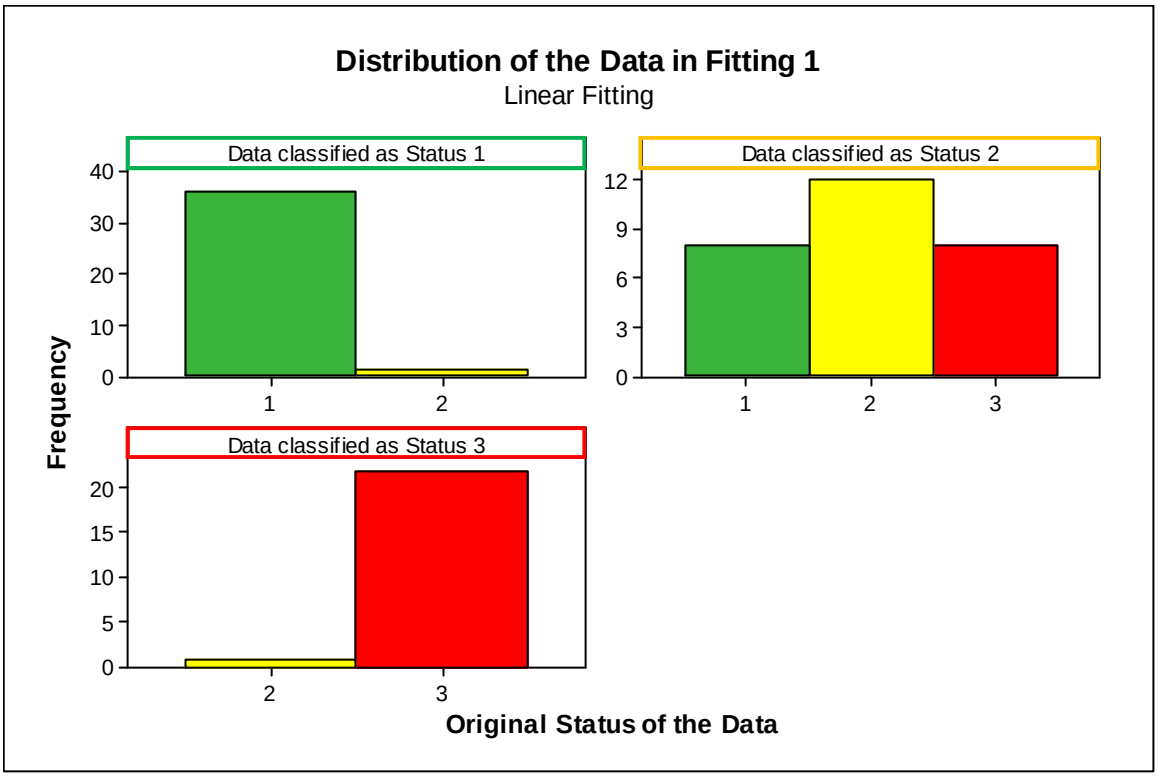

Figure 35: Comparison between status distribution of the data after discriminant analysis and original status in fitting 1.

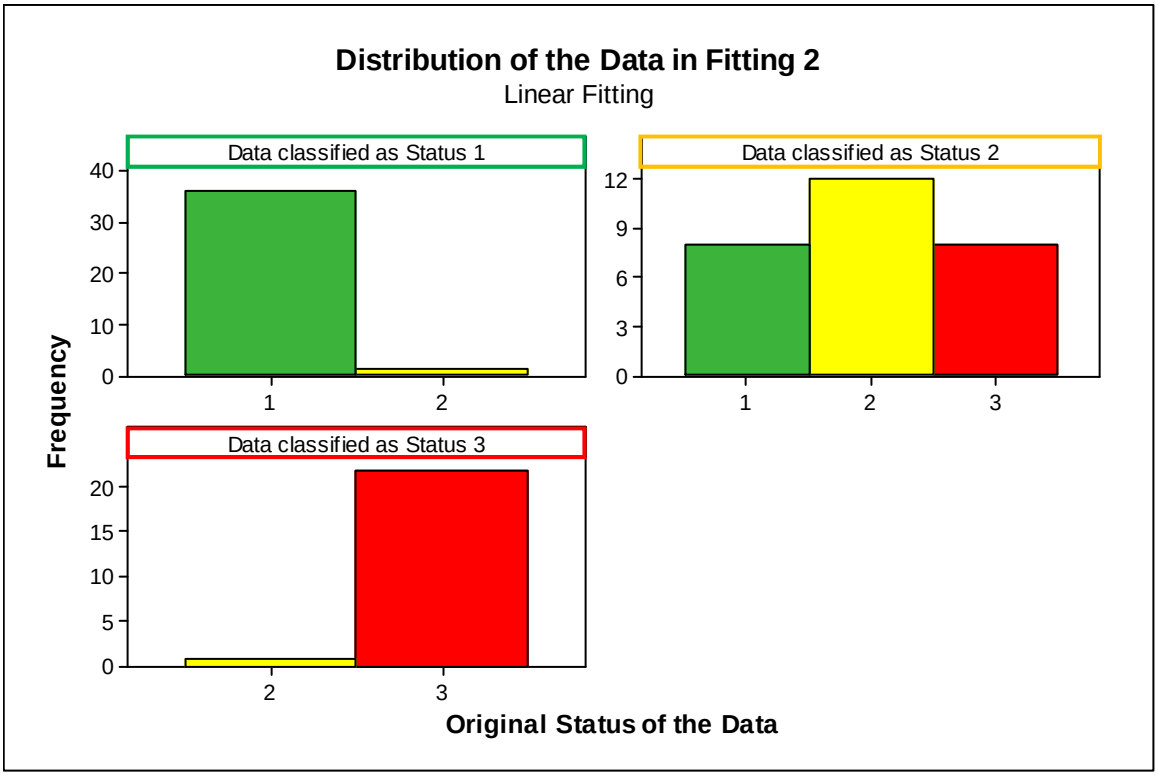

Figure 36: Comparison between status distribution of the data after discriminant analysis and original status in fitting 2.

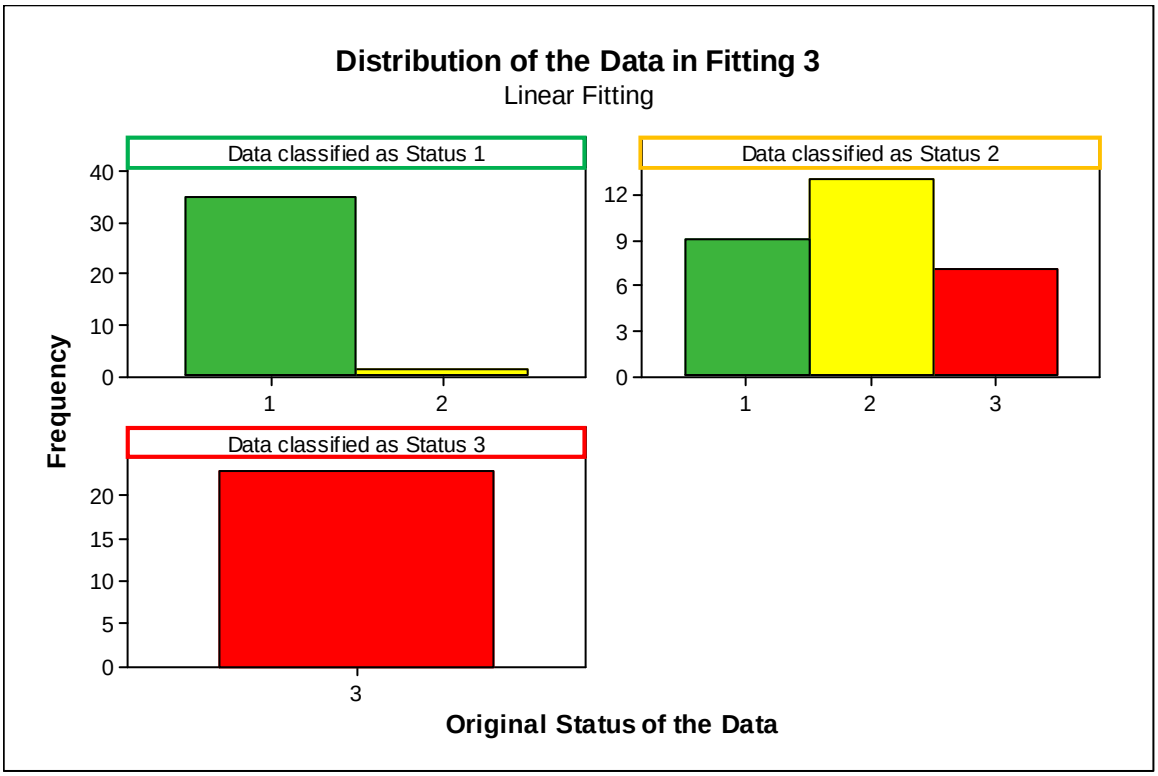

Figure 37: Comparison between status distribution of the data after discriminant analysis and original status in fitting 3.

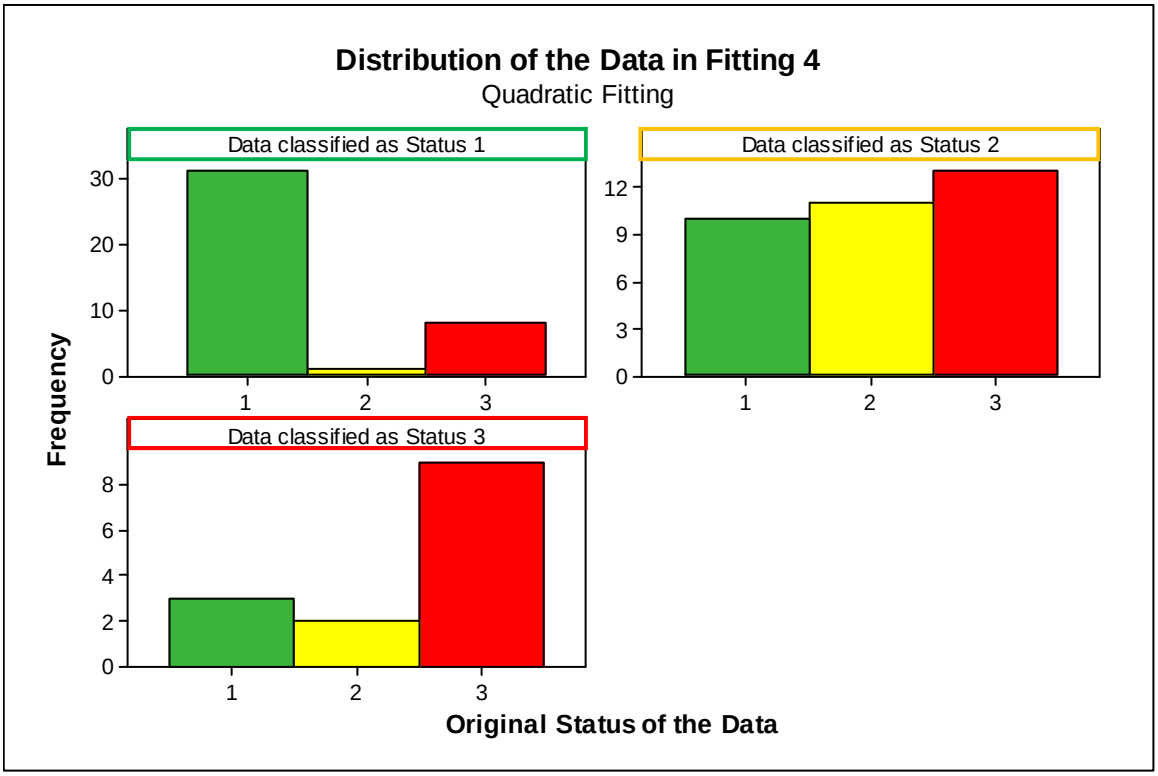

Figure 38: Comparison between status distribution of the data after discriminant analysis and original status in fitting 4.

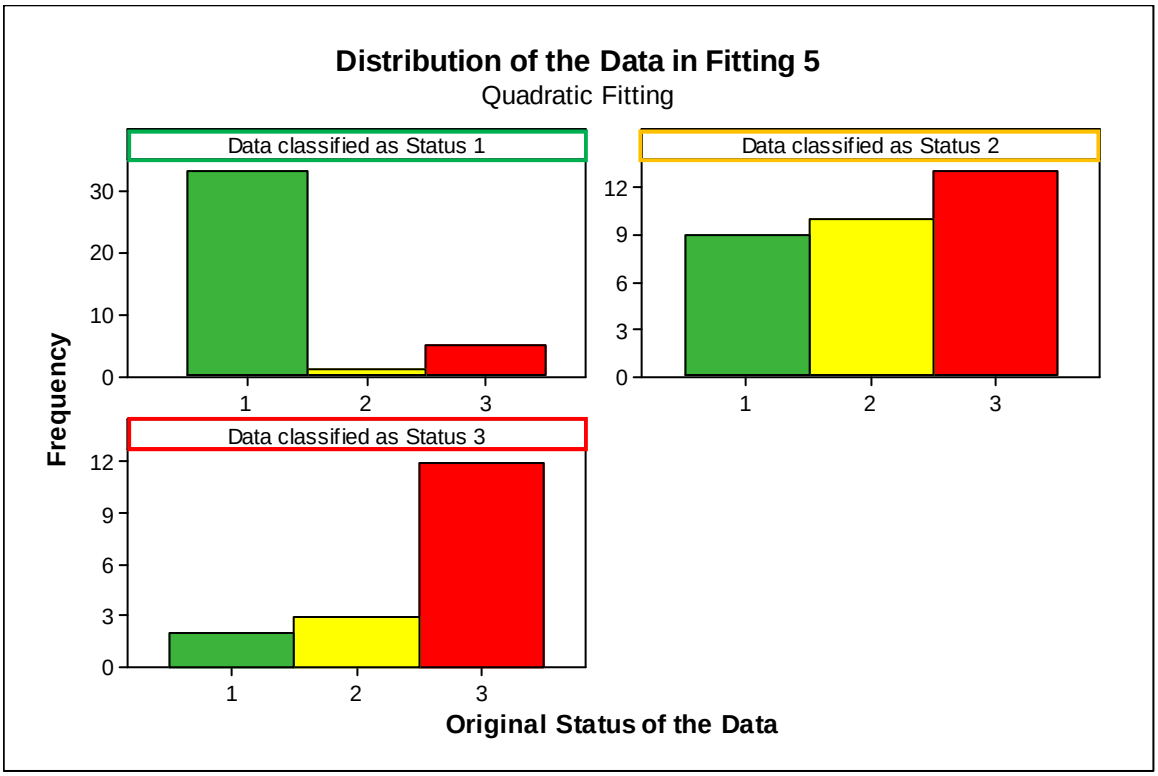

Figure 39: Comparison between status distribution of the data after discriminant analysis and original status in fitting 5.

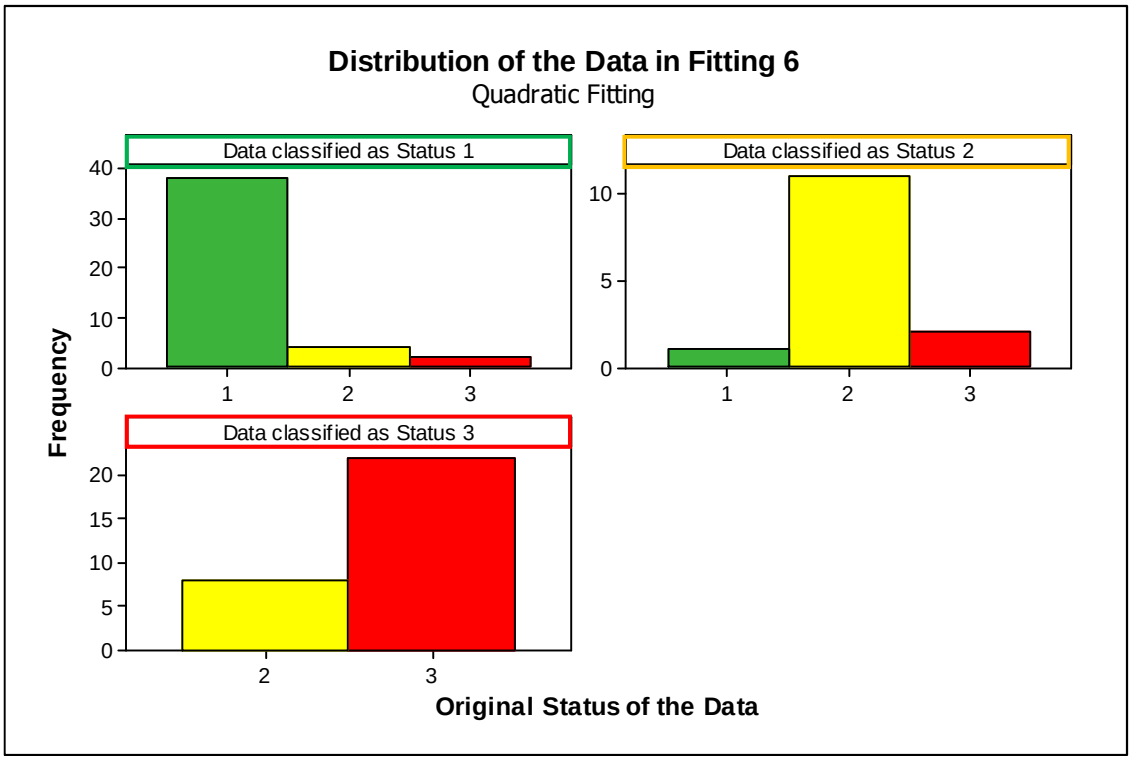

Figure 40: Comparison between status distribution of the data after discriminant analysis and original status in fitting 6.

These results have motivated the study of an alternative criterion for classification of these MWF samples, based on the fitting of a neural network model as a pattern recognition technique, which should be capable of associating a given pattern of distribution of the input information with the MWF status classes used by the machine operators. The results are shown in the next item.

5.8.2. Neural Network Fitting for Evaluating Status Classification

In this part of the study, the same groups of predictors used in the previous evaluation on discriminant analysis were adopted as inputs for the neural network, having the classification of the MWF status as the output. The input-output configurations are shown in Table 4. The results are presented in Figures 41 to 45, as original status versus status calculated by the ANN model, as well as the distribution of those calculated status, for better showing the overposition between

groups. For status 1/green, some of the models were able to calculate values in an acceptable range, but all results for status 2/yellow and 3/red resulted in poor fittings.

Evaluating the distribution of the calculated data, it is shown that in the training set the mean of the distribution is close to the expected value for the corresponding status, although there is overposition between the groups. However, in the validation set of fittings 1 to 3, the mean values of the distribution of Status 2 are closer to the value of 3 than the expected value of 2. In fittings 4 and 5, the results are even worse and the mean values of the distribution of Status 2 are higher than the ones from Status 3, i.e., it seems to be an inversion between both groups. In fitting 6 it was not possible to achieve any acceptable result, since all the tested conditions have returned the value of 0 for all observations and all groups, showing that, in this fitting and this data set, there are not enough inputs to allow fitting of a model and the only possible result for the output is that it has the value of 0 in all observations.

Table 4: Inputs used in the neural network fitting.

	Neural Network Fitting 1	**Neural Network Fitting 2**	**Neural Network Fitting 3**	**Neural Network Fitting 4**	**Neural Network Fitting 5**	**Neural Network Fitting 6**
Inputs	pH Concentration Nitrite Log(ATP) - - -	pH Concentration Nitrite Log(ATP) Wavelength Exponent - -	pH Concentration Nitrite Log(ATP) Wavelength Exponent Linear Coefficient of Wavelength Exponent Fitting	pH Concentration - - Wavelength Exponent - -	pH Concentration - - Wavelength Exponent Linear Coefficient of Wavelength Exponent Fitting	- - Nitrite Log(ATP) - - -
Outputs	Status	Status	Status	Status	Status	Status
Best Fitting	6 neurons in the hidden layer and 100,000 presentations of the data set	6 neurons in the hidden layer and 100,000 presentations of the data set	6 neurons in the hidden layer and 100,000 presentations of the data set	6 neurons in the hidden layer and 500,000 presentations of the data set	8 neurons in the hidden layer and 500,000 presentations of the data set	It was not possible to achieve any acceptable result

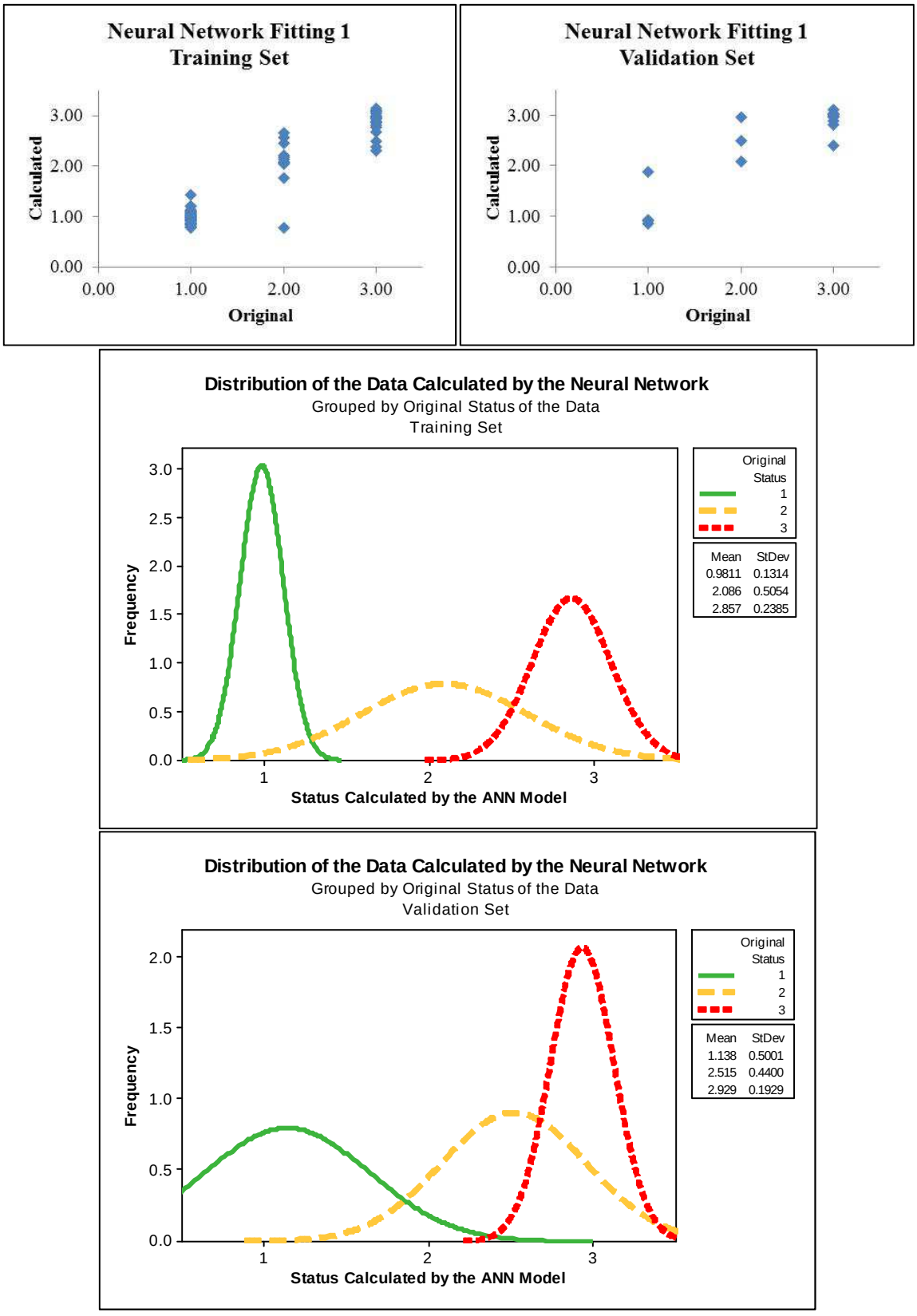

Figure 41: Comparison between calculated status by the neural network model in fitting 1 and original status of the data.

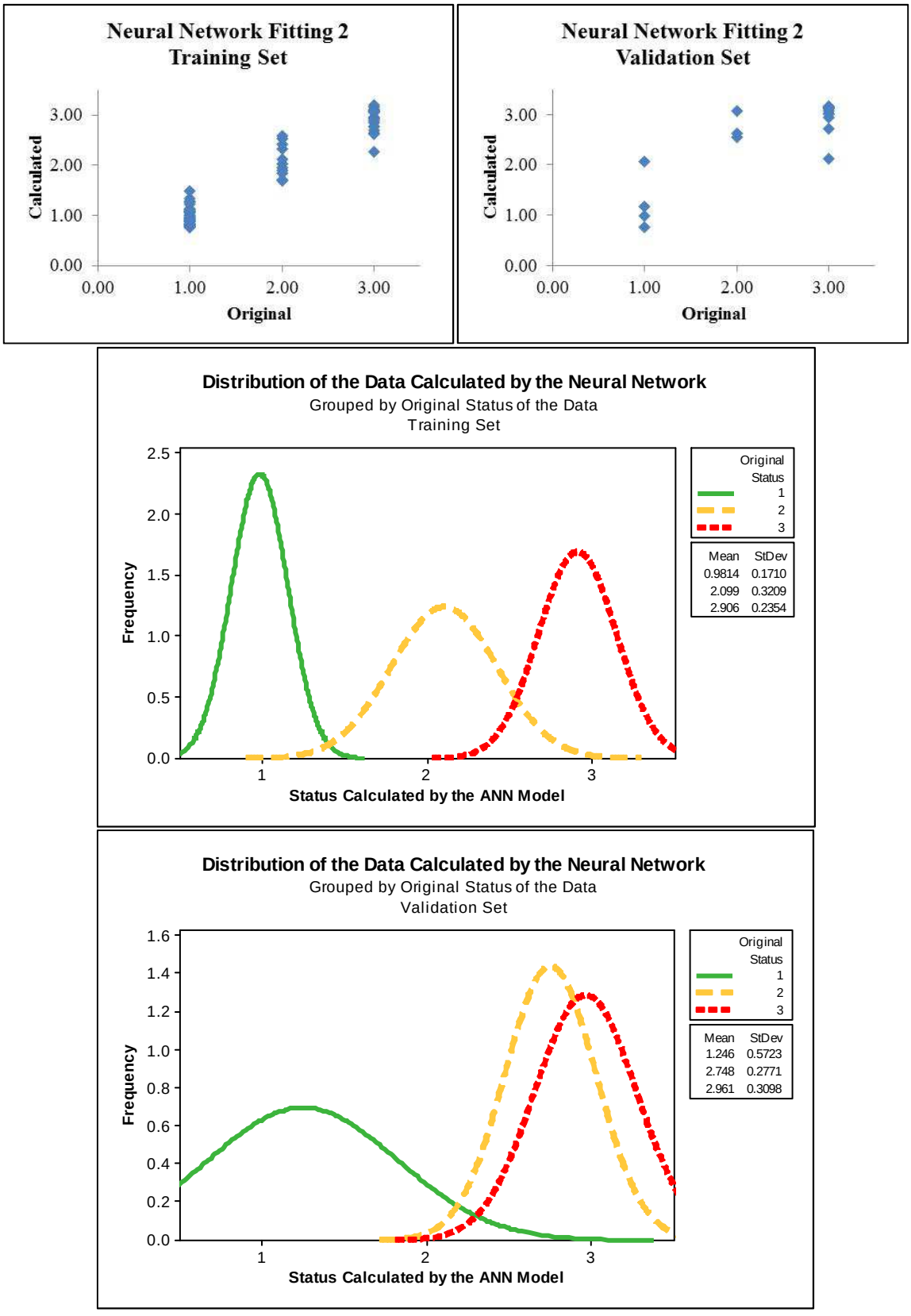

Figure 42: Comparison between calculated status by the neural network model in fitting 2 and original status of the data.

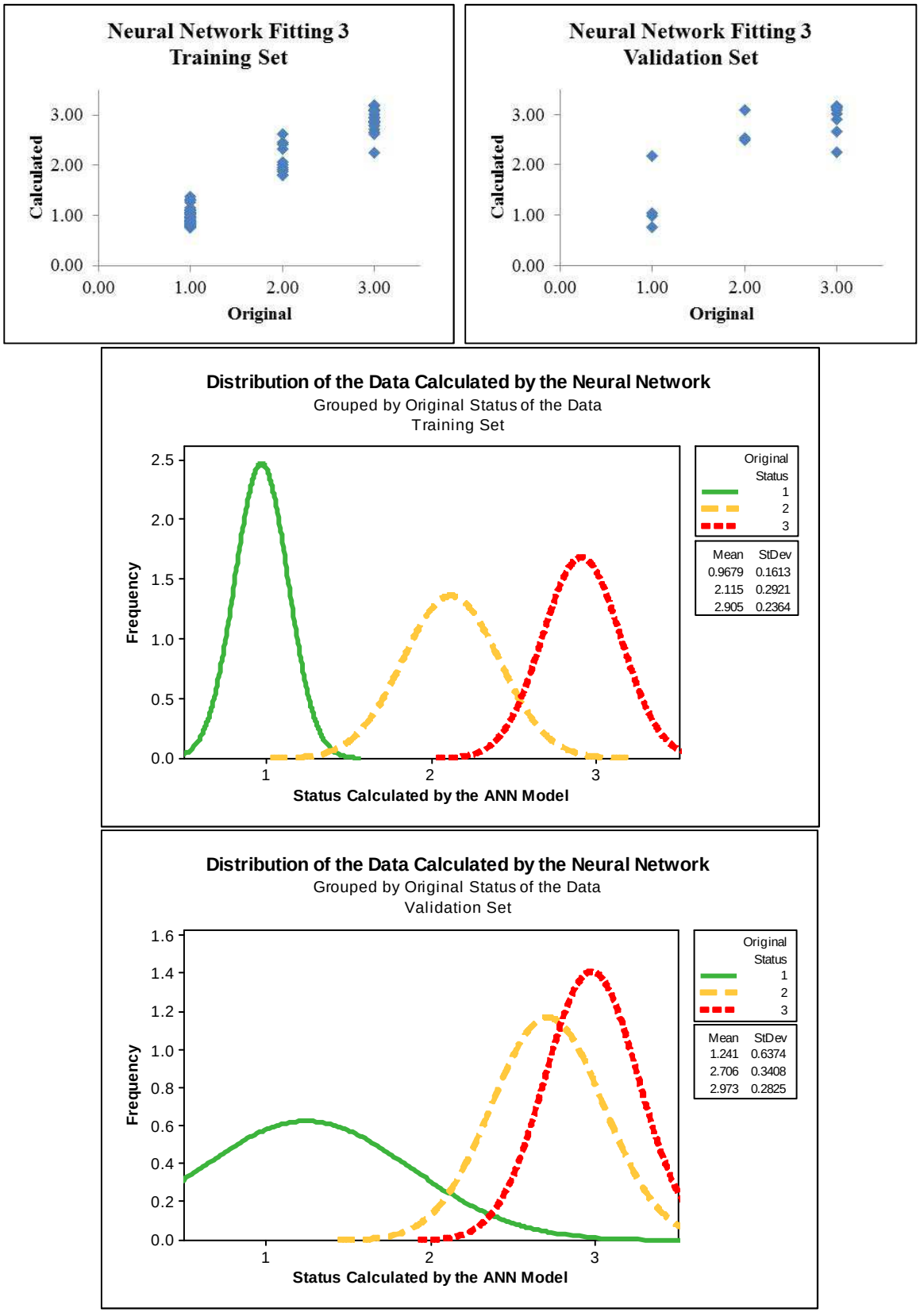

Figure 43: Comparison between calculated status by the neural network model in fitting 3 and original status of the data.

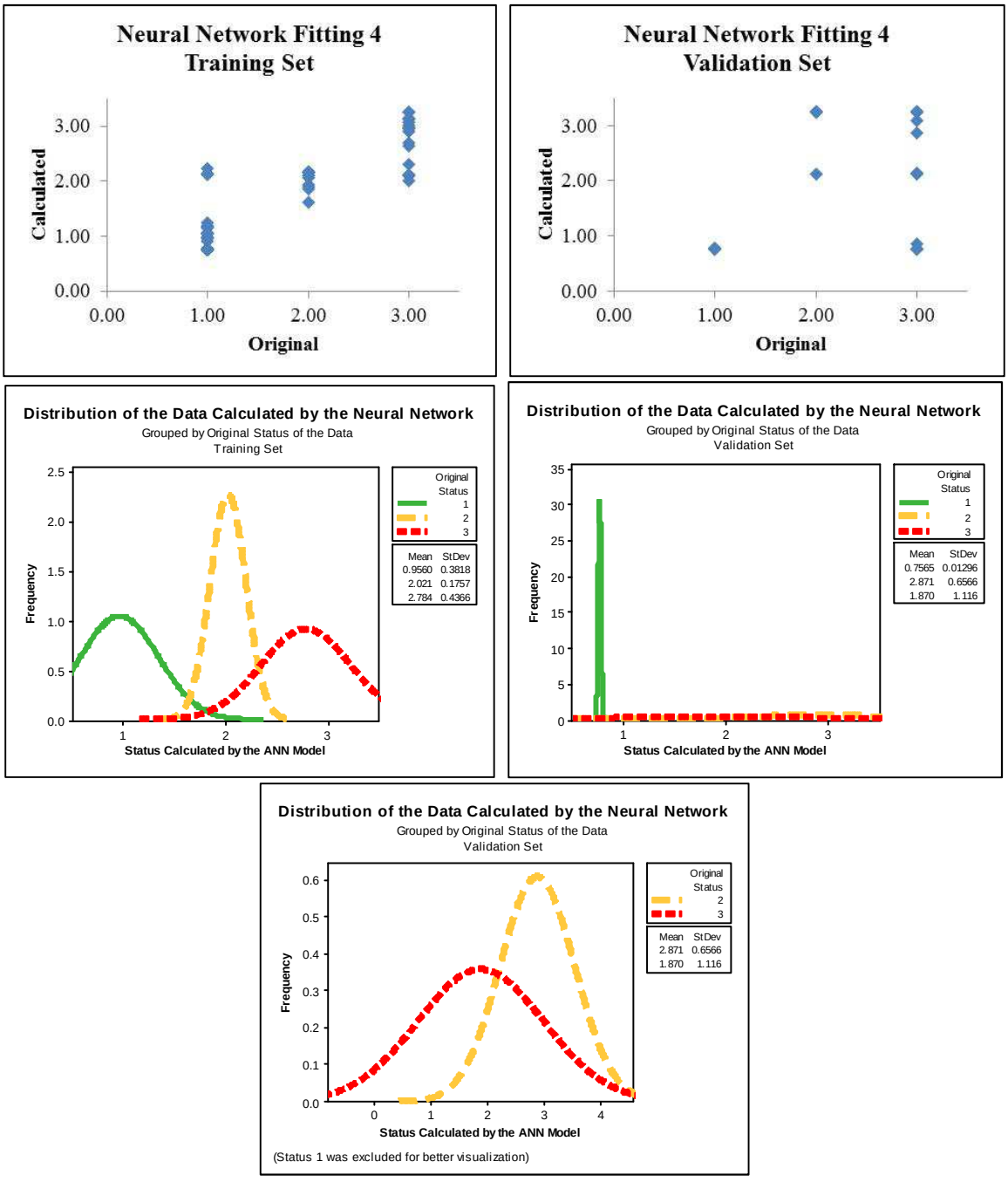

Figure 44: Comparison between calculated status by the neural network model in fitting 4 and original status of the data.

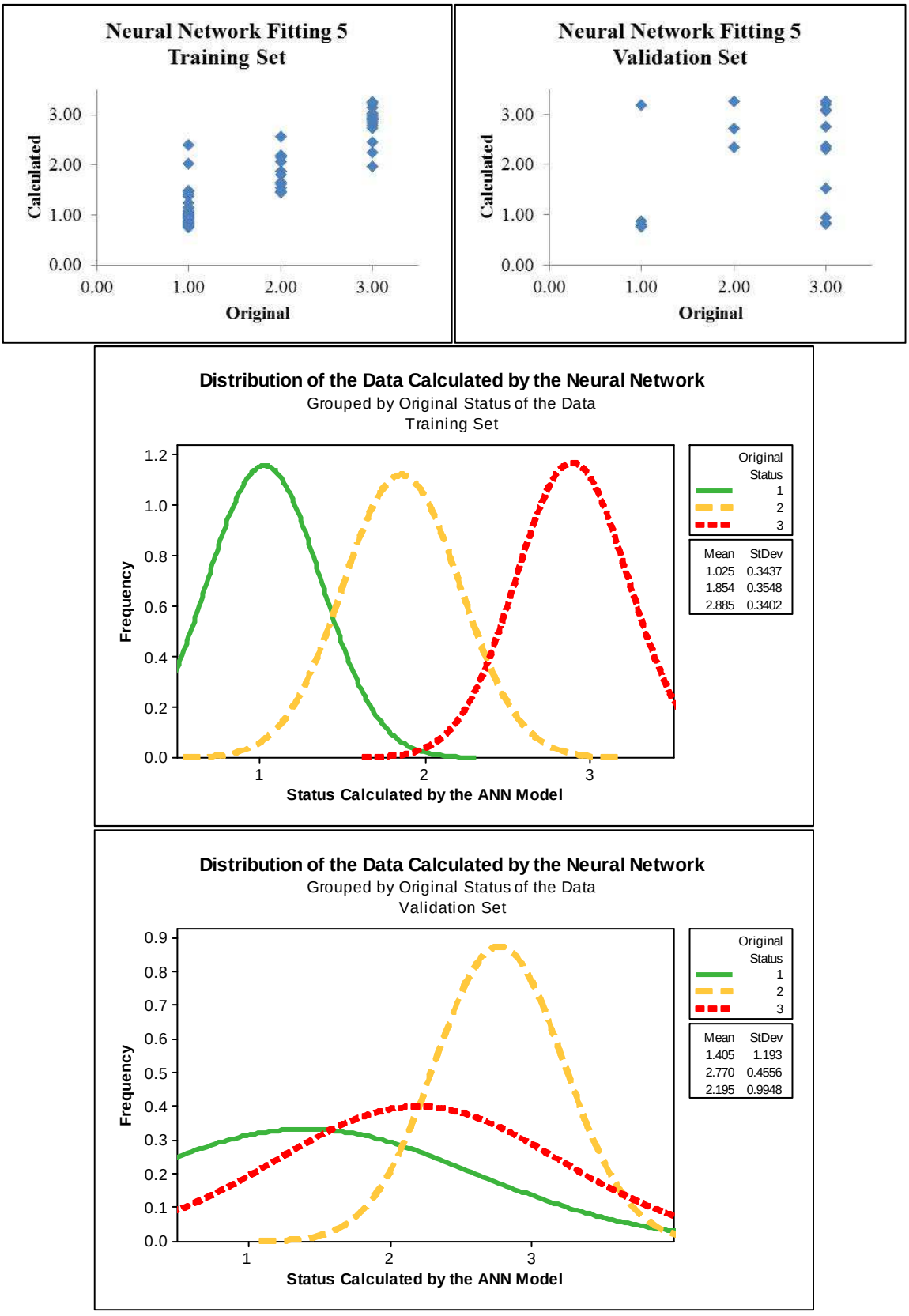

Figure 45: Comparison between calculated status by the neural network model in fitting 5 and original status of the data.

The interpretation of these results lead to hypotheses that are similar to the ones stated in the previous item, which are:

- *The data were not correctly classified by machine operators and actually should have received a different status classification*. If this hypothesis is true, then a new method is needed for quality monitoring of MWF.
- *The data were correctly classified by machine operators*. If this is true, then there may exist subjective or unmeasured variables besides the currently measured ones that may have affected the status classification.

Therefore, whatever the true hypothesis, the development of a new method for monitoring the aging of MWF seems necessary.

5.8.3. Coupling of the Spectroscopic Sensor and a Neural Network Model for the Monitoring of MWF Emulsion Destabilization

The present approach is based on the results obtained with a similar coupling, as described in item 5.7 of this thesis. Thus, the specific objective in this study is to use the ability of the neural network model to rebuild the droplet size distribution of the MWF emulsion from spectroscopic data, and then to adopt the presence of the population of coalesced droplets as an indicator of destabilization. The appearance of this second droplet population is shown in Figures 32a and 32b during the process of artificial destabilization of MWF emulsions.

With this purpose, a three-layer feed-forward neural network like the one presented in Figure 12 was used to fit the experimental data. A total of 27 variables were used as inputs: 23 absorbance values selected from 402 nm to 690 nm, arbitrarily selected in 12 nm intervals – larger intervals did not provide good results, as well as variables selected by PCA analysis –, MWF concentration, pH, calculated value for the wavelength exponent and linear coefficient obtained in the linear fitting used in the calculation of the wavelength exponent. Although the linear coefficient does not appear to have a physical meaning, apparently it has helped to discriminate

the spectra from different fluids. In fact, the optical properties of the fluids would be a more suitable option, but it was not possible to have access to this information, especially because these fluids are formulated from a number of substances, and the formulation itself is not made available by the MWF producers. As previously mentioned, although the previous studies showed the limitation of the application of the wavelength exponent method, the decrease of its accuracy with the increase of droplet size may have high impact in simpler systems, like the one previously studied, where other variables were probably providing equivalent information, but these measurements may still contribute to the evaluation of more complex systems, like in this long-term monitoring experiment, where the spectra are very noisy.

In the present study, data from all fluids and machines were used to fit one model, only. The outputs of the neural network consisted of 20 sizes classes, from 0.04 μm to 26.7 μm, ordered as multiples of $\sqrt{2}$. As in the previous fitting (item 5.6), this number of size classes was arbitrarily adopted in order to reconstruct the DSD of the samples with an appropriate resolution. The best fitting was obtained with 10 neurons in the hidden layer, after 50000 presentations of the data set to the neural network.

Figures 46 and 47 show representative results obtained in the fitting and validation of the model, for samples with different DSD characteristics, which correspond to different aging times, or status. The graphs at the left show the light extinction spectra of the MWF emulsions, as measured with the spectroscopic sensor, and the graphs at the right show the corresponding DSD (measured values and calculated by the neural network model). These figures show that the differences in the measured spectra are not clearly observed by visually, possibly due to the presence of contaminants from the machining process, as well as due to differences in the optical properties of the different MWFs. However, still it is possible to observe some evolution of the measured spectra with the destabilization of the emulsion.

In terms of the estimated DSD, good agreement between calculated and experimental values was obtained for 94% of the samples, for monomodal and bimodal distributions, and for different proportions of each droplet population. The rate of success of this fitting was calculated based on the number of observations for

which the relative squared error between calculated and observed values were under 1%.

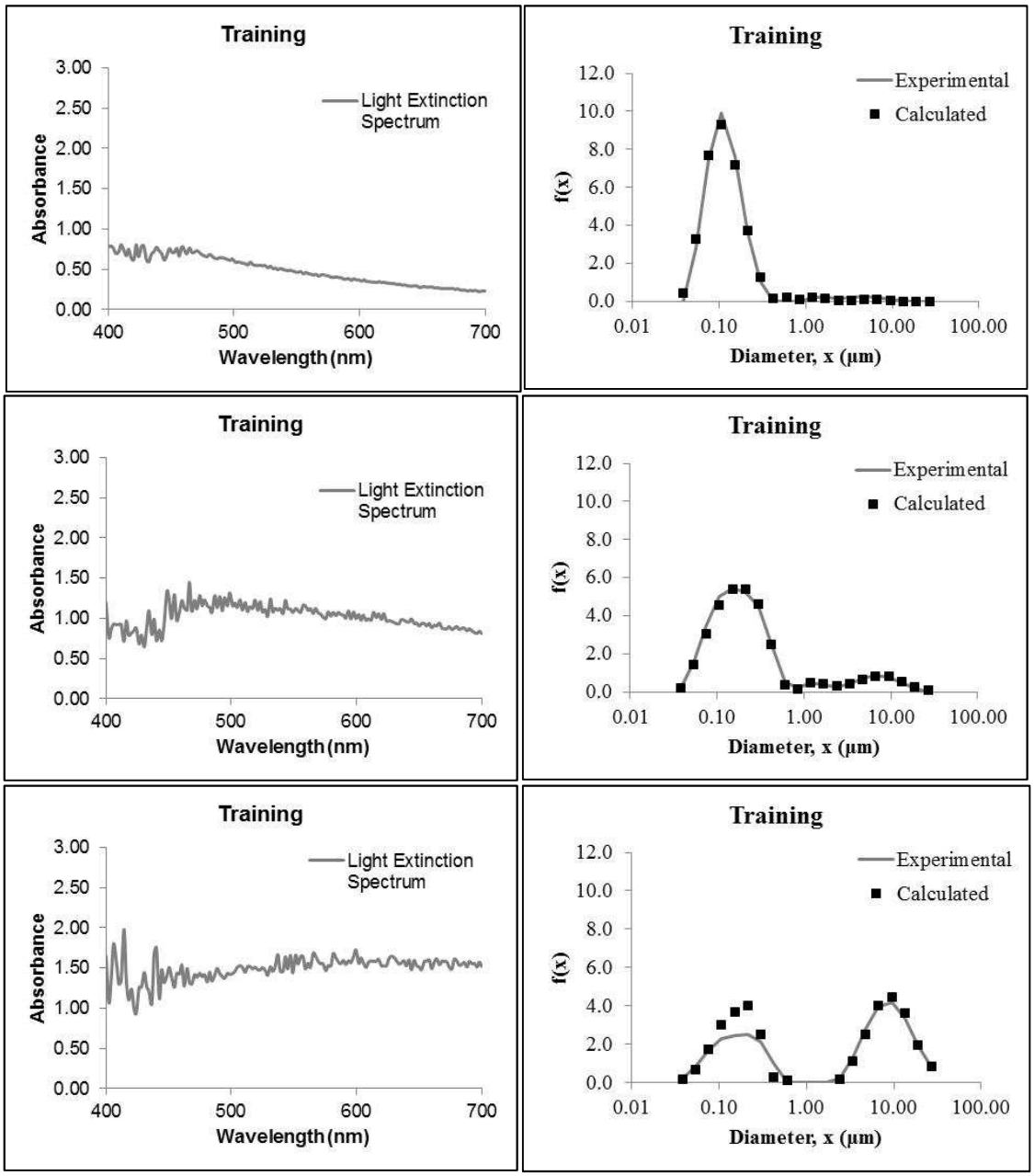

Figure 46: Neural network fitting results for the long-term monitoring study of commercial MWFs in a machining facility, with 27 inputs and 20 outputs (training set).

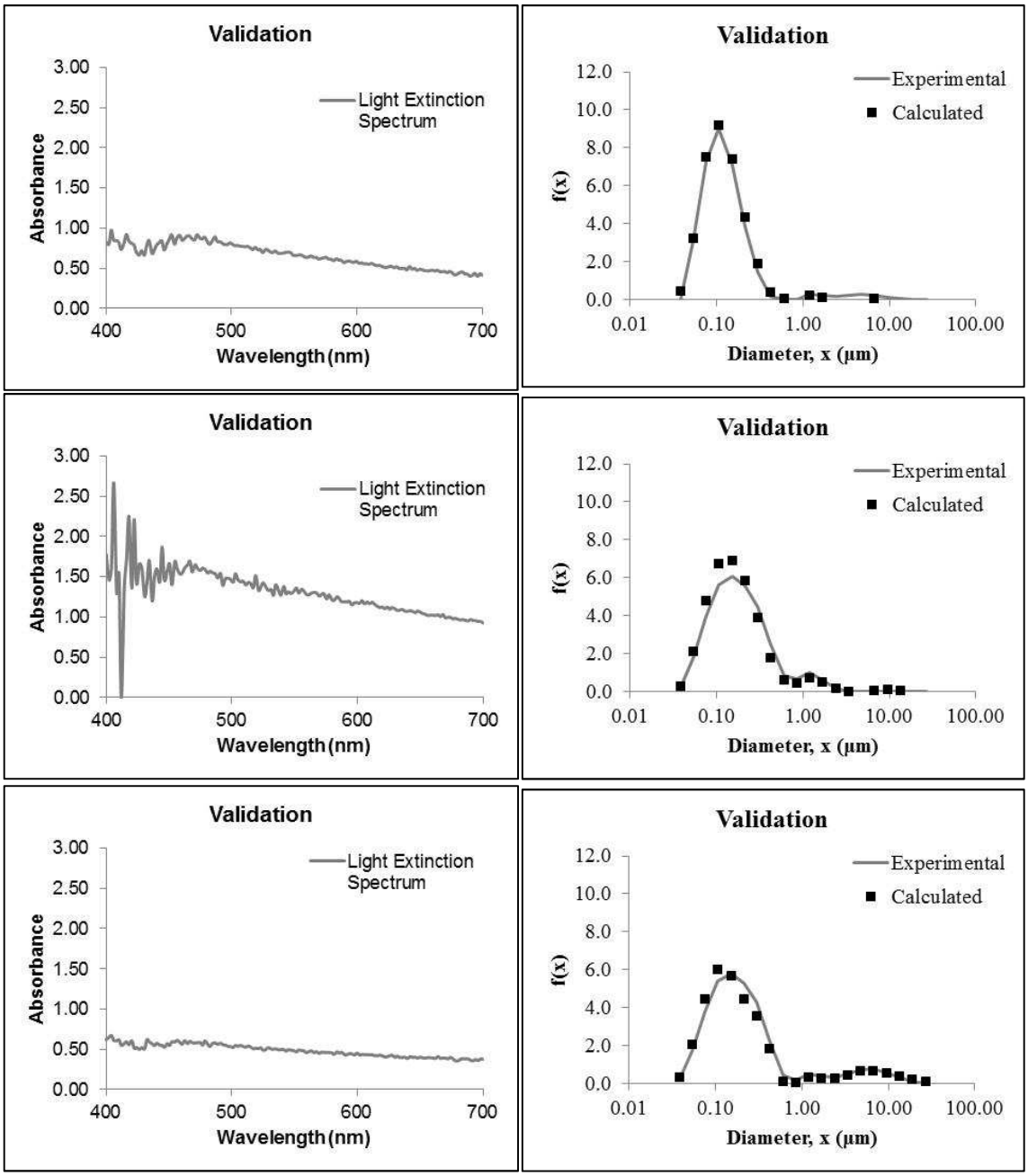

Figure 47: Neural network fitting results for the long-term monitoring study of commercial MWFs in a machining facility, with 27 inputs and 20 outputs (validation set).

Representative results for the 6% of the samples for which the model did not provide the expected result are shown in Figure 48. It is important to mention that in all the cases showing inaccurate results the model predicted the presence of a second population of coalesced droplets, which had not been detected in the measurements. Thus, in all these cases the model provided conservative results, i.e., the model associated the information with an aged MWF emulsion.

As mentioned in previous parts of this thesis, aging during real machining operation in a metalworking facility is complex and not easily detected. Besides microbiological contamination, fluids can be contaminated by solid particles and other oils in the process, and the MWF concentration can change due to water evaporation or new dilutions. An additional factor that can affect the results in this case is the possibly high variability of the collected data, because these data were collected by different machine operators in industrial scale facilities consisting of different metalworking equipments, as described. If these factors are taken into consideration, the resulting fraction of success obtained by the neural network model, i.e., 94% of the observations, can be considered as a satisfactory result for this system.

As reported in this item of the thesis, the neural network model was able to predict the presence of the second population of coalesced droplets in the MWF emulsion samples with a high percentage of success, i.e., for 94% of the observations. Since the formation of a second population with coalesced droplets, i.e., consisting of larger droplets, is an indication of emulsion destabilization, it is of interest that the spectroscopic sensor be able to detect this status in its early steps. Thus, it is of interest that the sensor plus neural network coupling be as sensitive as possible to the formation of this second droplet population. A study aimed at this was carried out, as reported in the next item.

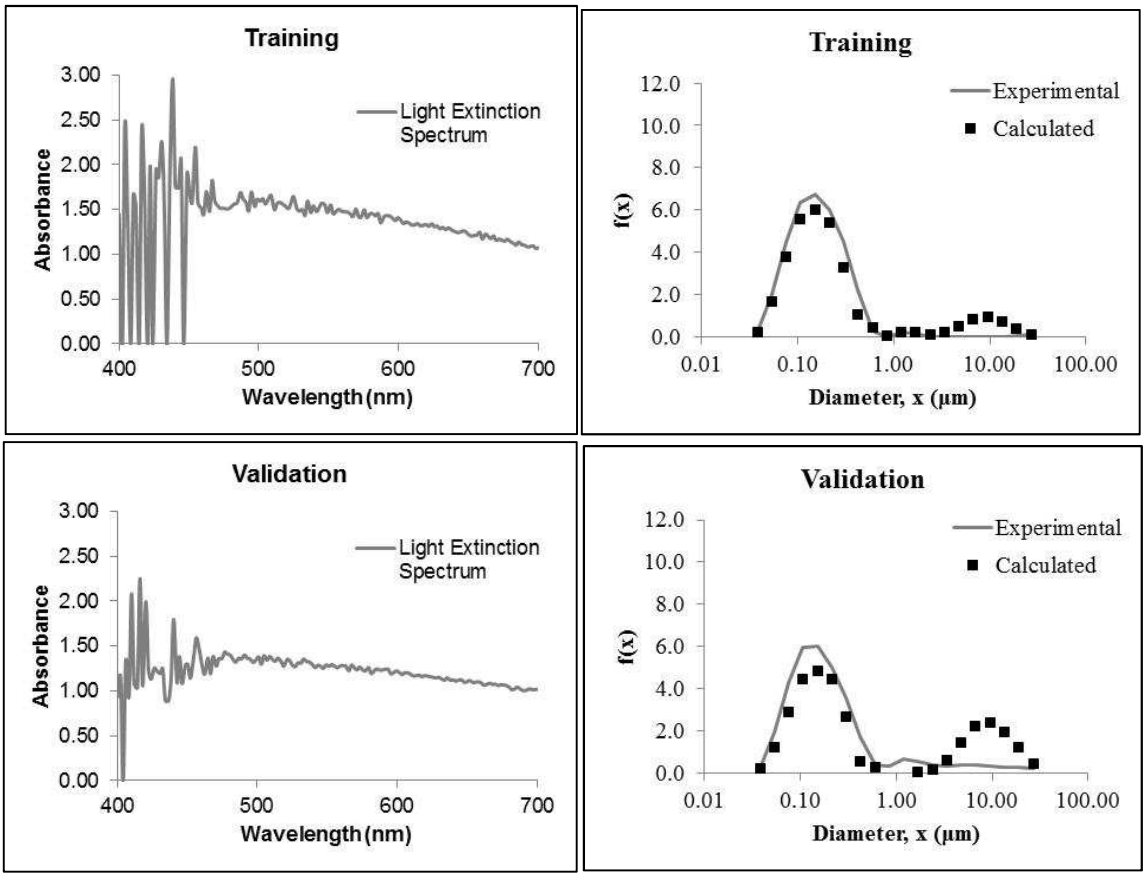

Figure 48: Neural network fitting results for the long-term monitoring study of commercial MWFs in a machining facility, with 27 inputs and 20 outputs (inaccurate fits).

5.8.4. Neural Network Fitting for Rebuilding Droplet Size Distribution of the MWF Using an Alternative Fitting Criterion

All the neural network models previously used in this study have been fitted to the data based on the conventionally adopted criterion, i.e., minimization of the squared error between calculated and measured values of each output variable, expressed in Equation 18, and repeated here:

$$E = \sum_{m=1}^{r} \sum_{k=1}^{p} \left(y_k^{(m)} - O_k^{(m)} \right)^2 \quad (18)$$

In order to increase the sensitivity of the neural network model, the criterion for model fitting was changed in order to increase the importance of the droplet population formed by coalesced droplets. The squared error in this case is expressed in the form of Equation 39, where *n* is the number of size classes used as outputs.

$$E_{mod} = \sum_{i=1}^{n-1}\left(A_{calc_i} - A_{exp_i}\right)^2 \quad (39)$$

In this equation, A_{calc} is the area under the calculated DSD curve and A_{exp} is the area under the experimental DSD curve, expressed by Equations 40 and 41.

$$A_{calc_i} = \left(\frac{y_{i+1}-y_i}{2}\right)_{calc}^2 . \Delta x_i \quad (40)$$

$$A_{exp_i} = \left(\frac{y_{i+1}-y_i}{2}\right)_{exp}^2 . \Delta x_i \quad (41)$$

In the present study the area under the DSD curve for the coalesced particles is much larger than the one for the smaller droplets because the size intervals increase as multiples of $\sqrt{2}$, and are thus larger for larger droplet sizes. This makes the squared error (Equation 39) much more sensitive to the formation of coalesced droplets.

Using this modified network, it was possible to reduce the total number of inputs to 12 variables: 8 absorbance values arbitrarily selected in 40 nm intervals, in the range of 402 nm to 690 nm, MWF concentration, pH, calculated value for the wavelength exponent and linear coefficient obtained in the calculation of the wavelength exponent. Once more, although the linear coefficient does not have a physical meaning, apparently it has helped to discriminate data from different fluids due to the lack of information on the optical properties of the MWF fluids. Data from

all fluids and machines were used to fit one single neural network model. As outputs of the neural network, 20 sizes classes were selected, from 0.04 μm to 26.7 μm, as multiples of $\sqrt{2}$. As in previous items, this number of size classes was arbitrarily adopted in order to reconstruct the DSD of the samples with appropriate resolution. The best fitting was obtained with 10 neurons in the hidden layer, after 50000 presentations of the data set to the neural network.

Figures 49 and 50 show results obtained in the fitting and validation of the model, for samples with different DSD and consequently different aging times, which are representative of the whole set. The graphs in the left represent the light extinction spectrum of the emulsion, measured with the spectroscopic sensor, and the graphs in the right represent the corresponding DSD (measured distribution and distribution calculated by the model). The change of the measured spectra with the increase of droplet size may not be so easily seen due to the presence of contaminants from the machining process, as well as differences between optical properties of the different MWFs, but still it is possible to observe some evolution of the measured spectra with the destabilization of the emulsion.

The modification of the ANN in the fitting criterion for the NN model from Equation 18 to Equation 39 resulted in improved agreement between calculated and experimental values of the DSD curves for all samples with monomodal and bimodal distributions and different proportions of each droplet population. Thus, the data from the 7 different MWF, collected from the described machining facility were successfully fitted by using a single ANN model. The data from the spectroscopic sensor, as well as all other inputs to the model can be easily obtained in any machining process. As a consequence of this configuration, a system consisting of the spectroscopic sensor coupled with a neural network model can be used to detect the emulsion destabilization in its early steps, by associating this with the presence of the second droplet population. Such a system can be adjusted for *in-line* and real-time measurements.

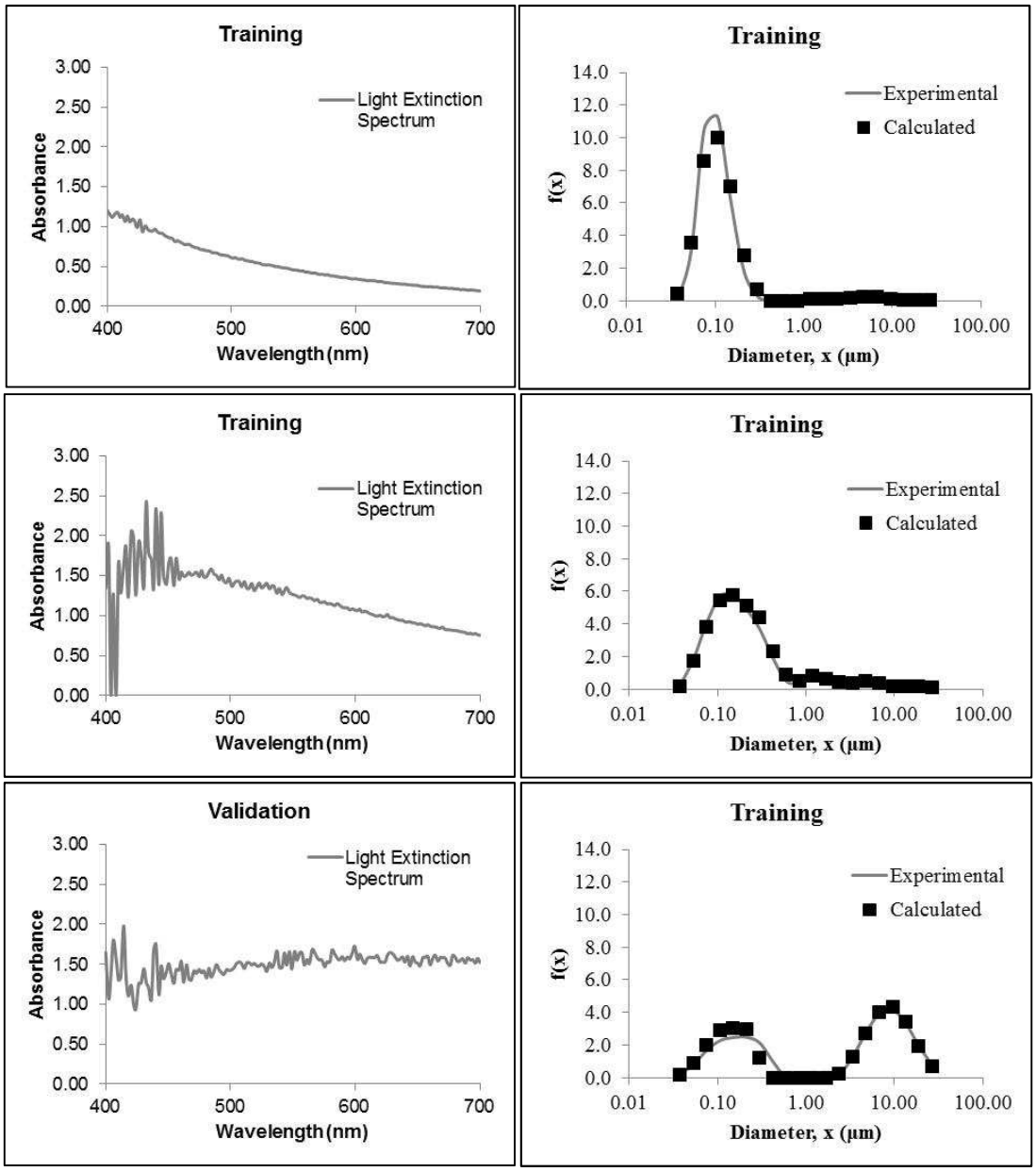

Figure 49: Neural network fitting results for the long-term monitoring study of commercial MWFs in a machining facility, using an alternative fitting criterion, with 12 inputs and 20 outputs (training set).

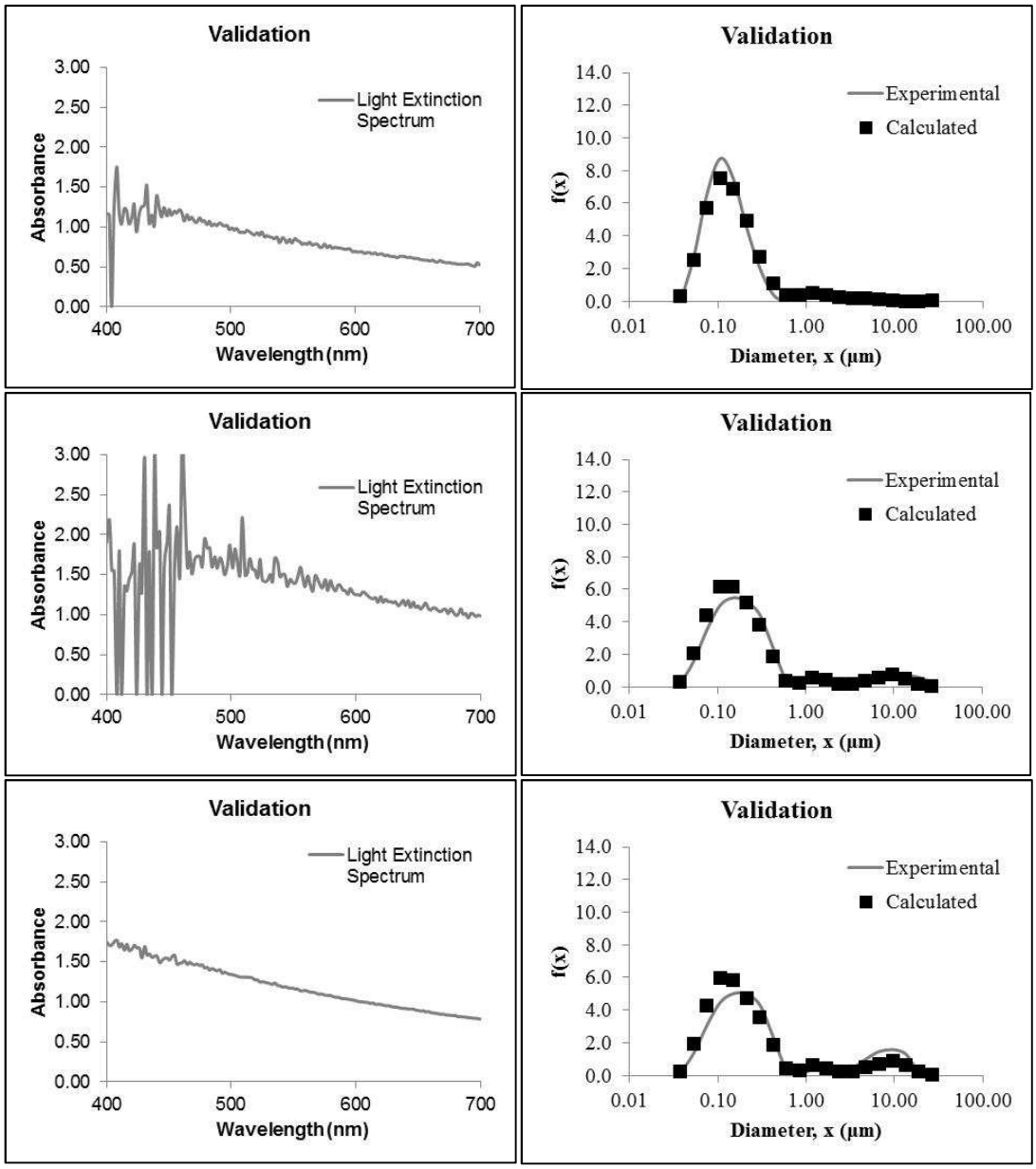

Figure 50: Neural network fitting results for the long-term monitoring study of commercial MWFs in a machining facility, using an alternative fitting criterion, with 12 inputs and 20 outputs (validation set).

6. CONCLUSIONS

Monitoring MWFs quality in machining process is critical for the control of process and product quality, and the conventional methods of quality control in machining facilities may not be the best alternative to provide the optimal useful life of these emulsions, with high impact in costs.

Literature suggests that the monitoring of emulsion destabilization could possibly be used as a better indicator of potential losses in MWFs performance. One possible method deals with the droplet size distribution, which is directly linked to the quality and physical stability of an emulsion. Thus, changes in DSD can be used as an indicator of partial destabilization of an emulsion.

Since changes in the DSD of an emulsion can cause changes in the light extinction spectra in spectroscopic measurements, one simple method of evaluating these changes is based on the so called wavelength exponent, *z*. The applicability of the wavelength exponent measurement as an indication of the emulsion stability was investigated in this thesis by monitoring both the turbidity spectra and the DSD of emulsions over time, for artificially aged MWF samples, as well as by evaluating the time evolution of the wavelength exponent and the quality of the fitting to the experimental data.

The results have shown that the wavelength exponent decreases gradually with the increase in the volumetric mean diameter of the droplets, which is in agreement with information in the literature. However, the destabilization of the MWF leads to the formation of a bimodal DSD, resulting in a significant reduction in the quality of the fitting to the data, expressed by the coefficient of determination, R^2, when the volumetric mean diameter, $D_{4.3}$, reaches approximately 1μm. The use of the wavelength exponent has been proposed under the assumption of a monomodal and monodisperse distribution and the decrease in its value with time has been associated with the growth in droplet size by coalescence. Thus, the droplet size of the emulsion may be a limitation for the use of this method, since the reduction in the

fitting quality reduces the reliability of the value obtained for *z* and, consequently, the reliability of this method in the evaluation of emulsion destabilization.

In this study, an alternative approach is proposed for the monitoring of MWF destabilization, based on neural network models for obtaining DSD of emulsions using the data from the spectroscopic sensor. This approach was tested with rapeseed oil emulsions and with artificially aged MWF. The results based on the fitting of neural network models showed that the combination of a UV/Vis spectroscopic system with a neural network results in an optical sensor, which is capable of detecting changes in the volumetric mean diameter, variance of droplet size distributions and DSD during aging of commercial MWF, as well as changes in DSD of rapeseed oil emulsions prepared in laboratory. However, the obtained models are limited to a set of inputs that may not be available in common applications; due to the high variability of the data in rapeseed oil emulsions and the addition of $CaCl_2$ to promote artificial aging of MWF. Nevertheless, these results pointed out the potential of this technique for monitoring such emulsions, with the advantage that apparently the results are not affected by multiple scattering, suggesting that this approach may even be applied to more concentrated emulsions.

In order to check the applicability of this method, a long-term monitoring study of commercial MWFs in a machining facility was carried out with the objective of obtaining information on the performance of the spectroscopic probe plus neural network as a sensor for monitoring MWF destabilization under long-term operation of machining equipment. In this campaign, the condition of the MWF was classified in three different categories by operation personnel based on routine analyses and experience. This classification is the current method of monitoring aging of MWF in this machining facility; however, a statistical analysis of these data based on multivariate discriminant analysis indicated that there is much confusion in the classification results, possibly indicating some failures in the current method of MWF monitoring. These results have motivated the development of a new method for monitoring aging of MWF, based on the fitting of a neural network model as a pattern recognition technique, to rebuild the droplet size distribution of the MWF emulsions from spectroscopic data, and then to adopt the presence of the population of coalesced droplets as an indicator of destabilization.

The obtained results on the fitting of long-term monitoring data have shown good agreement between calculated and experimental values for 94% of the samples, with monomodal and bimodal distributions and different proportions of each droplet population. This resulting fraction of success obtained by the neural network model can be considered as a satisfactory result for this system, however, the formation of a second population with coalesced droplets, i.e., consisting of larger droplets, is an indication of emulsion destabilization, so it is of interest that the sensor plus neural network coupling be as sensitive as possible to the formation of this second droplet population.

For this reason, the program for the fitting of ANN was modified for using a new criterion for the minimization of the error, considering the differences between experimental and calculated area under the DSD curve, which is a criterion more sensitive to the presence of bigger droplets, so it will be more accurate in evaluating emulsion destabilization. The obtained results on the fitting of long-term monitoring data with the modified fitting criterion of the ANN resulted in improved agreement between calculated and experimental values of the DSD curves for all samples with monomodal and bimodal distributions and different proportions of each droplet population. Thus, the data from the 7 different MWF, collected from the described machining facility were successfully fitted by using a single ANN model. The data from the spectroscopic sensor, as well as all other inputs to the model can be easily obtained in any machining process. As a consequence of this configuration, a system consisting of the spectroscopic sensor coupled with a neural network model can be used to detect the emulsion destabilization in its early steps, by associating this with the presence of the second droplet population. Such a system can be adjusted for in-line and real-time measurements, providing a tool for enabling the optimization of MWF service life. This is a new method for monitoring such emulsions with possible applications in similar systems, such as pharmaceutical products, emulsion polymerization processes, crystallization processes, among others.

REFERENCES

ABISMAÏL, B. et al. Emulsification by ultrasound: drop size distribution and stability. **Ultrasonics sonochemistry**, v. 6, n. 1-2, p. 75–83, mar. 1999.

ANGSTRÖM, A. On the Atmospheric Transmission of Sun Radiation II. **Geografiska Annaler**, v. 12, p. 130–159, 1930.

ASSENHAIMER, C. et al. Use of a spectroscopic sensor to monitor droplet size distribution in emulsions using neural networks. **The Canadian Journal of Chemical Engineering**, v. 92, n. 2, p. 318–323, 14 fev. 2014.

ASTM D3707. **Standard Test Method for Storage Stability of Water-in-Oil Emulsions by the Oven Test**PhiladelphiaAmerican Society for Testing and Materials (ASTM), , 2010.

ASTM D3709. **Standard Test Method for Stability of Water-in-Oil Emulsions Under Low to Ambient Temperature Cycling Conditions**PhiladelphiaAmerican Society for Testing and Materials (ASTM), , 2010.

BENITO, J. M. et al. Formulation, characterization and treatment of metalworking oil-in-water emulsions. **Clean Technologies and Environmental Policy**, v. 12, p. 31–41, 2010.

BERDNIK, V. V. et al. Characterization of spherical particles using high-order neural networks and scanning flow cytometry. **Journal of Quantitative Spectroscopy and Radiative Transfer**, v. 102, n. 1, p. 62–72, nov. 2006.

BERDNIK, V. V.; LOIKO, V. A. Particle sizing by multiangle light-scattering data using the high-order neural networks. **Journal of Quantitative Spectroscopy and Radiative Transfer**, v. 100, n. 1-3, p. 55–63, jul. 2006.

BOHREN, C.F., HUFFMAN, D. . **Absorption and scattering of light by small particles**. New York: [s.n.].

BRINKSMEIER, E. et al. Current Approaches in Design and Supply of Metalworking Fluids. **Tribology Transactions**, v. 52, n. 5, p. 591–601, 2009.

BYERS, J. P. **Metalworking Fluids**. 2. ed. Boca Raton: CRC Press, 2006.

CELIS, M.; GARCIA-RUBIO, L. H. Continuous Spectroscopy Characterization of Emulsions. **Journal of Dispersion Science and Technology**, v. 23, n. 1, p. 293–299, 2002.

CELIS, M.; GARCIA-RUBIO, L. H. Characterization of Emulsions: A Systematic Spectroscopy Study. **Journal of Dispersion Science and Technology**, v. 29, n. 1, p. 20–26, jan. 2008.

CELIS, M.-T. et al. Spectroscopy measurements for determination of polymer particle size distribution. **Colloids and Surfaces A: Physicochemical and Engineering Aspects**, v. 331, n. 1-2, p. 91–96, dez. 2008.

CELIS, M.-T.; GARCIA-RUBIO, L. H. Stability of Emulsions from Multiwavelength Transmission Measurements. **Industrial & Engineering Chemistry Research**, v. 43, n. 9, p. 2067–2072, abr. 2004.

CHANAMAI, R.; MCCLEMENTS, D. J. Dependence of creaming and rheology of monodisperse oil-in-water emulsions on droplet size and concentration. **Colloids and Surfaces A: Physicochemical and Engineering Aspects**, v. 172, n. 1-3, p. 79–86, out. 2000.

CHENG, C.; PHIPPS, D.; ALKHADDAR, R. M. Treatment of spent metalworking fluids. **Water research**, v. 39, n. 17, p. 4051–63, out. 2005.

CHESTNUT, M. H. Confocal microscopy of colloids. **Current Opinion in Colloid & Interface Science**, v. 2, p. 158–161, 1997.

CHISTYAKOV, B. E. Theory and practical application aspects of surfactants. In: V.B. FAINERMAN, D. M. AND R. M. (Ed.). . **Studies in Interface Science**. 1st ed. ed.Oxford: Elsevier, 2001. p. 511–618.

COUPLAND, J. N.; JULIAN MCCLEMENTS, D. Droplet size determination in food emulsions: comparison of ultrasonic and light scattering methods. **Journal of Food Engineering**, v. 50, n. 2, p. 117–120, nov. 2001.

DELUHERY, J.; RAJAGOPALAN, N. A turbidimetric method for the rapid evaluation of MWF emulsion stability. **Colloids and Surfaces A: Physicochemical and Engineering Aspects**, v. 256, n. 2-3, p. 145–149, abr. 2005.

DICKINSON, E. Interfacial interactions and the stability of oil-in-water emulsions. **Pure and Applied Chemistry**, v. 64, n. 11, p. 1721–1724, 1992.

DOLL, K. M.; SHARMA, B. K. Emulsification of chemically modified vegetable oils for lubricant use. **Journal of Surfactants and Detergents**, v. 14, p. 131–138, 2011.

EGGER, H.; MCGRATH, K. M. Aging of oil-in-water emulsions: The role of the oil. **Journal of Colloid and Interface Science**, v. 299, p. 890–899, 2006.

EL BARADIE, M. A. Cutting Fluids Part 1: Characterisation. **Journal of Materials Processing Technology**, v. 56, p. 786–797, 1996.

ELICABE, G. E.; GARCIA-RUBIO, L. H. Latex Particle Size Distribution From Turbidimetry Using a Combination of Regularization Techniques. **Advances in Chemistry Series**, v. 227, p. 83–104, 1990.

GLASSE, B. et al. Turbidimetric Spectroscopy for the Evaluation of Metalworking Fluids Stability. **Tribology Transactions**, v. 55, n. 2, p. 237–244, mar. 2012.

GLASSE, B. et al. Analysis of the Stability of Metal Working Fluid Emulsions by Turbidity Spectra. **Chemical Engineering & Technology**, v. 36, n. 7, p. 1202–1208, 6 jul. 2013.

GLASSE, B. et al. Turbidimetry for the stability evaluation of emulsions used in machining industry. **The Canadian Journal of Chemical Engineering**, v. 92, n. 2, p. 324–329, 31 fev. 2014.

GLASSE, B. **Monitoring of Metal Working Fluid Emulsion Quality by in-process Light Spectroscopy**. [s.l.] Universität Breman, 2015.

GREELEY, M.; RAJAGOPALAN, N. Impact of environmental contaminants on machining properties of metalworking fluids. **Tribology International**, v. 37, p. 327–332, 2004.

GROSCHE, L. C. **Study of the interactions between emulsion flow and a spectrometer probe based on numerical simulations**. [s.l.] Universidade de São Paulo, 2014.

GUARDANI, R.; NASCIMENTO, C. A. O. **Análise Estatística Multivariada Aplicada a Processos Químicos - Técnicas de Discriminação e de Classificação de Dados**São PauloUniversidade de São Paulo, , 2007.

GUARDANI, R.; NASCIMENTO, C. A. O.; ONIMARU, R. S. Use of neural networks in the analysis of particle size distribution by laser diffraction: tests with different particle systems. **Powder Technology**, v. 126, n. 1, p. 42–50, jun. 2002.

GUIMARÃES, A. P. et al. Destabilization and Recuperability of Oil Used in the Formulation of Concentrated Emulsions and Cutting Fluids. **Chemical and Biochemical Engineering Quarterly**, v. 24, n. 1, p. 43–49, 2010.

HARUSAWA, F.; MITSUI, T. Stability of emulsions. **Progress in Organic Coatings**, 1975.

HASS, R. et al. Optical monitoring of chemical processes in turbid biogenic liquid dispersions by Photon Density Wave spectroscopy. **Analytical and Bioanalytical Chemistry**, v. online, p. 1–12, 2015.

HAYKIN, S. **Neural Networks: A Comprehensive Foundation**. 2. ed. New Jersey: Prentice Hall, 1999.

HIEMENZ, P. C.; RAJAGOPALAN, R. **Principles of Colloid and Surface Chemistry**. Third ed.New York: CRC Press, 1997.

HOLLINGSWORTH, K. G. et al. Fast emulsion droplet sizing using NMR self-diffusion measurements. **Journal of Colloid and Interface Science**, v. 274, n. 1, p. 244–250, 2004.

JOHNS, M. L.; HOLLINGSWORTH, K. G. Characterisation of emulsion systems using NMR and MRI. **Progress in Nuclear Magnetic Resonance Spectroscopy**, v. 50, n. 2-3, p. 51–70, mar. 2007.

JOHNSON, R. A.; WICHERN, D. W. **Applied Multivariate Statistical Analysis**. 6th. ed. Upper Saddle River: Prentice-Hall, 2007.

JOLLIFFE, I. T. **Principal Component Analysis**. New York: Springer, 1986.

JUNG, C. H.; KIM, Y. P. Simplified Analytic Model to Estimate the Ångstrom Exponent in a Junge Aerosol Size Distribution. **Environmental Engineering Science**, v. 27, n. 9, p. 789–795, 2010.

KEMP, S. J.; ZARADIC, P.; HANSEN, F. An approach for determining relative input parameter importance and significance in artificial neural networks. **Ecological Modelling**, v. 204, n. 3-4, p. 326–334, jun. 2007.

KIOKIAS, S.; RESZKA, A. A.; BOT, A. The use of static light scattering and pulsed-field gradient NMR to measure droplet sizes in heat-treated acidified protein-stabilised oil-in-water emulsion gels. **International Dairy Journal**, v. 14, n. 4, p. 287–295, 2004.

KLOCKE, F.; EISENBLÄTTER, G. Dry Cutting. **Annals of CIRP**, v. 46, n. 2, p. 519–526, 1997.

LAWRENCE, S.; GILES, C. L.; TSOI, A. C. **Lessons in neural network training: overfitting may be harder than expected** (AAAI Press, Ed.)14th National Conference on Artificial Intelligence. **Anais**...Menlo Park: AAAI Press, 1997

MACHADO, A. R.; WALLBANK, J. The effect of extremely low lubricant volumes in machining. **Wear**, v. 210, n. 1-2, p. 76–82, set. 1997.

MCCLEMENTS, D. J.; COUPLAND, J. N. Theory of droplet size distribution measurements in emulsions using ultrasonic spectroscopy. **Colloids and Surfaces A: Physicochemical and Engineering Aspects**, v. 117, n. 1-2, p. 161–170, out. 1996.

MIE, G. Beiträge zur Optik trüber Medien, speziell kolloidaler Metallösungen. **Annalen der Physik**, v. 330, n. 3, p. 377–445, 1908.

MOLLET, H.; GRUBENMANN, A. **Formulation Technology: Emulsions, Suspensions, Solid Forms**. 1st. ed. Weinheim: Wiley-VCH Verlag GmbH & Co. KGaA, 2001.

MORRISON, I. D.; ROSS, S. **Colloidal Dispersions – suspensions, emulsions and foams**. 1 edition ed.New York: Wiley-Interscience, 2002.

NASCIMENTO, C. A. O.; GUARDANI, R.; GIULETTI, M. Use of Neural Networks in the Analysis of Particle Size Distribution by Laser Diffraction. **Powder Technology**, v. 90, p. 89–94, 1997.

NOVALES, B. et al. Characterization of emulsions and suspensions by video image analysis. **Colloids and Surfaces A: Physicochemical and Engineering Aspects**, v. 221, n. 1-3, p. 81–89, 2003.

OLIVEIRA, J. F. G. DE; ALVES, S. M. Adequação ambiental dos processos usinagem utilizando Produção mais Limpa como estratégia de gestão ambiental. **Produção**, v. 17, n. 1, p. 129–138, abr. 2007.

REDDY, S. R.; FOGLER, H. S. Emulsion stability: Determination from Turbidity. **Journal of colloid and interface science**, v. 79, n. 1, p. 101–104, 1981.

RUMMELHART, D., MCCLELLAND, J. **Parallel distributed processing explorations in the microstructure of cognition**. [s.l: s.n.].

SEINFELD, J. H.; PANDIS, S. N. **Atmospheric Chemistry and Physics From Air Pollution to Climate Change**. [s.l: s.n.].

SONG, M. et al. Rapid Evaluation of Water-in-Oil (w/o) Emulsion Stability by Turbidity Ratio Measurements. **Journal of colloid and interface science**, v. 230, n. 1, p. 213–215, 1 out. 2000.

TÁPIA, M. **Redes neurais artificiais: uma aplicação na previsão de preços de ovos**. [s.l.] Universidade Federal de Santa Catarina, 2000.

VARGAS, A. K. N. et al. Use of biowaste-derived biosurfactants in production of emulsions for industrial use. **Industrial and Engineering Chemistry Research**, v. 53, p. 8621–8629, 2014.

VARGAS, A. K. N. **Study of emulsion stability using computational fluid dynamics**. [s.l.] Universidade de São Paulo, 2014.

VIÉ, R.; JOHANNET, A.; AZÉMA, N. Settling of mineral aqueous suspensions. Classification and stability prediction by neural networks. **Colloids and Surfaces A: Physicochemical and Engineering Aspects**, v. 459, p. 202–210, 2014.

WILDE, P. J. Interfaces: Their role in foam and emulsion behaviour. **Current Opinion in Colloid and Interface Science**, v. 5, n. 3-4, p. 176–181, 2000.

ZIMMERMAN, J. B. et al. Design of Hard Water Stable Emulsifier Systems for Petroleum- and Bio-based Semi-synthetic Metalworking Fluids. **Environmental Science and Technology**, v. 37, n. 23, p. 5278–5288, 2003.

APPENDIX A – Publications Resulting from the Present Study

1. Papers published in journals

- *Use of a spectroscopic sensor to monitor droplet size distribution in emulsions using neural networks*. ASSENHAIMER, C., Machado, L. J., Glasse, B., Fritsching, U., Guardani, R.. Canadian Journal of Chemical Engineering, v. 92, n. 2, p. 318-323, 2014.
- *Turbidimetry for the stability evaluation of emulsions used in machining industry*. Glasse, B., ASSENHAIMER, C., Guardani, R. and Fritsching, U. Canadian Journal of Chemical Engineering, v. 92, n. 2, p. 324-329, 2014.
- *Analysis of the stability of metal working fluid emulsion by turbidity spectra*. Glasse, B., Fritsching, U., ASSENHAIMER, C., Guardani, R.. Chemical Engineering & Technology, v. 36, n. 7, p. 1202-1208, 2013.

2. Oral Presentations

- *Use of a Spectroscopic Sensor to Monitor Droplet Size Distribution in Emulsions Using Neural Networks*. ASSENHAIMER, C., Machado, L. J., Glasse, B., Fritsching, U., Guardani, R. Emulsification: Modeling, Technologies and Application, Lyon (France), November, 2012.
- *Evaluation of emulsion stability using turbidimetry*. Glasse, B., Fritsching, U., ASSENHAIMER, C., Guardani, R. Emulsification: Modeling, Technologies and Application, Lyon (France), November, 2012.
- *Use of a Spectroscopic Sensor to Monitor Emulsion Stability Based on Turbidity Spectra*. ASSENHAIMER, C., Glasse, B., Lisboa, J. S., Fritsching, U., Guardani, R. XIX Congresso Brasileiro de Engenharia Química – COBEQ 2012, Búzios (RJ), September, 2012.
- *Uso da Espectroscopia UV-Visível para Estimar a Distribuição de Tamanho de Gotas em Emulsões Oleosas*. ASSENHAIMER, C., Guardani, R., Paiva, J. L.,

Glasse, B., Fritsching, U. XXXV Congresso Brasileiro de Sistemas Particulados - ENEMP 2011, Vassouras (RJ), October, 2011.

3. Poster Presentations

- *Avaliação do Tratamento de Efluentes Contendo Resíduos de Fluido de Corte por Processo UV-H_2O_2*. ASSENHAIMER, C., Seto, L. N., Guardani, R.. XX Congresso Brasileiro de Engenharia Química – COBEQ 2014. Florianópolis (SC), October, 2014.
- *Estudo da Degradação Térmica de Emulsões de Fluidos de Corte*. Postal, V., Correia, J., ASSENHAIMER, C., Guardani, R.. Congresso Brasileiro de Engenharia Química – COBEQ 2014. Florianópolis (SC), October, 2014.
- *Estudo Comparativo de Técnicas Numéricas de Inversão para Obtenção de Distribuição de Tamanho de Gotas em Emulsões*. Silva, C. F. B., ASSENHAIMER, C., Guardani, R.. Congresso Brasileiro de Engenharia Química – COBEQ 2014. Florianópolis (SC), October, 2014.

APPENDIX B – Exploratory Studies to Estimate the Droplet Size Distribution of Rapeseed Oil Emulsions Based on Optical Models and the Mie Theory

An algorithm based on the model proposed by ELIÇABE and GARCIA-RUBIO (1990) for estimating droplet size distribution in emulsions, as described in Chapter 3.3.2, was used to rebuild the DSD from spectroscopic measurements. The author based his model on the optical model (Equation 2, previously presented) and used regularization techniques and inversion algorithms in data treatment. Based on the referenced paper, an algorithm was written in Matlab® code and used in this study. The script was tested with an artificially estimated distribution and with real rapeseed oil emulsions. For the artificially estimated case, the expected spectra of a droplet population with normal distribution were calculated by the optical model (Equation 2, previously presented) and used in the script for evaluation of the rebuilt DSD.

As shown in Figures B.1 and B.2, the calculated distributions do not correspond to the artificially estimated DSD. This difference may be due difficulties in implementation of the regularization technique and, for the real emulsion, also due to multiple scattering effects, not considered in the optical model. Besides, differences in the optical properties and even numerical limitations of the algorithm can be responsible for the poor agreement observed.

Although further studies could be done in this approach in order to investigate the reason for the poor results and to improve them, a different methodology that was investigated at the same time, based on the association of light scattering spectra and DSD by multivariate calibration techniques, showed better results. Besides, Glasse (2015) have intensively studied the application of several inversion methods for retrieving DSD from the spectroscopic measurements and poor results were obtained for real emulsions like rapeseed oil emulsion and MWF; only synthetic data produced good results. In this way, it was decided to focus only in this second approach, using multivariate calibration techniques, such as neural networks models.

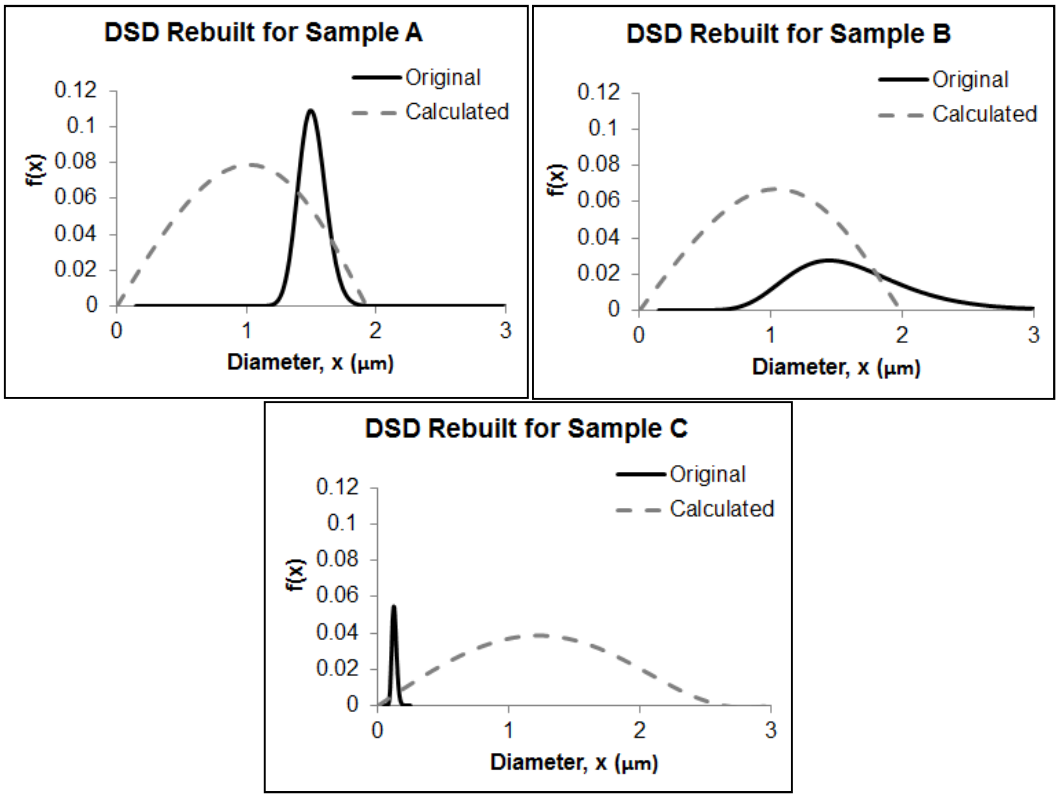

Figure B.1: Theoretical DSD of three emulsions and the corresponding DSD calculated by the algorithm proposed by Eliçabe and Garcia-Rubio (1990).

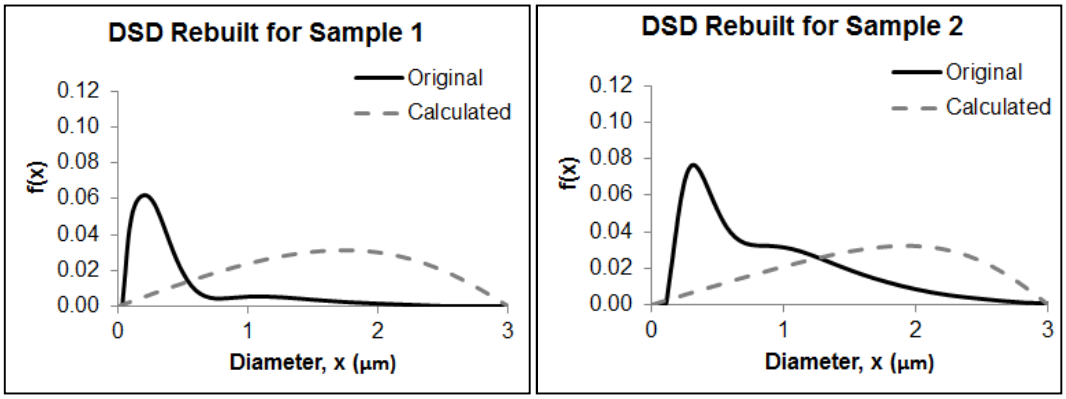

Figure B.2: DSD of two rapeseed oil emulsion samples, measured by Malvern Mastersizer®, and DSD of these samples calculated by the algorithm proposed by Eliçabe and Garcia-Rubio (1990).

APPENDIX C – Algorithm Written in Matlab® Code Based on the Model Proposed by Eliçabe and Garcia-Rubio

The following scripts were used in APPENDIX B for droplet size distribution estimation and are based on the model proposed by Eliçabe and Garcia-Rubio (1990), described in Chapter 3.3.2.

1. Script for Computation of Mie Efficiencies (used in the described tests for estimation of droplet size distribution based on light scattering models and inversion techniques)

```
function result = Mie(m, x)

if x==0
    result=[0 0 0 0 0 1.5];
elseif x>0
    nmax=round(2+x+4*x.^(1/3));
    n1=nmax-1;
    n=(1:nmax);cn=2*n+1; c1n=n.*(n+2)./(n+1); c2n=cn./n./(n+1);
    x2=x.*x;
    f=Mie_ab(m,x);
    anp=(real(f(1,:))); anpp=(imag(f(1,:)));
    bnp=(real(f(2,:))); bnpp=(imag(f(2,:)));
    g1(1:4,nmax)=[0; 0; 0; 0];
    g1(1,1:n1)=anp(2:nmax);
    g1(2,1:n1)=anpp(2:nmax);
    g1(3,1:n1)=bnp(2:nmax);
    g1(4,1:n1)=bnpp(2:nmax);
    dn=cn.*(anp+bnp);
    q=sum(dn);
    qext=2*q/x2;
    en=cn.*(anp.*anp+anpp.*anpp+bnp.*bnp+bnpp.*bnpp);
    q=sum(en);
    qsca=2*q/x2;
    qabs=qext-qsca;
    fn=(f(1,:)-f(2,:)).*cn;
    gn=(-1).^n;
    f(3,:)=fn.*gn;
    q=sum(f(3,:));
    qb=q*q'/x2;
    asy1=c1n.*(anp.*g1(1,:)+anpp.*g1(2,:)+bnp.*g1(3,:)+bnpp.*g1(4,:));
    asy2=c2n.*(anp.*bnp+anpp.*bnpp);
    asy=4/x2*sum(asy1+asy2)/qsca;
    qratio=qb/qsca;
    result=[qext qsca qabs qb asy qratio];
```

```
end;
```

2. Script for Computation of Mie Coefficients (used in the last presented algorithm)

```
function result = Mie_ab(m,x)

z=m.*x;
nmax=round(2+x+4*x.^(1/3));
nmx=round(max(nmax,abs(z))+16);
n=(1:nmax); nu = (n+0.5);

sx=sqrt(0.5*pi*x);
px=sx.*besselj(nu,x);
p1x=[sin(x), px(1:nmax-1)];
chx=-sx.*bessely(nu,x);
ch1x=[cos(x), chx(1:nmax-1)];
gsx=px-i*chx; gs1x=p1x-i*ch1x;
dnx(nmx)=0+0i;
for j=nmx:-1:2
    dnx(j-1)=j./z-1/(dnx(j)+j./z);
end;
dn=dnx(n);
da=dn./m+n./x;
db=m.*dn+n./x;

an=(da.*px-p1x)./(da.*gsx-gs1x);
bn=(db.*px-p1x)./(db.*gsx-gs1x);

result=[an; bn];
```

3. Script for rebuilding Droplet Size Distribution from Spectroscopic Measurements

```
format long
clear all
clear global
clf
clc
global m turb X I1 I2
Messung_import = xlsread ('messung');

tau= (Messung_import (:,1));
turb=(Messung_import (:,2));
```

```
wv_up=950;
wv_dn=350;

tau_2=[];
turb_2=[];
for i=1:(length(tau))
    tau_i=tau(i);
    turb_i=turb(i);
    if tau_i>wv_dn && tau_i<wv_up
        tau_2=[tau_2 tau_i];
        turb_2=[turb_2 turb_i];
    end
end
tau=reshape(tau_2, length(tau_2),1);
turb=reshape(turb_2, length(turb_2),1);

if tau(1,1) > tau((length(tau)),1)
    tau =flipud (tau);
    turb=flipud(turb);
end

M=length(tau);

n_max=  51;
D_min= 5e-9;
D_max= 3000e-9;
delta_D=(D_max-D_min)/(n_max-1);
Vector_D=D_min:delta_D:D_max;
Vector_D=transpose (Vector_D);

A_ij_vector=[];


for i=1:M
    tau_i=tau(i,1)*1e-9;
    lambda=tau_i*1000;

    im=0.0000001;
    nm=(1.29+((0.47*(lambda)^2)/((lambda)^2-(0.119)^2))-
((0.08*(lambda)^2)/(2.92^2-(lambda)^2)))^0.5;
    np=1.45797+0.00598 * (lambda^-2) -0.00036*(lambda^-4);
    m=1.35/1.33;

for n1=1:1:n_max

    if n1==1

        D_n1=(Vector_D(1,1));
        D_n2=(Vector_D(2,1));
        D_n3=0;

    elseif n1==n_max
        D_n1=(Vector_D((n_max-1),1));
        D_n2=(Vector_D(n_max,1));
        D_n3=0;

    else
        D_n1=(Vector_D(n1,1));
```

```
        D_n2=(Vector_D((n1+1),1));
        D_n3=(Vector_D((n1-1),1));
    end


    x_n1=((pi*nm*D_n1)/tau_i);
    x_n2=((pi*nm*D_n2)/tau_i);
    x_n3=((pi*nm*D_n3)/tau_i);

    Mie_maetzler_n1=Mie(m,x_n1);
    Mie_maetzler_n2=Mie(m,x_n2);
    Mie_maetzler_n3=Mie(m,x_n3);

    Q_ext_n1=Mie_maetzler_n1(:,1);
    Q_ext_n2=Mie_maetzler_n2(:,1);
    Q_ext_n3=Mie_maetzler_n3(:,1);

    kernel_n1= pi/4*Q_ext_n1*D_n1^2;
    kernel_n2= pi/4*Q_ext_n2*D_n2^2;
    kernel_n3= pi/4*Q_ext_n3*D_n3^2;

    A1=D_n2*kernel_n1-D_n1*kernel_n2+((kernel_n2-kernel_n1)/(2*(D_n2-
D_n1)))*((D_n2)^2-(D_n1)^2);
    A2=0.5*kernel_n1*((D_n2)^2-(D_n1)^2)-(((kernel_n2-
kernel_n1)*D_n1)/(2*(D_n2-D_n1)))*((D_n2)^2-(D_n1)^2)+(((kernel_n2-
kernel_n1)*((D_n2)^3-(D_n1)^3))/(3*(D_n2-D_n1)));

    if n1==1
    a_ij=(D_n2/delta_D)*A1-(1/delta_D)*A2;
    A_ij_vector=[A_ij_vector a_ij];

    elseif n1==n_max
    a_ij=(1/delta_D)*A2-(D_n1/delta_D)*A1;
    A_ij_vector=[A_ij_vector a_ij];

    else
    A3=D_n1*kernel_n3-D_n3*kernel_n1+((kernel_n1-kernel_n3)/(2*(D_n1-
D_n3)))*((D_n1)^2-(D_n3)^2);
    A4=0.5*kernel_n3*((D_n1)^2-(D_n3)^2)-(((kernel_n1-
kernel_n3)*D_n3)/(2*(D_n1-D_n3)))*((D_n1)^2-(D_n3)^2)+(((kernel_n1-
kernel_n3)*((D_n1)^3-(D_n3)^3))/(3*(D_n1-D_n3)));
    a_ij=(1/delta_D)*A4-(D_n3/delta_D)*A3+(D_n2/delta_D)*A1-(1/delta_D)*A2;
    A_ij_vector=[A_ij_vector a_ij];

    end
end
end

A_ij_vector=reshape (A_ij_vector, n_max, M);
A_ij_vector=A_ij_vector';

A=A_ij_vector;
beta=1000;
n=n_max;
m=M;

clear n1 n2 A1 A2 A3 A4 D_n1 D_n2 D_n3 M im np nm lambda delta_D a_ij
clear Q_ext_n1 Q_ext_n2 Q_ext_n3 i n_max x_n1 x_n2 x_n3 Mie_maetzler_n1
Mie_maetzler_n2 Mie_maetzler_n3 kernel_n1 kernel_n2 kernel_n3
```

```
zero_rows = zeros(2,n);
zero_matrix = zeros(n-2,2);
unit_matrix = eye(n-2,n-2);
    MATRIX1 = [zero_rows; [zero_matrix unit_matrix] ];

zero_row = zeros(1,n);
zero_column = zeros(n-2,1);
unit_matrix = eye(n-2,n-2);
    MATRIX2 = [zero_row ; [zero_column unit_matrix zero_column] ;
zero_row];

zero_rows = zeros(2,n-2);
zero_columns = zeros(n,2);
    MATRIX3 = [[unit_matrix; zero_rows] zero_columns];

MATRIX4 = toeplitz([[0 -2] zeros(1,n-2)]);
MATRIX4(n,:)=zeros(1,n);
    MATRIX4(:,n)=zeros(n,1);

MATRIX5 = toeplitz([[0 -2] zeros(1,n-2)]);
MATRIX5(1,:)=zeros(1,n);
    MATRIX5(:,1)=zeros(n,1);

    MATRIX6=toeplitz([0 0 1 zeros(1,n-3)]);

H = MATRIX1 + 4*MATRIX2 + MATRIX3 + MATRIX4 + MATRIX5 + MATRIX6;

BETA_MATRIX = [beta^2 zeros(1,n-1); zeros(n-2,n); zeros(1,n-1) beta^2];
FINAL_MATRIX = BETA_MATRIX + H;

[K,p]=chol(FINAL_MATRIX);
X=A*K^(-1);

clear zero_column zero_columns zero_matrix zero_row zero_rows unit_matrix
options tau_i p MATRIX1 MATRIX2 MATRIX3 MATRIX4 MATRIX5 MATRIX6


gamma_amount=1000;
gamma_min=-35;
gamma_max=-5;
gamma_chain=logspace(gamma_min,gamma_max,gamma_amount);


V_gamma_vec=[];
I1=eye(n);
I2=eye(m);
for i=1:gamma_amount
    gamma=gamma_chain (1,i);
    V_gamma=(  m*(((norm((I2-((X*((transpose(X)*X + gamma.*I1)^-
1)*transpose(X))))*turb))^2)/((trace(I2-((X*((transpose(X)*X + gamma*I1)^-
1)*transpose(X)))))^2)));
    V_gamma_vec=[V_gamma_vec V_gamma];
end
[V_gamma_value V_index]=min(V_gamma_vec);
gamma_opt=gamma_chain(V_index);
```

```
f = ((transpose (A))*A+gamma_opt*FINAL_MATRIX)^-1*(transpose(A))*turb;

Vector_D_plot=Vector_D*10^9;
f_plot=f/sum(f);
hold all
xlabel('Droplet Size in nm');
ylabel('normalized f(D)');
semilogx(Vector_D_plot,f_plot);
hold off
```